Kickstart Procedure of a Pumped Storage Tidal Power Plant

Capozucca, M.

Award date:
2021

Department of Mechanical Engineering

Power and Flow Research Group

Kickstart Procedure of a Pumped Storage Tidal Power Plant

Thesis for Master's Program: Sustainable Energy Technology

Matteo Capozucca

Supervisors:

Dr. B.P.M. van Esch

TU/e, Mechanical Engineering Department, Power & Flow Research Group

Dr. ir. J. van Berkel

HZ University of Applied Sciences, Delta Power Group

Eindhoven, May 2021

TU/e EINDHOVEN UNIVERSITY OF TECHNOLOGY

Declaration concerning the TU/e Code of Scientific Conduct for the Master's thesis

I have read the TU/e Code of Scientific Conduct[i].

I hereby declare that my Master's thesis has been carried out in accordance with the rules of the TU/e Code of Scientific Conduct

Date

08/05/2021

Name

MATTEO CAPOZUCCA

ID-number

1350404

Signature

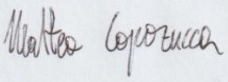

Insert this document in your Master Thesis report (2nd page) and submit it on Sharepoint

[i] See: http://www.tue.nl/en/university/about-the-university/integrity/scientific-integrity/
The Netherlands Code of Conduct for Academic Practice of the VSNU can be found here also.
More information about scientific integrity is published on the websites of TU/e and VSNU

Version 202007

Abstract

Nowadays, tidal energy is still an underutilized form of renewable energy. However, it theoretically could play a major role in the energy transition from fossil fuels to green energy sources, given its very high predictability. This feature, which is not shared by other renewable sources like sun and wind, could play a major role from the point of view of grid stabilization, which is one of the biggest issues of the delocalization of energy production. In order to generate sufficient water level differences between two bodies of water, tidal barrages are constructed in coastal or delta areas, creating artificial lakes. This is the case of the lake Grevelingen, that was created when several estuaries of the North Sea were closed as part of the "Deltaplan" for safety protection of the coastal areas of the Netherlands. Since then, the ecological condition of the area has been deeply affected, since the water recirculation has been hindered by the dam, and therefore the quality of life of flora and fauna of the area has been negatively influenced. Consequently, the touristic and economic appeal of the region has been affected as well. For this reason, the Dutch government decided to reintroduce the tide in the lake via new openings in the dam, and this intervention could be coupled with the installation of pump-turbines. These hydraulic machines would have the primary role of managing the water safety of the area by regulating the water level in the lake, but would also give the possibility to recover some of the energy spent, working as tidal turbines. The project framework "Playing with current(s)" is taking this possibility as a case study to evaluate this technical solution for different applications in many locations around the globe. The power plant could also play an important role in the stabilization of the energy grid, being able to operate as an energy sink, storing energy in form of water head (pumped storage), or as an energy producer (turbine operation). It is of utmost importance that, in order to be able to be competitive on the energy market and respond to the grid instabilities, the power plant is able to start operating in generation mode as quickly as possible. In particular, a 10-seconds window has been established. To comply with this restriction, it could be important to "kickstart" the system, accelerating the flow with pump operation to reach generating conditions faster than with just natural flow. A 0-D model has been developed to study the start-up of the system with three different strategies: natural flow, kickstart at fixed frequency, and kickstart with adoption of a frequency controller. The comparison between these three starting strategies revealed that it is possible to comply with the 10 seconds restriction only using a kickstart procedure with frequency controller.

Table of Content

List of Figures

List of Tables

1 Introduction

Nowadays, the effects generated by global warming on Earth's climate are well known and documented in scientific literature. In particular, rising sea levels, floods, storms and general extreme weather caused by rising temperatures represent major threats to coastal and delta areas. By 2070, hundreds of millions of people will be threatened by these phenomena in hundreds of coastal locations around the world [1][2]. In the second half of the 20th century, the scientific community proved that the rising temperatures are mainly associated with the release of CO_2 and other greenhouse gases in the Earth's atmosphere. These greenhouse gases are the product of fossil fuels combustion for energy generation, transportation, industrial processes and other human activities [3][4]. Human society has struggled to completely abandon fossil fuels use since then for different reasons. In fact, fossil fuels present great advantages in terms of accessibility, energy density and utilization. Moreover, from an electric grid point of view, power plants fed with fossil fuels grant a very stable output, with the ability of quickly adjusting it to the energy demand, therefore helping to maintain stability on the distribution network. Despite all these positive aspects, the rapid depletion of the Earth's resources and the climate crisis cannot be ignored. In order to contain a global temperature rise an energy revolution must be pursued, and increasing the energy generation via renewable energy sources is vital for the climate stability.

1.1 Tidal Energy

Tidal energy is a renewable energy source that exploits the kinetic energy of the tidal streams or the potential energy difference between two distinct water heads. This water level difference can be obtained with the construction of a dam, separating a new artificial basin from another body of water (e.g. sea). The tides generated by the gravitational pulls of the Sun-Earth-Moon system and the centrifugal force generated by the rotation of Earth and Moon, combined with the presence of the dam, allow to establish the desired water head [5].

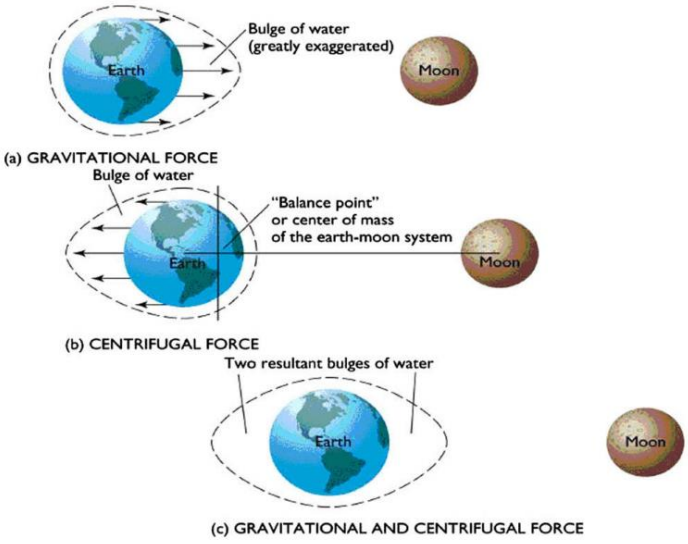

Figure 1.1: Tidal phenomenon generation [6]

In particular, a bulge of water is created by the gravitational pull of the Moon on the side of the Earth facing its natural satellite. Another bulge is generated on the opposite side by the centrifugal force created by the rotation of the Earth-Moon system. The two resulting tides have the same order of magnitude. When a landmass is lined up to this bulge, the coastal areas will experience a high tide. In contrast, when a land mass is angled at 90° with the bulge, a low tide will occur [6]. The low-to-high tidal cycle repeats twice every 24 hours and 50 minutes (although local tides could be influenced by other factors like local geology), so each day on average two low tides and two high tides will be experienced, with a drift of 50 minutes [7]. As of today, tidal energy is still underutilized, but it could play a very important role in the needed energy transition from fossil fuels to renewable, with literature assessing how, for example, about 20% of United Kingdom's energy requirements could be satisfied with 51 tidal power sites around the British islands [8]. In addition, tidal energy has one of its strengths in its predictability. In fact, while energy sources like sun and wind are extremely variable with time, posing very arduous challenges about grid balancing and power distribution, tidal energy availability is exactly predicted both geographically and temporally by our current models [8].

There are two kinds of tidal power plants: tidal streams turbines and tidal barrages. Tidal stream turbines extract the kinetic energy of the currents in order to generate electricity. These turbines utilize principles similar to wind turbines, but they also face different working conditions. In fact, despite the lower stream velocity of tidal currents when compared to winds, the turbines have to resist to greater loads given the much higher density of the fluid. Tidal stream turbines can have vertical or horizontal axis of rotation. This technology is out of the scope of this graduation project, so it will not be investigated further. Tidal barrage systems exploit the potential energy difference on the two sides of a dam built across a bay or an estuary, transforming this potential energy in electricity via hydraulic turbines. The electricity generation follows the same principles of the hydroelectric power plants, with the difference that water flow across the turbine will happen in both directions. In fact, power generation can be realized at time of ebb tide, flood tide, or both [6].

1. Ebb generation: the basin is filled with water during the flood tide. When the maximum water level is reached, the gates of the dam are closed. When the tide has retired sufficiently, gates are opened again to allow water to flow from the basin to the sea, generating torque on the turbine-shaft-generator system.
2. Flood generation: during the flood tide, the gates are kept close until a sufficient water level difference is reached. The gates are then opened to realize power generation. This method is less favourable due to its environmental and shipping activity impact, caused by an average lower water level in the basin.
3. Two-way generation: generation is realized in both ebb and flood tide. This method has the advantage of a shorter non-generating period and a reduction in the costs of generators, due to a lower peak power, caused by a lower tidal range in the basin [9].

Examples of these three different generation modes are shown in the picture below.

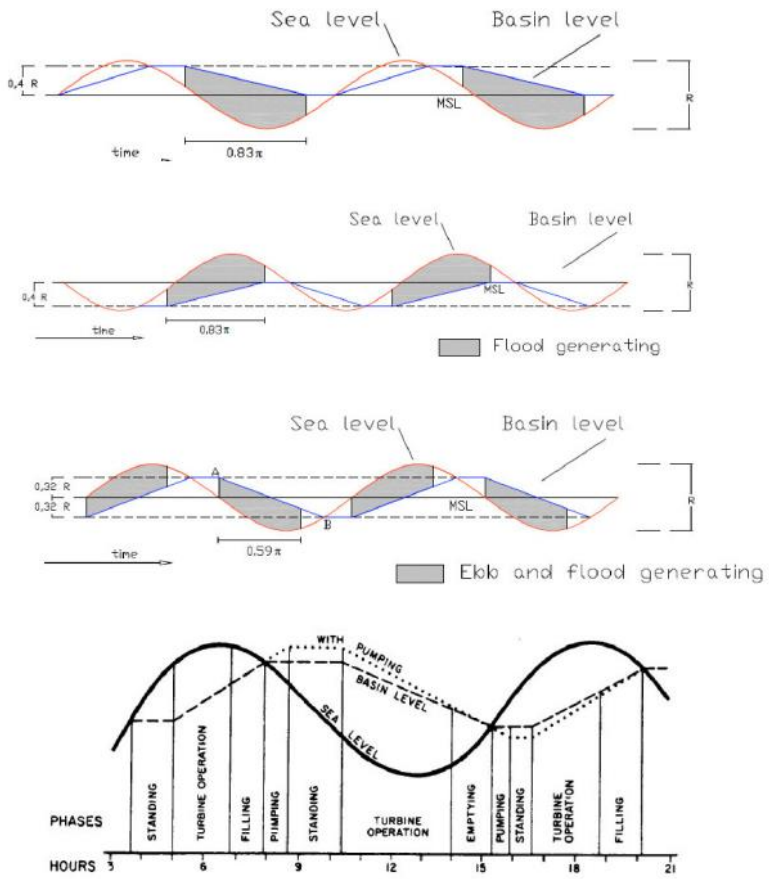

Figure 1.2: From top to bottom: ebb, flood, two-ways generation, two-ways generation with pumped storage [10]

The first ever tidal barrage power plant was built in La Rance, France, between 1961 and 1967, and it is still active today with an output of approximately 500 GWh per year. One of the biggest drawbacks of tidal barrages is their environmental impact. In fact, the construction of a dam in a delta or estuary area deeply affects the water currents, compromising water recirculation, oxygen levels and sediment transportation. As a consequence, marine life could be negatively affected [11]. Safety of fishes and other water animals is also threatened due to the passage through the turbines [12]. Moreover, construction costs of these systems are extremely high, given the amount of material needed for both closing coastal areas and allowing the structure to be able to resist the loads of the two bodies of water. As of today, given the modern technology improvements of turbine design, maintenance and repair is not considered an issue [6]. A technique often coupled with tidal barrages power plants is pumped storage. In pumped storage, the impeller can be used both as a turbine and as a pump, in which case it absorbs energy from the grid and stores it in the form of potential energy into water columns. This often offers benefits not just from a grid balance point of view, but also for water safety measures, environmental protection, and financial gains. Paragraph 2.4 will expand on the advantages of pumped storage.

1.2 Brouwersdam

The region of Zeeland, located in the western Netherlands, has suffered from major casualties caused by extraordinary floods in 1953. After that disaster, the Dutch government instituted the "Delta Committee" to try and limit possible future floods. As part of the "Deltaplan", numerous estuaries of the North Sea have been closed with the use of dams, providing needed safety to human activities in the area. One of the infrastructures fulfilling this role since then is the Brouwersdam.

Figure 1.3: Aerial View of the Brouwersdam

The Brouwersdam separates lake Grevelingen from the North Sea. Its construction started in 1964 to prevent high floods and was concluded in 1971. The construction of the Brouwersdam transformed the estuary in a saltwater lake, the lake Grevelingen. Given the presence of a very small opening connecting the sea and the lake, the tidal range of the lake has been reduced to less than 5 cm. This very small range severely harmed water recirculation, which in turn deeply affected the water quality of the lake in terms of oxygenation. For this reason, the deepest layers of the lake started suffering of hypoxia, affecting the life of organisms living in those areas. Moreover, poor water quality in the lake harms recreational activities in the area, making it less attractive and damaging it economically. For all these reasons the Dutch government decided to reintroduce a damped tide inside lake Grevelingen. Studies by the company Deltares showed that in order to reintroduce sufficient amounts of oxygen and nutrients in the lake, a tidal range of at least 40 cm has to be achieved (whereas, the average tidal range at the same location without the dam would be 2,5 meters). The Dutch government's goal is to introduce an oscillation between -10 cm and -50 cm NAP (normal Amsterdam sea level) at the Brouwersdam.

The reintroduction of the tide requires the construction of a number of culverts in the Brouwersdam. This can represent a valid solution today, but could present problems in the future. Sea levels are expected to rise due to global warming, and this would produce two effects:

- Increase of the static head difference during flood tide. This will increase the amount of water flowing into lake Grevelingen at every flood.
- Reduction of the static head difference available during ebb tide. This will reduce the amount of water flowing out of lake Grevelingen at every ebb.

The combination of these two aspects will gradually make it more difficult to drain water from the lake back to the sea, and therefore will affect the water safety management of the area. In order to improve the management of water flow between the lake and the sea, hydraulic pumps could be installed in the conduits. The energy spent to drive the pumps could be partially or entirely recovered utilizing them also as turbines.

1.3 Tidal Power Plant

The "Playing with current(s)" project framework, in its current state, would consider a system of fifteen conduits placed in the submerged part of the dam structure. Each conduit has a square geometry with 8-meters long sides, and would house a reversible bulb pump-turbine with a diameter of 8 meters. While initially the project contemplated a conduit length of 49 meters, this length has later been doubled to guarantee more space to the road laying on top of the dam.

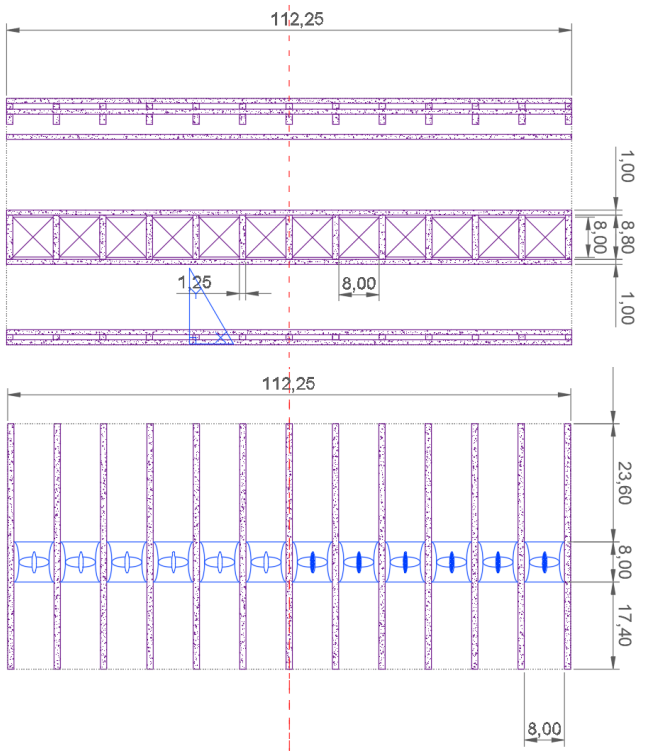

Figure 1.4: Conduits Geometry, Front and Top View

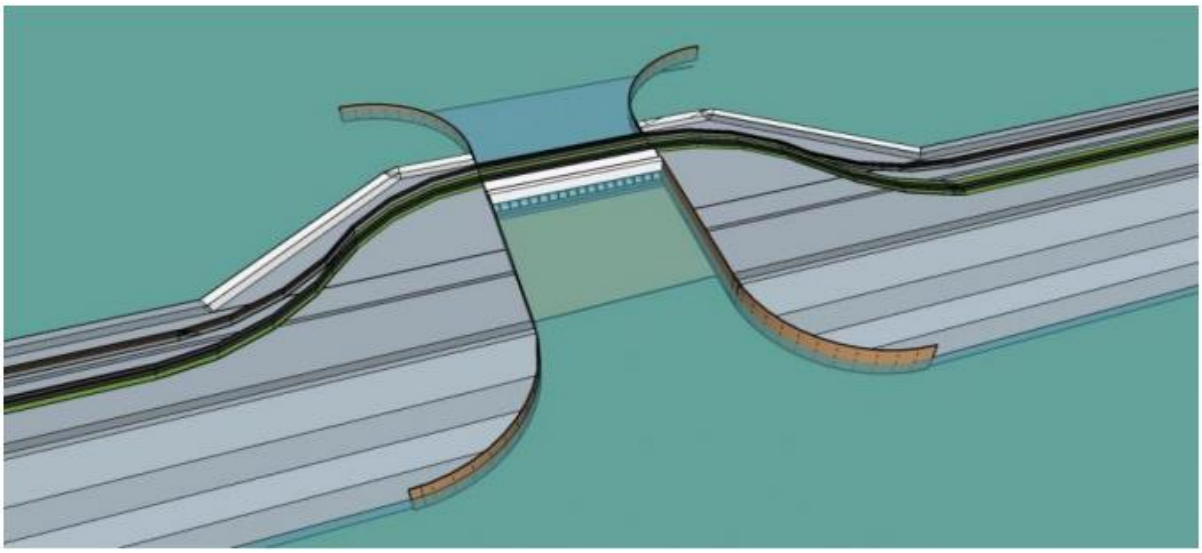

Figure 1.5: Digital Representation of the Tidal Power Plant [13]

Axial flow turbines such as bulb turbines are a widely used technology in the tidal power sector. In fact, they are used in the largest tidal power plants in the world, such as the Sihwa Lake tidal power station in South Korea and the already mentioned Rance tidal power station in France. From a working range point of view, the use of a tidal barrage power plant at the Brouwersdam presents some challenges. In fact, commercial tidal power plants usually work with a tidal range (defined as the difference between the average high and low water levels in a year) of about 6-8 meters, while at the location of the Brouwersdam the average tidal range is 2,5 meters. The average maximum water head difference across the dam is about 1 meter during ebb tide and 1,9 meters during flood tide. These working conditions lie at the edge of operational range for low pressure turbines [14].

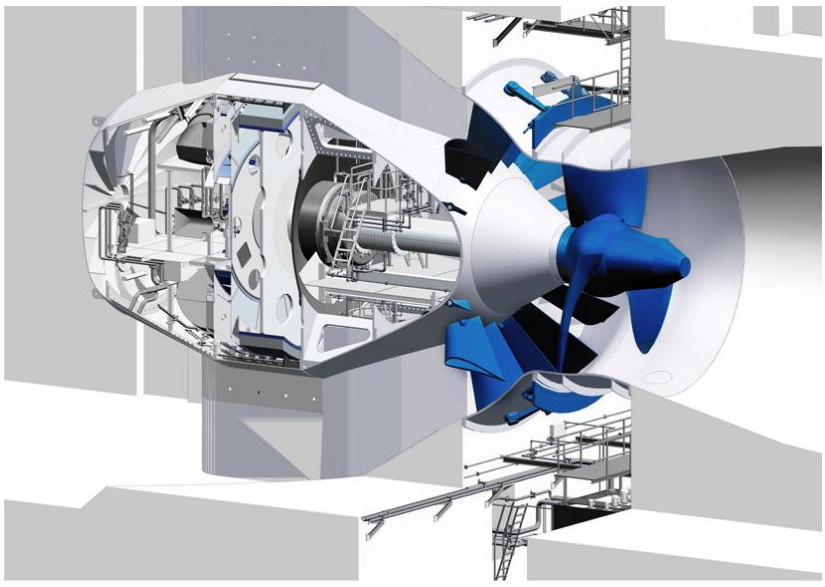

Figure 1.6: Bulb turbine example

A preliminary economic analysis for the project of the tidal power plant at Brouwersdam, shown in figure 1.7, has been performed in 2015. The stakeholders analyzed a few different configurations, of which two would utilize bulb turbines. The parameters of these two configurations are listed in the two rightmost columns. The table shows from top to bottom, for the near full scale and the full scale configuration, the installed capacity, the type of turbine, the yearly energy production, the estimated number of households the plant could supply energy to, the investment cost, the financial result over the life of the project (NPV), and the internal rate of return (IRR). The final economic result over the life of the investment would be of -30 and -63 million euros for the near full-scale and full-scale configuration respectively [15].

	Doorlaat	Seizoen-centrale	Vrije stroming klein	Vrije stroming groot	Near Full Scale	Full Scale
Geïnstalleerd vermogen (MW)	n.v.t.	4-5	4-5	14	25	41
Type turbine	n.v.t.	Vrije stroming	Vrije stroming	Vrije stroming	Bulb	Bulb
Energieproductie per jaar (GWh/j)	n.v.t.	11	16	28	85	116
Aantal huishoudens	n.v.t.	3.200	4.800	9.000	25.500	34.900
Investering nominaal (mln€)	100*	161**	161**	185**	250**	353**
Projectresultaat NCW (mln€)	-27	-43**	-40**	-41**	-30**	-63**
Projectresultaat na optimalisatie* NCW (mln€)	0	+/-	+/-	+/-	+	+/-
Internal Rate of Return	n.v.t.	0%	0%	0%	+	+

Figure 1.7: Economical analysis for six different project configurations [15]

1.4 Tide at the Brouwersdam

A hypothetical scenario of the North Sea tide and the damped tide of Lake Grevelingen is shown in the picture below. A tidal range of 2.5 meters around the NAP has been assumed for the sea tide, described by a sinusoidal function with a period of 12 hours. The water level in the lake has been assumed to be varying between -0.5 m and -0.1 m NAP. Turbine operation, highlighted in grey, has been assumed to start when there is at least 0.5 meters of static head difference, and has been assumed being interrupted when the static head would be lower than 0.5 meters as well. In addition, the static head difference between the North Sea and lake Grevelingen has been plotted.

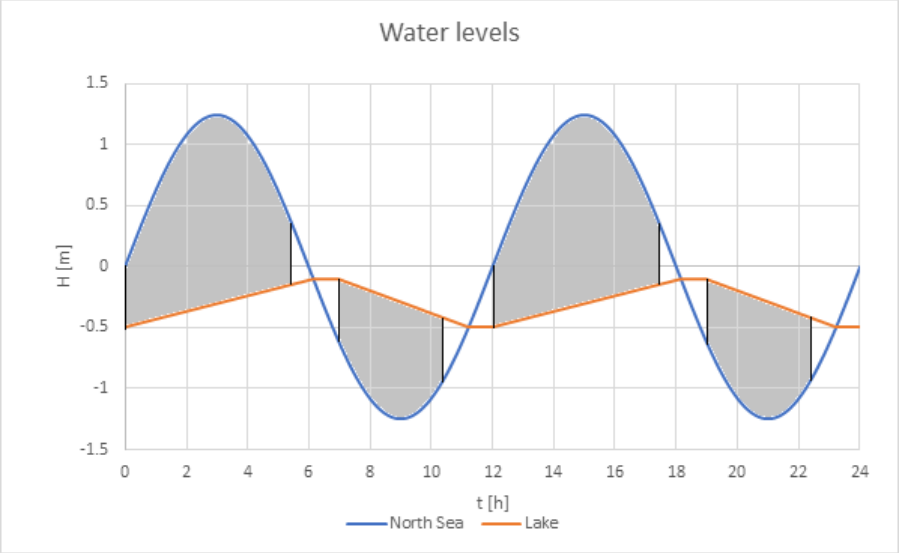

Figure 1.8: Two-ways operation at the Brouwersdam. Turbine operation highlighted in grey

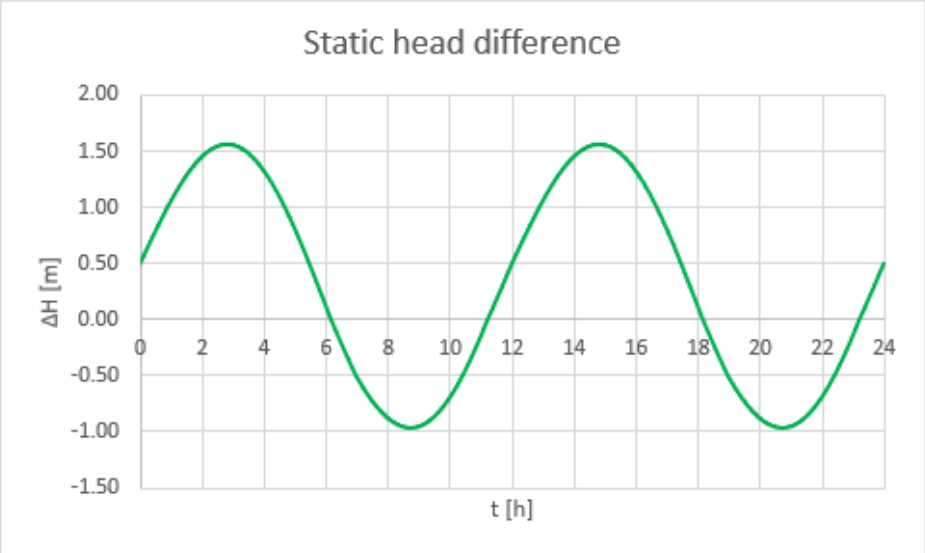

Figure 1.9: Water level difference between North Sea and Lake Grevelingen

The average discharge of the power plant, in absence of other sluice gates, to allow the desired oscillation of the water level in the lake, given a lake surface area of 110 km^2, would be:

$$Q_{flood} = \frac{A_{lake} * \Delta H_{lake}}{t} = \frac{110 * 10^6\ m^2 * 0.4\ m}{19620\ s} = 2243\ m^3/s \qquad (1.1a)$$

$$Q_{ebb} = \frac{A_{lake} * \Delta H_{lake}}{t} = \frac{110 * 10^6\ m^2 * 0.4\ m}{12492\ s} = 3522\ m^3/s \qquad (1.1b)$$

These values correspond to an average flow rate of 150 m^3/s and 235 m^3/s respectively, for each single conduit. The higher flow rate required during ebb generation is cause by the asymmetry of the system, which allows for a flood turbine operation of 5 hours and 27 minutes, and an ebb turbine operation of

3 hours and 28 minutes. Assuming a constant head loss of 10% in the conduits, the head of the pump has been calculated subtracting the head loss to the static head. The hydraulic power of the system is:

$$P_h = Q * H_p * \rho * g \tag{1.2}$$

The resulting power generated during 24 hours of operation has been shown in the picture below. The power plant average output over a day is about 18 MW.

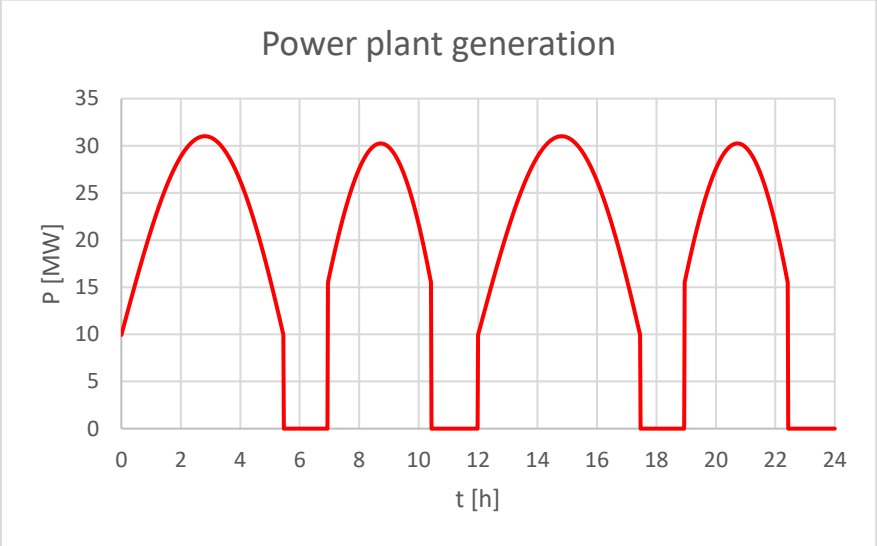

Figure 1.10: Estimated power generation in a day for the Brouwersdam power plant

1.5 Research Goals

In conclusion, the project framework "Playing with current(s)" led by HZ University of Applied Sciences, which this graduation project belongs to, aims to investigate the possibility of combining the use of dam systems for flood protection in bay areas with the use of tidal pump-turbines. The hydraulic machines could provide different benefits such as:

1. Enabling water safety measures by regulating the basin's water level pumping water out of the lake.
2. Favouring water recirculation and oxygenation in the basin, which, as previously stated, are usually hindered by dams, improving the quality of life for the local flora and fauna.
3. If operated as turbines, they could be able to partially or entirely recover the energy spent in pump operation.
4. Operating as energy sinks and storage systems (working in pump mode) when the grid is overloaded or the conditions on the electricity market are favourable.

As a case study, the project framework is evaluating the possibility of installation of pump-turbines in ducts under the Brouwersdam. In particular, this graduation project focuses on the possibility of reaching nominal generating conditions in a few seconds after the start-up of the system. This would

allow the power plant to be able to respond to energy imbalances in the grid very quickly and be more competitive in the energy market. However, it is still not clear how fast the system would be able to reach generating conditions naturally. As a matter of fact, if the flow would be driven just by the natural head difference between the two water columns, it could take too much time for the flow rate to reach values suitable for energy generation. In order to solve this issue, a kickstart procedure could be adopted. Said procedure would consist in starting the impeller in pump mode to accelerate the flow more rapidly, and reach nominal generating conditions faster. It has to be considered that, during a power demand peak, it could be problematic to utilize a procedure such as a kickstart that is also requesting power from the grid. Depending on the amount of power needed by the power plant during this operation, a possible solution could lie in the installation of batteries. Those batteries, during generation mode, would store the amount of energy necessary to allow a future kickstart of the power plant.

One of the main stakeholders of the energy distribution side of the project is the Dutch energy company PZEM. The company works in the energy trading sector, and is responsible for supplying energy to different energy market parties in the Netherlands. In addition, it supplies regulating power and reserve power to TenneT, one of the main energy distributors in the Netherlands. In communications with the managers of the "Playing with current(s)" project, PZEM stated that the response time for start-up of the power plant should be less than 10 seconds, and that the shorter the start-up, the better. In conclusion, the project aims to answer the following research question:

- *Is it possible to design a starting procedure, for a single pump-turbine, that allows the system to reach nominal generating conditions in less than ten seconds?*

In order to answer this question, three different starting procedures will be compared:

1. A start-up where the system is accelerated just by the natural flow caused by the static head difference.
2. A kickstart procedure at fixed motor frequency, where the drivetrain is initially accelerated by an electric motor. The impeller would initially work as a pump, accelerating the flow faster compared to the natural flow acceleration.
3. A kickstart procedure with a frequency controller. The variation of the motor frequency at start-up would allow the system to work at higher shaft speeds compared to the normal kickstart procedure, accelerating the flow even faster. In addition, a frequency controller is often needed in variable speed application such as wind turbines and tidal pump-turbines, since this device allows the frequency of the motor/generator current to be adjusted between the machine and the grid.

These procedures have been designed using a 0-D, time dependent numerical model in a Matlab-Simulink environment. The time needed for the system to reach nominal generating conditions, for each

procedure and for three different static head scenarios have been analyzed and discussed. In order to model the characteristics of the pump-turbine, experimental data gathered by the company Nijhuis Pompen BV using a small-scale experimental setup have been used. These data have been reported in appendix A. This research has been summarized in a scientific paper, submitted to the European and Tidal Wave Energy Conference Series (EWTEC) for its 2021 edition. The paper has been attached in appendix B.

1.6 Thesis Overview

The report at hand is composed of seven chapters. The first one has been an introductory chapter, with a general description of tidal energy technology and of the geographical area the project focuses on. The research goals have also been stated. Then, a description of pumped storage operation follows in chapter 2, with explanations about the performance characteristics, the possible configurations of a pumped storage system and its different operating modes. In chapter 3 the model built to represent the physical phenomenon is described (governing equations, numerical solver). Chapter 4 is dedicated to the numerical verification of the model and to its validation. In chapter 5 the results of the simulations are shown, whereas these results are commented in chapter 6. Chapter 7 includes the final comments and recommendations for the improvement of the model and future possible researches.

2 Pumped Storage

2.1 Working Principles of Hydraulic Turbomachines

Hydraulic turbomachines are devices able to transfer energy between a fluid and a rotor. According to the more general classification, if energy is transferred from the rotor to the flow (meaning that mechanical energy is transformed into hydraulic energy) the machine is considered a pump. Instead, if the energy is transferred from the flow to the rotor the machine is considered a turbine. This energy transfer is realized thanks to the interaction between the flow and the impeller blades. These systems work according to three conservation laws: conservation of mass, momentum and energy.

For a pipe system with a hydraulic pump, pumping water from an elevation z_1 to a higher elevation z_2, the energy conservation law is [16]:

$$\frac{p_1}{\rho g} + \frac{v_1^2}{2g} + z_1 + H_p = \frac{p_2}{\rho g} + \frac{v_2^2}{2g} + z_2 + H_{loss} \tag{2.1}$$

where:

- p_1 and p_2 are the pressures at the suction side and pressure side of the pump respectively
- v_1 and v_2 are the velocities at the suction side and pressure side of the pump respectively
- H_{loss} are the head losses in the system
- H_p is the head generated by the pump, defied as $H_p = \Delta z + H_{loss}$

The first term of on each side of the equation represents the pressure head, whereas the second is the dynamic head. The net power of the pump is defined as:

$$P_p = \dot{m} g \Delta z + P_{loss,pipe} = \eta_p P_{shaft} \tag{2.2}$$

where:

- $\dot{m}$ is the mass variation over time
- $P_{loss,pipe}$ is the power lost in the pipe
- η_p is the efficiency of the pump
- P_{shaft} is the shaft power

For a turbine, the energy conservation law is:

$$\frac{p_1}{\rho g} + \frac{v_1^2}{2g} + z_1 = \frac{p_2}{\rho g} + \frac{v_2^2}{2g} + z_2 + H_t + H_{loss} \tag{2.3}$$

with $H_t = \Delta z - H_{loss}$. The net power of the turbines is defined as:

$$P_t = \dot{m} g \Delta z - P_{loss,pipe} = \frac{P_{shaft}}{\eta_t} \tag{2.4}$$

where η_t is the efficiency of the turbine. As mentioned previously, the interaction between the flow and the impeller blades is essential in order for power to be transferred between shaft and flow. In fact, this power transfer is obtained thanks to the flow deviation caused by the blades. The angular momentum conservation law for an hydraulic machine is:

$$\sum M = \dot{m}_0 (\vec{r} \times \vec{v})_0 - \dot{m}_1 (\vec{r} \times \vec{v})_1 \tag{2.5}$$

where $\vec{r}$ is the radial vector and $\vec{v}$ is the velocity vector. The effect of the angular momentum change is a torque on the shaft, therefore:

$$T = \dot{m}_0 r_0 v_{\theta 0} - \dot{m}_\iota r_i v_{\theta i} \tag{2.6}$$

Where $v_{\theta 0}$ and $v_{\theta i}$ indicate the swirl velocity at the inlet and outlet of the machine. Consequently, the shaft power is:

$$P_{sh} = nT \tag{2.7}$$

where n is the angular speed of the hydraulic machine. The usual way of representing pump performances is via characteristic curves. These are curves that relate parameters of pumps such as head, net positive suction head, torque, power and efficiency to flow rate, for different shaft speed values. In the picture below, examples of these curves are shown for a centrifugal pump.

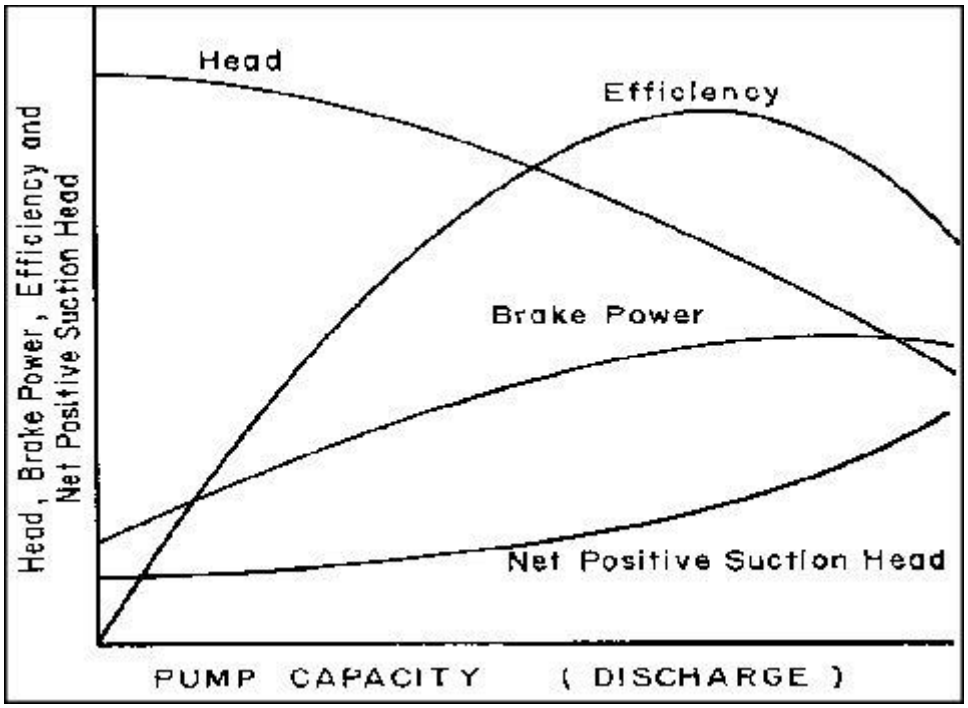

Figure 2.1: Centrifugal pump characteristic curves [17]

2.2 Scaling of Performance

In the study of turbomachines, it is often useful to be able to compare the performances or behavior of one machine to the one of a similar machine under different conditions, for example size and speed. Dimensionless numbers serve this purpose, allowing to use the principle of similarity to compare different devices, such as test-scale models with the real application machines. The following dimensionless numbers are defined as follows[16]:

$$\phi = \frac{Q}{nD^3} \tag{2.8}$$

ϕ is called flow number. Q is the flow rate, n is the shaft speed and D is the diameter of the machine.

$$\psi = \frac{gH}{n^2D^2} \tag{2.9}$$

ψ is called head number, and H is the head of the turbomachine.

$$Re = \frac{\rho n D^2}{\mu} \tag{2.10}$$

Re is called Reynolds number, and μ is the dynamic viscosity of the fluid. Reynolds number represent the ratio between inertia forces and viscous forces. Two machines with same Reynolds number yield the same hydraulic efficiency. These numbers are the base for performance scaling. For example, scaling from a shaft speed n_1 to n_2 requires that ϕ and ψ are constant, therefore:

$$\frac{Q_2}{Q_1} = \frac{n_2}{n_1} \tag{2.11}$$

$$\frac{H_2}{H_1} = \left(\frac{n_2}{n_1}\right)^2 \tag{2.12}$$

For the power defined as $P = \frac{\rho g Q H}{\eta}$, with η constant, this means:

$$\frac{P_2}{P_1} = \left(\frac{n_2}{n_1}\right)^3 \tag{2.13}$$

The scaling according to diameter follows the same principle. In conclusion, the performance characteristics of a pump can be scaled according to the pump diameter and its shaft speed according to:

$$Q_2 = Q_1 * \left(\frac{n_2}{n_1}\right) * \left(\frac{D_2}{D_1}\right)^3 \tag{2.14a}$$

$$H_2 = H_1 * \left(\frac{n_2}{n_1}\right)^2 * \left(\frac{D_2}{D_1}\right)^2 \quad (2.14b)$$

$$P_2 = P_1 * \left(\frac{n_2}{n_1}\right)^3 * \left(\frac{D_2}{D_1}\right)^5 \quad (2.14c)$$

$$T_2 = T_1 * \left(\frac{n_2}{n_1}\right)^2 * \left(\frac{D_2}{D_1}\right)^5 \quad (2.14d)$$

Regarding efficiency, when scaling up the characteristics of a small impeller, the efficiency does not scale up accordingly, since the head and power scaling presents some inaccuracy due to the fact that the frictional losses depend on the Reynolds number. In order to have an evaluation of what the efficiency would be when the impeller is scaled up maintaining geometrical similarity, the following formula is usually utilized [25]:

$$\frac{(1-\eta_{turbine})}{(1-\eta_{model})} = \left(\frac{Re_{model}}{Re_{turbine}}\right)^n \quad (2.15)$$

where n is called power factor (usually assumed between 0.1 and 0.5) and $Re = \frac{\rho \frac{Q}{A} D_h}{\mu}$ is the Reynolds number for a pipe. Equation (16) presents a scaling based on Reynolds number which assumes that all losses in the pump are due to friction, and that the internal surface of the pump is perfectly smooth. This formula highlights how, in case of large-scale systems for which the Reynolds number is larger, the efficiency will also be higher compared to the model-scale system. The picture below shows the efficiency of a system in function of the non-dimensional flow number. The coloured scale represents the Reynolds number corresponding to each recorded data point. The graph demonstrates how, for higher Reynolds numbers, the efficiency of the system is higher.

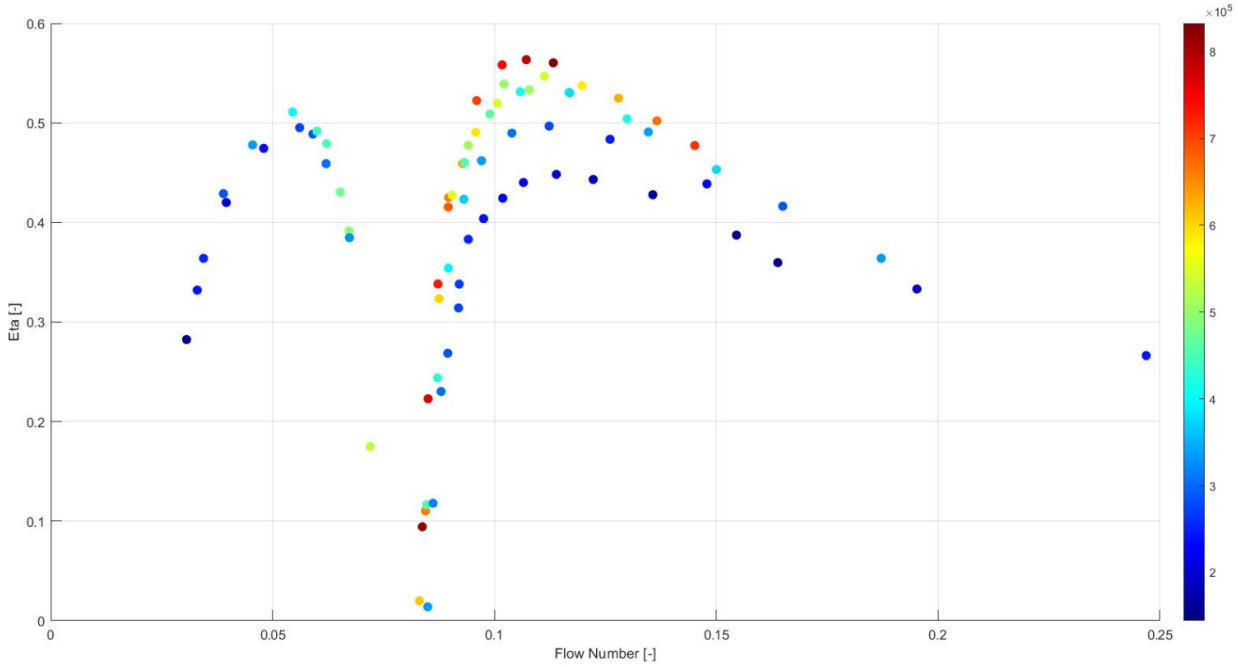

Figure 2.2: Efficiency as a function of flow number and Reynolds number

2.3 Types of Hydraulic Turbomachines

One of the possible classifications of hydraulic turbomachines is based on the flow direction. This could be radial (like in the case of centrifugal pumps and Francis turbines), axial (like bulb and Kaplan turbines) or a combination of two (mixed flow machines). Another type of turbine is the Pelton wheel, which is an impulse-based water turbine. This kind of turbine extracts energy from the impulse of high-pressure moving water. A common way of categorizing hydraulic machines is based on their specific speed and specific diameter. These values, at best efficiency point, are defined as:

$$N_s = \frac{\phi^{\frac{1}{2}}}{\psi^{\frac{3}{4}}} = \frac{n\sqrt{Q}}{(gH)^{\frac{3}{4}}} \tag{2.16a}$$

$$D_s = \frac{\psi^{\frac{1}{4}}}{\phi^{\frac{1}{2}}} = \frac{D(gH)^{\frac{1}{4}}}{\sqrt{Q}} \tag{2.16b}$$

These numbers are valid for all turbomachines. For equal N_s and D_s two machines are considered geometrically similar. In figure 2.3 different types of pumps and turbines are shown classified for their specific speed, and their maximum efficiencies are specified (in green). In figure 2.4, different types of turbine and their operating ranges in terms of specific speed and head are shown.

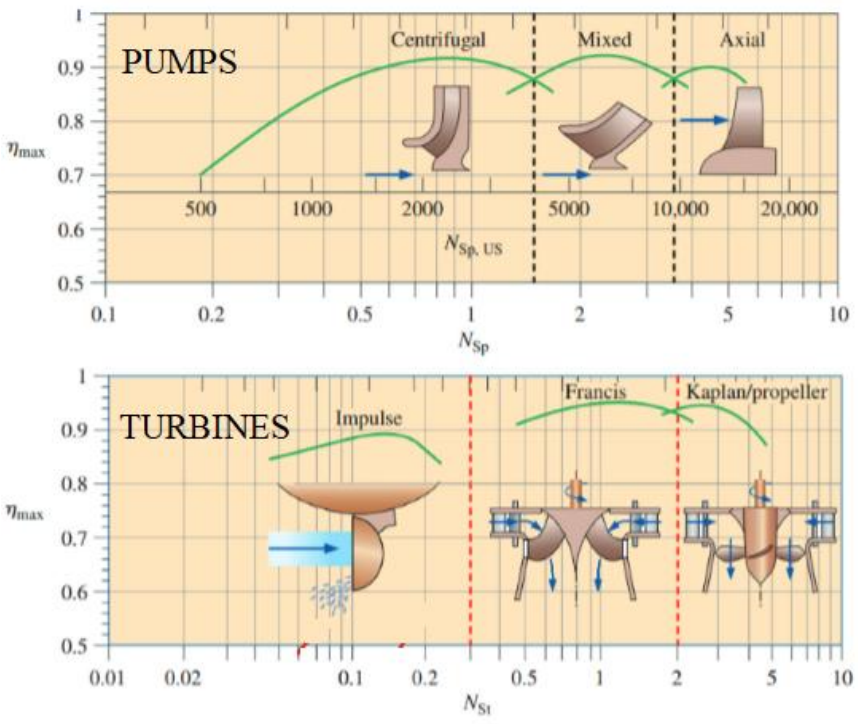

Figure 2.3: Efficiency of pumps and turbines in function of specific speed [16]

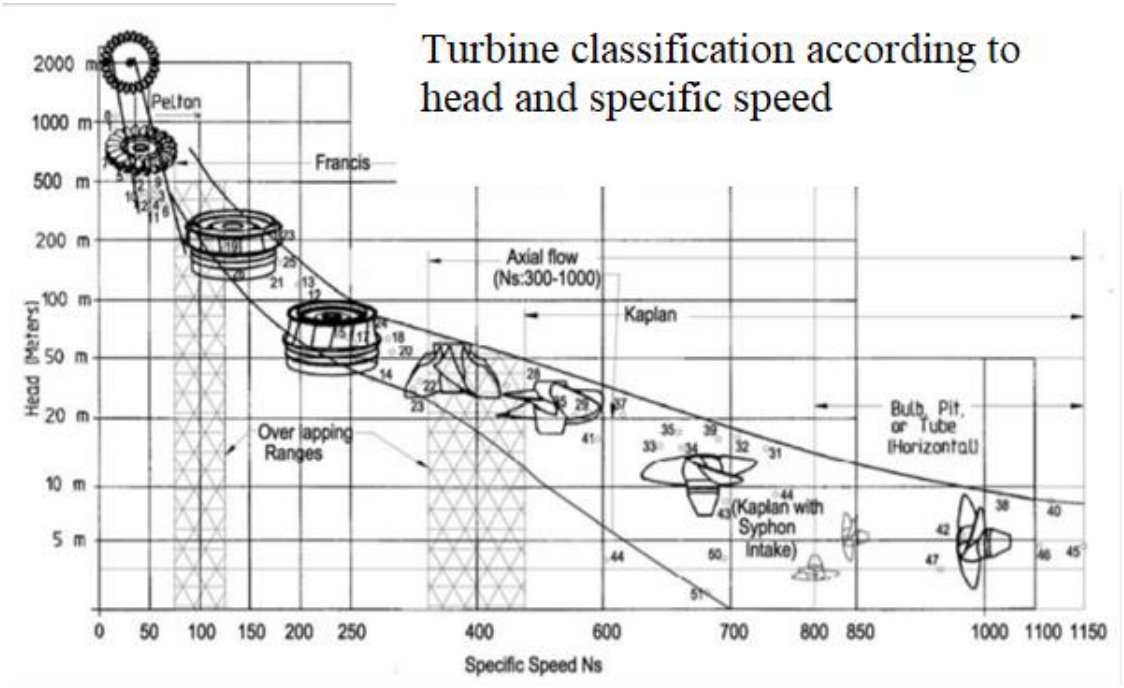

Figure 2.4: Turbines operating ranges according to head and specific speed [18]

In order to evaluate the best dimensions for impellers, turbomachine designers use the Cordier diagram. For a given operating point (flowrate and pressure, and a rotating speed), the optimum diameter of high-efficiency impellers can be found in the Cordier diagram. The Cordier diagram is an empirical diagram based on measurements. It shows the specific speed of a machine as a function of its specific diameter.

The Cordier diagram indicates that the higher the specific speed, the smaller the machine. This suggests that for low head, high capacity applications, the most suitable machine design are bulb turbines. In fact, the selection an impeller of smaller specific speed would require an even larger machine.

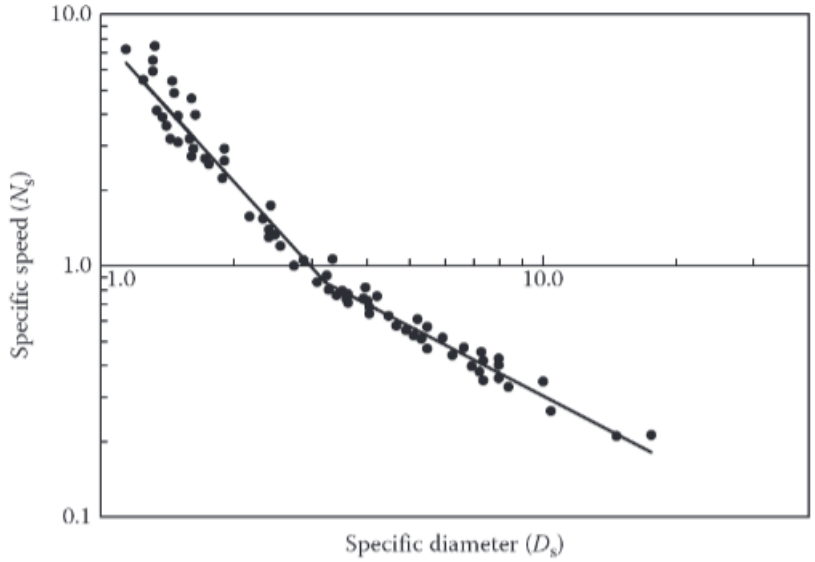

Figure 2.5: Cordier diagram [16]

2.4 Pumped Storage Strategy and Configurations

Pumped storage is an energy storage technology used in hydroelectric and tidal barrage power plants. Its main purpose is to maintain power balance on the grid. This method stores energy in form of gravitational potential energy by pumping water from a lower elevation to a higher one, working as a power sink when the grid tends to be overloaded and the price of electricity is low (generation higher than demand), to have it available when the demand rises and selling energy is more profitable (peak hours). The pumping and generation phases are realized via use of one or two hydraulic machines, each connected to electrical machines. Hydraulic pumps have proved to be very useful in the management of water safety procedures as well, which is also considered a high priority by the Rijkswaterstaat in the lake Grevelingen area. Despite the fact that the pumped storage process causes a net consumption of power, the revenues can still be high thanks to the economic strategy just described. These systems are often coupled with wind and solar energy installations, given their ability to store the extra power generated by these more fluctuating sources, and to release it when necessary [19][20]. This is a demonstration of the important role that pumped storage tidal power could play in the energy transition, where one of the biggest challenges is represented by the matching of the energy demand and the fluctuating generation. As mentioned before, in order to be able to both generate energy and apply pumped storage concepts, it is necessary to use both a pump and a turbine, coupled with one or more electrical machines working as motor and generator. All these elements can be coupled in three different configurations [21]:

- Quaternary configuration: makes use of four different devices. A pump is coupled with an electric motor, while a turbine is coupled with a generator. This makes the system easy to control, as switching between the two modes is generally fast, especially if two separate pipes for the pump-motor and the turbine-generator systems are used. However, this configuration is very expensive, given the fact that two hydraulic machines and two electric machines are needed.
- Ternary configuration: a pump and a turbine are connected to a single electric machine, acting as a motor/generator. This system is easy to control and less expensive given that only one electrical machine (and a single powerhouse) is needed. The switching time is slower compared to the quaternary configuration, since it is limited by pipeline dynamics.
- Binary configuration: a reversible pump-turbine is used as hydraulic machine, connected to a single electric machine working as a motor/generator. This is the cheapest and most used configuration worldwide. The downside is that the start-up is usually slow given the fact that the shaft rotation has to be reversed between pump and turbine mode. Pipeline dynamics also affects the switching time. The system usually grants a low efficiency as a turbine, since the hydraulic machine design is optimized for pump operation.

For the Brouwersdam project, a binary configuration is considered.

2.5 Four-quadrant Operation

A pump-turbine can work in eight different modes, depending on the direction of the flow, on the angular speed, on the head, and the torque acting on the shaft. Figure 2.6 represents these eight modes in a four-quadrant graph, from the point of view of a pump. Q represents the flow rate, H indicates the manometric head, T represents the hydraulic torque and N indicates the shaft speed.

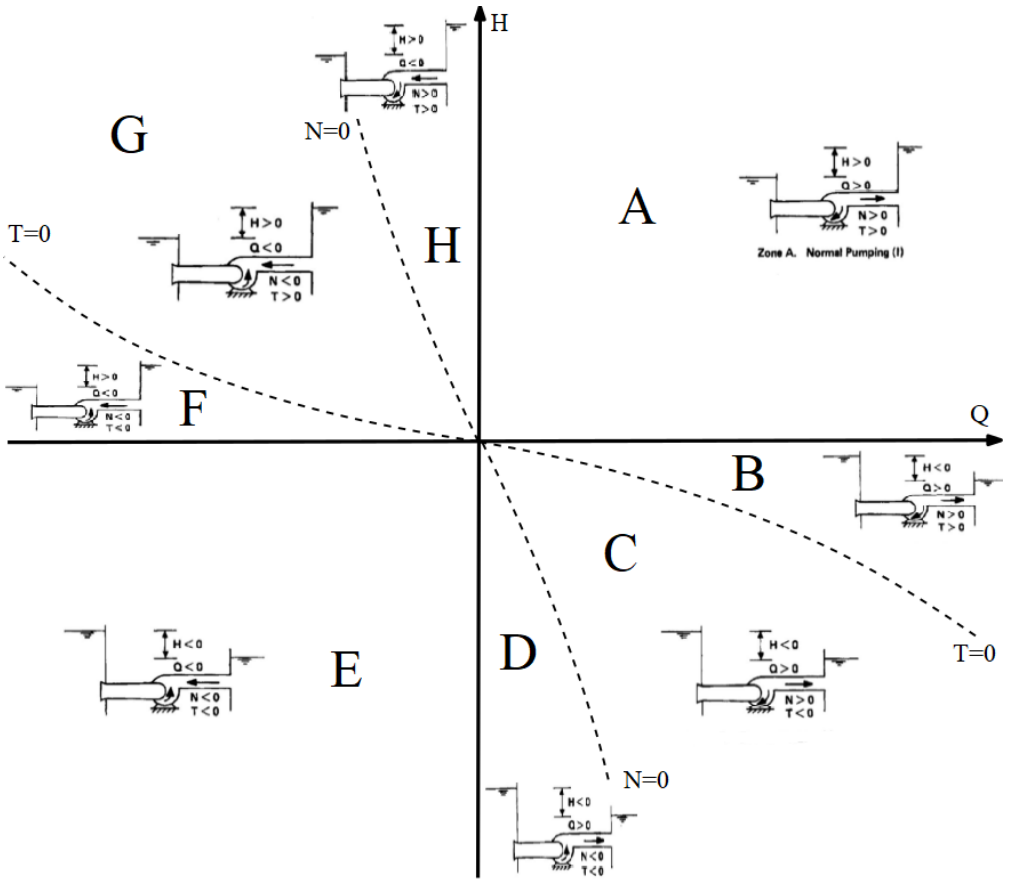

Figure 2.6: Pump-turbine operation zones

A. Pump mode: positive flow rate, positive head (increasing pressure across the impeller), positive torque/power (impeller is consuming power provided by the electric motor), positive shaft speed.
B. Pump-assisted drainage (also called brake mode): positive flow rate, negative head, positive torque, positive shaft speed. The impeller is absorbing power from the electric machine, but flow rate would be higher without it.
C. Reverse turbine: positive flow rate, negative head, negative torque/power (the impeller is transferring mechanical power to the electric machine through the shaft), positive shaft speed.
D. Dissipative mode: the same as reverse turbine mode, but the shaft is rotating in the opposite direction.

For a perfectly symmetrical axial hydraulic machine, modes E (reverse pump), F (reverse brake), G (turbine) and H (dissipative mode) mirror the conditions of mode A, B, C and D. Pumped storage is performed operating the machine in pump mode A and then generating in turbine mode G with opposite flow direction and opposite shaft rotation. However, for this study, the flow and the shaft speed do not reverse between the initial pumping and the generation phase. In fact, using a kickstart procedure, the system passes from pump mode A, to pump-assisted drainage B, to reverse turbine C, where the generation is performed. In Figure 2.7 an example of Q-H and Q-P graphs for a hydraulic machine is

depicted. The black curves represent the characteristic curves, meaning the flow rate/head and flow rate/power relations of the hydraulic machine at four different shaft speeds n_1, n_2, $-n_1$ and $-n_2$ with $n_1 > n_2$. The red curve represents the runaway curve, so all the Q-H points where the impeller is in a free spin situation (torque and power equal to 0).

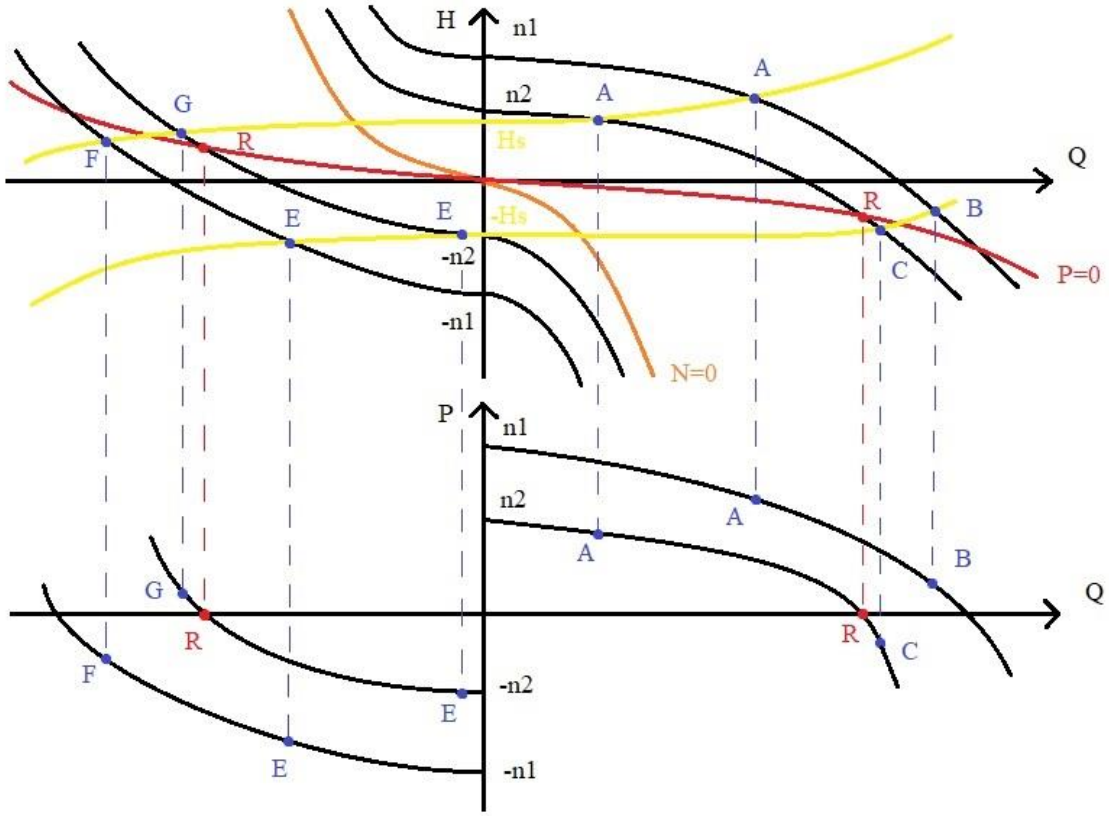

Figure 2.7: Q-H and Q-P graphs. Pump-turbine characteristic curves (black), system resistance curves (yellow), runaway curve (red)

The yellow curves represent different system resistance curves. Resistance curves are a graphical representation of the pump head, also called manometric head, that is required to move fluid through a pipe or a duct at a steady flow rate in pump mode, or the head that can be extracted from a steady flow in turbine mode. The difference between the water levels at the pressure side and the suction side (in pump mode) is denoted by H_s, the so-called static head (or system head). This static head is represented by the resistance curve at Q=0. The intersection points between a resistance curve and the characteristic curves are the equilibrium points of the system at different shaft speeds. These points have been highlighted in blue, also adding the indication of the respective operating mode. In pump mode and reverse pump mode (first and third quadrant respectively) the pump head necessary to move water at a certain flow rate is always higher than the available static head. This is because the pump has to compensate for head losses due to friction, so the difference between the static head correspondent to that particular resistance curve and the manometric head required at any other point of the curve is exactly the amount of head lost in the piping system. The higher the friction in the pipe (due for example to a very rough surface material) the steeper the resistance curve. In turbine, reverse turbine and brake

mode (second and fourth quadrant) the head that the impeller is able to extract from the flow is less than the available static head, since part of it is going to be lost because of friction. In the Q-P graph, the runaway curve is represented by the x-axis. As an example, the transition from pumping to generation will be described, for both of pumped storage operation and kickstart procedure.

2.6 Switching Modes

2.6.1 Switching in Pumped Storage

In pumped storage operation, the system is initially pumping water to a higher elevation, working in pump mode A at a constant shaft speed, on one of the equilibrium points shown in Figure 2.7. To start generating power, the motor stops supplying power to the shaft. In pump mode, the fluid torque on the impeller is directed opposite to shaft rotation direction. As a consequence, if the motor is disconnected, the shaft speed reduces, and the operating point moves along the resistance curve to lower flow rate. Assuming that the deceleration happens slowly (because of a large rotor inertia), the operating point remains on the resistance curve (quasi-steady operation). The flow rate reaches zero and becomes negative, driven by the positive static head. The shaft speed continues to decrease, reaches zero and reverses direction. The operating point then enters the turbine region G, generating power. Without connecting the generator to the grid, the (negative) shaft speed would increase until the operating point reaches the runaway curve at runaway speed.

2.6.2 Switching in Kickstart Procedure

During a kickstart, which is the procedure this research focuses on, the system is in a situation of negative static head, whereas the operation of the machine at the opening of the gate-valves starts in pump mode A. Moreover, the operation is not quasi-steady, therefore the system does not move on the resistance curve while transitioning from pump mode A to reverse turbine mode C, without changing the direction of the flow and of the shaft rotation. When the gate-valves of the conduit are opened, natural flow starts developing. At the same time, the shaft is accelerated by the electric motor. During this first phase at low flow rate values, the system operates in region A. The shaft accelerates and the operation point moves towards characteristic curves of higher shaft speed. When the flow rate increases, the system crosses the pump-assisted drainage region first. Then, for higher flow rate values, the system reaches the reverse turbine mode C, where it is the flow that supplies power to the shaft, and therefore power is generated through the electric machine. An example of the trajectory of the operating point is highlighted in orange in the figure below.

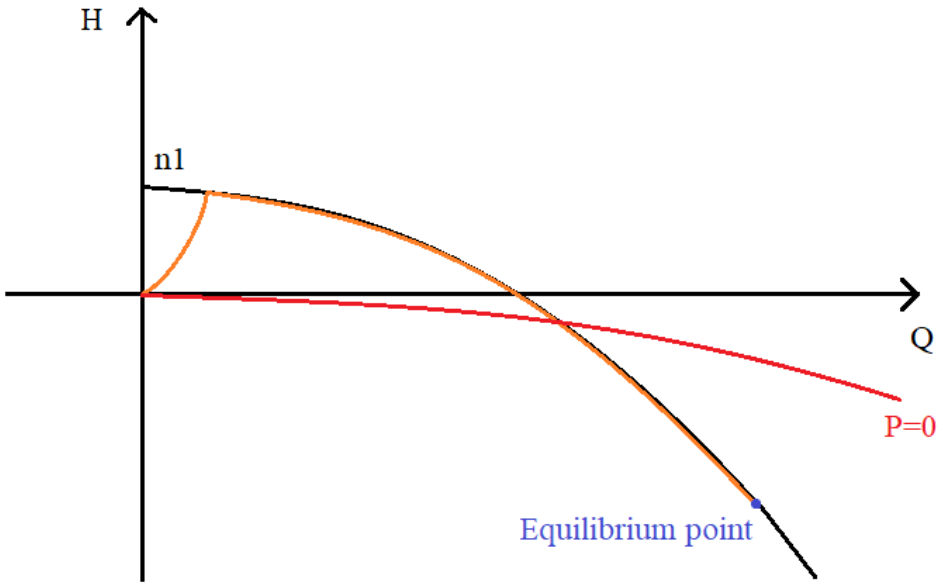

Figure 2.8: Operating points during kickstart procedure

2.7 Brouwersdam Pump-turbine

To evaluate the performance of the pump-turbine of the Brouwersdam project, experimental data have been used. The experiments were performed by the Dutch company Nijhuis Pumpen BV with the use of an experimental setup composed of two water tanks connected by a duct where the pump-turbine has been placed. There are no stator vanes upstream or downstream of the impeller. A shaft connects the pump-turbine to an electrical machine. The pump-turbine is a 5-bladed impeller with a diameter of 30 centimeters and with symmetrical blades, meaning that the blades have a symmetrical profile at each section. Symmetrical impellers represent a compromise between pump and turbine operation, theoretically providing the same efficiency between pump and reverse pump mode, and turbine and reverse turbine mode. The pump-turbine to be used in the Brouwersdam power plant is assumed to have the same geometry (scaled up to an 8-meters diameter) of the one used in the experimental setup.

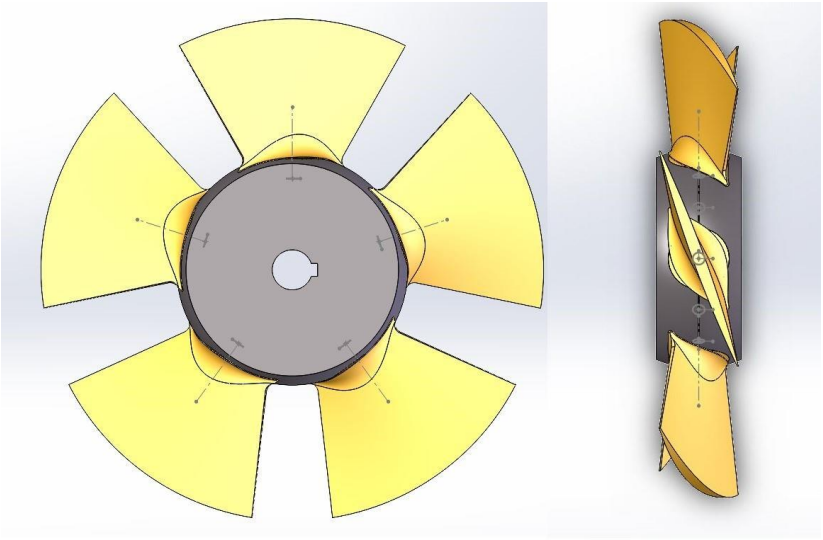

Figure 2.9: Front and side view of the impeller used for experiments

In order to evaluate the head generated by the pump-turbine ΔH_p, experiments at steady-state conditions were performed by Nijhuis Pompen, with use of the model-scale impeller shown in figure 2.9. These experiments were run for both directions of flow, with shaft angular speed switched according to the direction of flow. This way, data points in pump and reverse pump mode, brake and reverse brake, turbine and reverse turbine mode were collected. No experiments were performed with conditions representing dissipation mode D and H. The steady-state condition of the system was guaranteed by a bypass pipe connecting the bottom of the two tanks. When water was pumped from the low-water tank to the high-water tank, a reverse flow in the bypass pipe naturally developed in the opposite direction. In turbine experiments, when water was flowing from the high tank to the low tank, another pump placed in the bypass pipe was supplying return flow. During the experiments of Nijhuis, the setup was able to record data sets comprising of:

- Static heads H_{s1}, H_{s2} and manometric head H_p
- flow rate Q
- power consumed/generated P_{sh}
- impeller speed ω

The static pressures in the water tanks and across the pump-turbine have been measured with pressure transducers. These are sensors that translate an applied pressure into a voltage difference thanks to a piezoelectric diaphragm. Knowing the calibration of the sensors it is possible to translate the electric signal back to a value of static pressure. Once the static pressure p is known, in bar, the correspondent head is calculated according to:

$$H = \frac{10^5 * p}{\rho g} \tag{2.17}$$

For the measurement of the manometric head, the static pressure has been measured from four taps placed around the pipe, at 90 degrees from each other, on both sides of the impeller. These four taps are linked to each other and then connected to the pressure transducer. The manometric head is calculated as the difference between the head on the pressure side and on the suctions side of the impeller. The manometric head sensors are highlighted in yellow in the picture below.

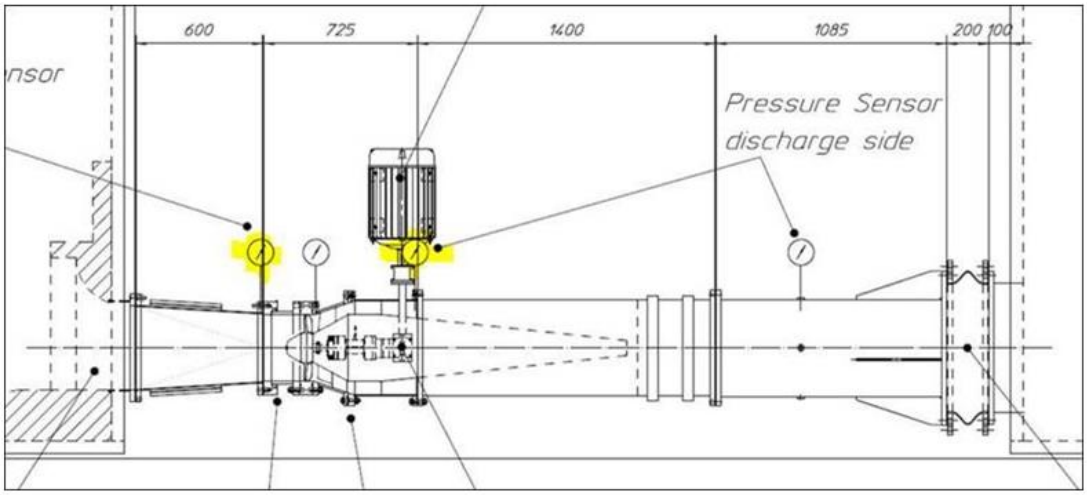

Figure 2.10: Position of manometric head sensors (highlighted in yellow)

The flow rate has been measured using an electromagnetic flowmeter, placed in the bypass pipe. This is a transducer that measures a fluid's flow rate by the voltage induced by its flow through a magnetic field. A magnetic field is applied to the metering tube, which results in a potential difference proportional to the flow velocity perpendicular to the flux lines. This voltage is then measured and converted back to a flow rate value, knowing the calibration of the device. The calibration of all instruments has been performed and documented before their use in the experiments. Torque and mechanical efficiency for each data point are then derived from the measured quantities according to:

$$T = \frac{P_{sh}}{\omega} \tag{2.18}$$

$$\eta_{mech,pump} = \frac{Q * H_p * \rho * g}{P_{sh}} \tag{2.19a}$$

$$\eta_{mech,turbine} = \frac{P_{sh}}{Q * H_p * \rho * g} \tag{2.19b}$$

Equation (2.19a) is associated to operation in pump mode, reverse pump mode and pump-assisted drainage. Equation (2.19b) is associated to turbine and reverse turbine mode. To assess the reliability of the manometric head measurements, pressure losses were evaluated for four different experiments, with constant static head difference $H_s = H_{s2} - H_{s1}$ of -0.5 m, -0.7 m, -1 m, -1.5 m respectively, and increasing shaft speed. In these experiments the impeller was operating in reverse turbine condition, thus the pressure losses are defined as:

$$H_{loss} = H_m - H_s \tag{2.20}$$

The head losses with respect to flow rate are shown below, for all four experiments:

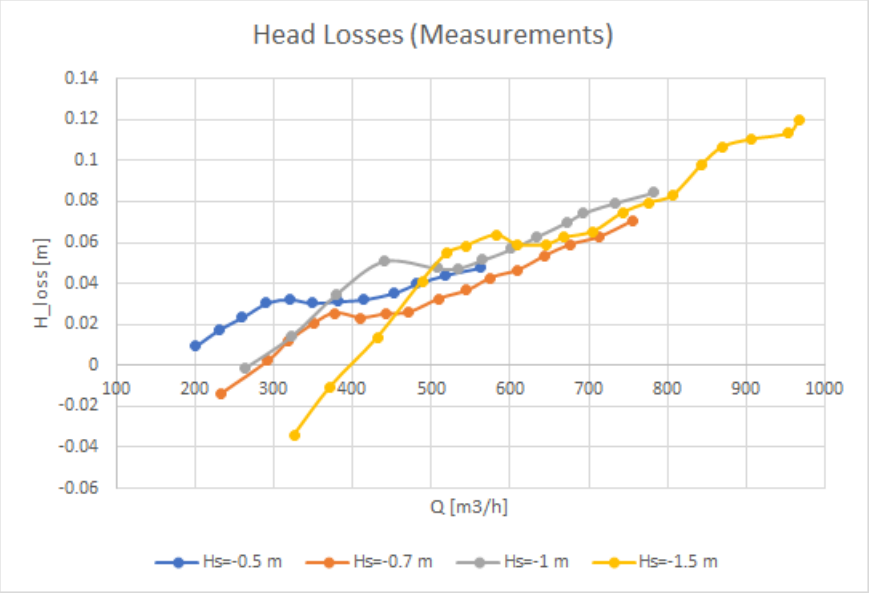

Figure 2.11: Measured head losses with respect to flow rate

The results for head losses present some issues:

- The expected quadratic dependence of head losses on flow rate is not recognizable [23].
- There is a significant deviation between head losses values at the same flow rate. This is physically not realistic, since the characteristics of the system that influence friction losses (conduit length, diameter, pipe surface roughness, fluid density and viscosity) are the same for all experiments, so friction losses are expected to be equal for equal flow rate.
- Some points yield negative losses, meaning that the static head is higher than the manometric head. This is impossible in turbine and reverse turbine mode, since it would mean that the turbine is able to extract from the flow a head higher than the one available in the water columns.

The inaccuracies in the static head measurements could be related to disturbances caused by swirling in the flow generated by the impeller rotation, given the proximity of the sensors to the impeller (about one impeller diameter away from the impeller section) and the absence of guide vanes which are usually utilized to orient the flow lines in the axial direction. For all the aforementioned reasons, the manometric head measurements are considered unreliable, and another approach for the evaluation of the manometric head is used. This consists in the estimation of head losses for each data point, and the derivation of the manometric head from the static head according to:

- $H_m = H_s + H_{loss}$ for positive flow rate
- $H_m = H_s - H_{loss}$ for negative flow rate

To estimate losses, the strategy involves, as a starting point, their calculation at the point of highest efficiency, following the assumption that this would coincide with a state of minimum swirl, even

though the absence of stator vanes on both sides of the impeller means a certain swirl in the flow will still be present. Once the best efficiency point in each experiment is identified, the estimation of the Darcy friction factor f for that point is performed using Serghide's correlation. Serghide's correlation is an approximated explicit form of Colebrook's equation, which expresses the Darcy friction factor as a function of Reynolds number and pipe relative roughness $\frac{D_h}{\varepsilon}$. Colebrook's equation as shown below was derived from experimental data on turbulent flow.

$$\frac{1}{\sqrt{f}} = -2\log\left(\frac{\varepsilon}{3.7 * D_h} + \frac{2.51}{Re * \sqrt{f}}\right) \tag{2.21}$$

This equation can be solved iteratively to find the Darcy friction factor. For this project, Serghide's approximation was used:

$$f = \left[A - \frac{(B-A)^2}{C - 2B + A}\right] \tag{2.22}$$

where:

$$A = -2\log\left(\frac{\varepsilon}{3.7 * D_h} + \frac{12}{Re}\right) \tag{2.23a}$$

$$B = -2\log\left(\frac{\varepsilon}{3.7 * D_h} + \frac{2.51A}{Re}\right) \tag{2.23b}$$

$$C = -2\log\left(\frac{\varepsilon}{3.7 * D_h} + \frac{2.51B}{Re}\right) \tag{2.23c}$$

with Reynolds number defined as:

$$Re = \frac{\rho U D_h}{\mu} = \frac{\rho Q D_h}{A\mu} \tag{2.24}$$

Despite its simplicity, this approximation shows a very good accuracy, as its average percent absolute deviation from Colebrook's equation is equal to 0.0002%, and its max percent absolute deviation is equal to 0.0023% [24]. Once the Darcy friction factor has been calculated, the K factor has been derived from it, as defined by:

$$K_f = f\frac{L}{D_h} \tag{2.25}$$

The head losses for all the data points of each measurement have then been calculated according to:

$$H_{loss} = K_f \frac{\left(\frac{Q}{A}\right)^2}{2g} \tag{2.26}$$

The resultant head losses curves in function of flow rate are shown below.

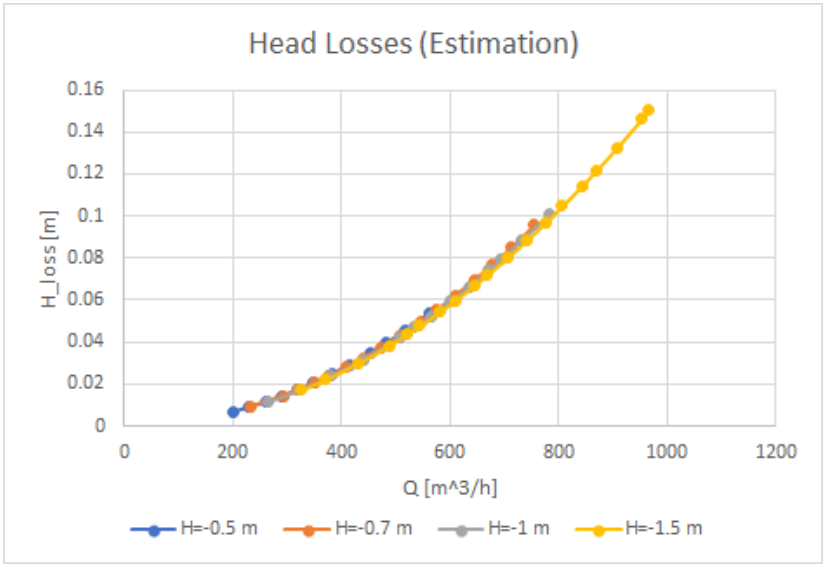

Figure 2.12: Estimated head losses with respect to flow rate

In conclusion, the characteristics curve for manometric head and torque recorded during Nijhuis' experiments are shown in the pictures below, for different shaft speeds and for an impeller diameter of 8 meters.

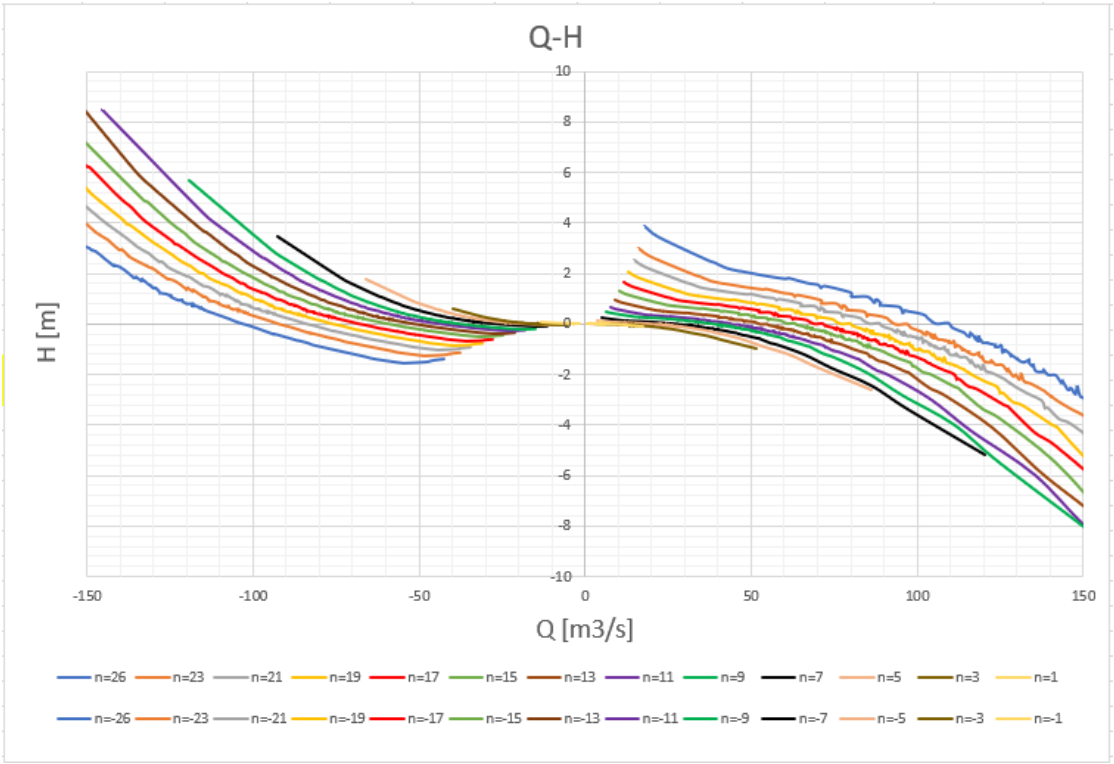

Figure 2.13: Manometric head as a function of flow rate, for different shaft speeds

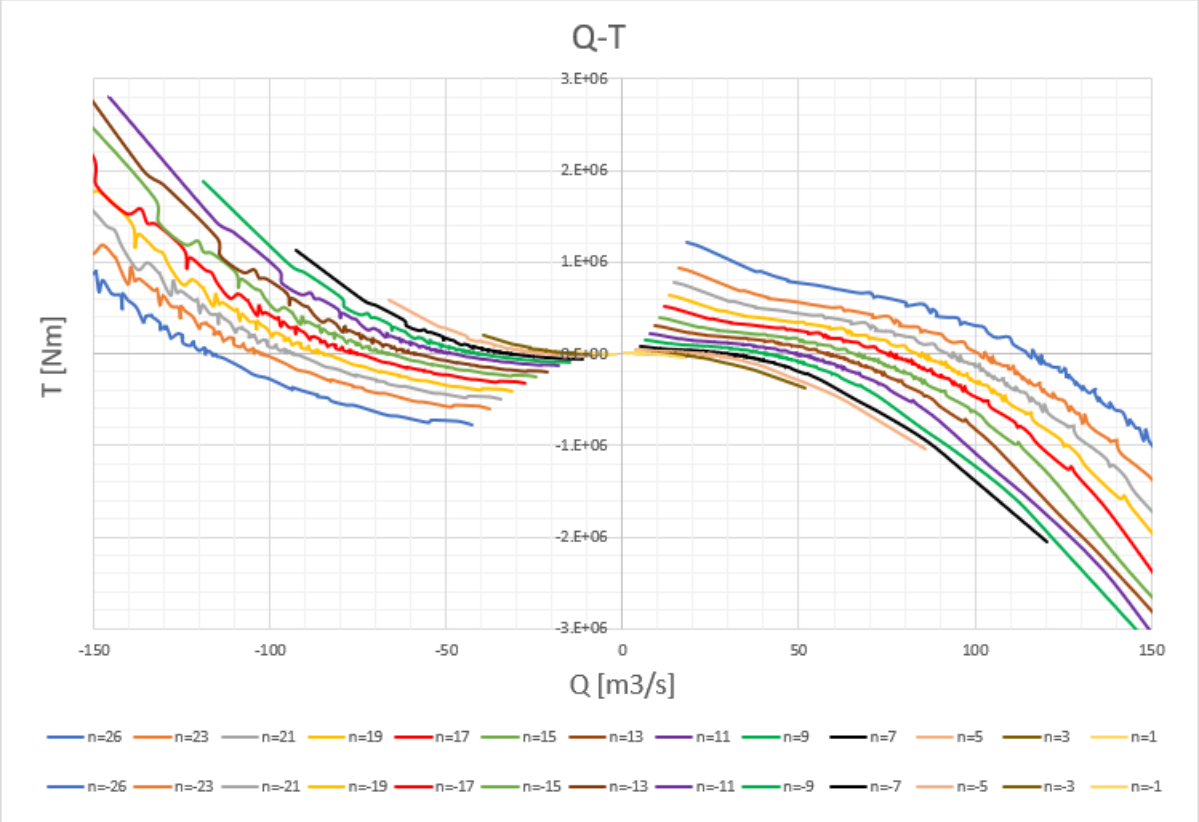

Figure 2.14: Torque as a function of flow rate, for different shaft speeds

3 Modelling of the System

A numerical analysis of the operation of the full-scale pump-turbine system at the Brouwersdam is performed. The model solves a system of four explicit, first-order, coupled ODEs that describe the dynamics of the complete system, including the effects of fluid friction in the conduit, the hydraulic performance of the pump-turbine, and the inertia of the liquid and rotor system. Subsequently, in section 4, numerical model will be verified with a simplified test case for which an analytical solution exists, and validated by experiments on a model-scale pump-turbine test setup at HZ University of Applied Sciences.

3.1 Governing Equations

The system to be represented is composed of five elements:

- the two water columns on both the North Sea side and basin side with their respective heads H_{s1} and H_{s2}
- the conduit of constant cross-sectional area A and length L
- the pump-turbine
- the electric machine

A set of four 0-D, time-dependent, explicit, first-order ODEs has been used to describe the system. To model the water flow in the conduit, the conservation law of momentum in its integral form can be applied to the system [22], considering water as a rigid material column, to exclude any compressibility effect. The starting equation is shown below:

$$\rho AL\frac{du}{dt} = \rho gA(H_{s1} - H_{s2}) + \rho gA \cdot \Delta H_p - \frac{u^2}{2g}\rho gA(K_c + K_i + K_o) \tag{3.1}$$

where:

- $\rho AL\frac{du}{dt}$ is the sum of the forces applied to the water in the system
- $\rho gA(H_{s1} - H_{s2})$ is the force generated by the static head difference between the two water columns
- $\rho gA \cdot \Delta H_p$ is the force applied by the impeller
- $-\frac{u^2}{2g}\rho gA(K_s + K_i + K_o)$ is the force generated by friction in the system
- K_f, K_i, K_o are called K values, and represent the percentage of kinetic energy lost in the conduit because of friction, at the inlet and at the outlet. Moreover, $K_c = f \cdot \frac{L}{D}$ where f is the Darcy friction factor.

There was no need to take into account the variation of dynamic head between inlet and outlet, since they have equal cross-sectional area, therefore the flow speed at those sections is the same. Rewriting the equation in terms of flow rate $Q = u \cdot A$ and solving for $\frac{dQ}{dt}$ we find:

$$\frac{dQ}{dt} = \frac{gA}{L}(H_{s1} - H_{s2}) + \frac{gA}{L} \cdot \Delta H_p - \frac{\left(f \cdot \frac{L}{D} + K_i + K_o\right)}{2AL} Q^2 \tag{3.2}$$

This is a non-linear equation, where the non-linearity is introduced by the losses term and by the pump head, which is a non-linear function of shaft speed ω and flow rate Q. This equation describes the variation of flow rate caused by the difference in water head, by the pressure jump generated by the pump-turbine, and by the pressure losses in the conduit. This equation is part of a system of four first-order ODEs represented in a Matlab-Simulink simulative environment to investigate the behavior of the system in the starting transitory. Equation (3.2) is coupled with the two equations representing the change in static head levels in the two bodies of water. The changes in static head are described by:

$$\frac{dH_{s1}}{dt} = \frac{Q}{A_{s1}} \tag{3.3a}$$

$$\frac{dH_{s2}}{dt} = \frac{Q}{A_{s2}} \tag{3.3b}$$

where A_{s1} and A_{s2} are the surface areas of the two bodies of water. The fourth equation of the system, which describes the drivetrain dynamics, is:

$$T_h + T_m - T_f = \left(I_m + I_p + I_w\right) * \frac{d\omega}{dt} \tag{3.4}$$

where:

- T_h is the hydraulic torque applied on the impeller by the fluid. Its value is negative for pump operation and positive for turbine operation. This term, which is a function of Q, ω, D, is obtained from the scaling of the Nijhuis experiments of section 2.7.
- T_m is the torque applied on the shaft by the electric machine. It is positive when the machine works as a motor, negative when it works as a generator.
- T_f is the friction torque on the bearings.
- I_m is the moment of inertia of the electric machine.
- I_p is the moment of inertia of the pump-turbine.
- I_w is the added moment of inertia of water entrained between the impeller blades.
- ω is the angular velocity of the machine/shaft/impeller system.

In conclusion, the model is composed by four differential equations: (3.2), (3.3a), (3.3b) and (3.4). This system of ODEs is solved for the four unknown variables $Q, H_{s1}, H_{s2}, \omega$. This kind of model can be compared to an RLC circuit, where the static head difference between the two water columns is the analogous of a voltage difference between two capacitor's plates. In the model representing the Brouwersdam system, two very large bodies of water are modelled, and the water level of both sides is basically unaffected by the volume of water flowing between them during the starting procedure. This would mimic the case of a circuit with a capacitor of infinite capacity. In the experimental setup used for the verification of the model, described in section 4.2.1, obviously the flow rate affects the water level in the two tanks. Moreover, the resistance in the pipe could be modelled as an electric resistor, while the impeller represents an inductor: the presence of the impeller prevents the water flow to rapidly change its flow rate (which is represented by the current in the electrical analogy) but given enough time a constant flow will pass through it.

In order to evaluate the last term of equation (3.2), corresponding to the variation of flow rate caused by head losses, the three K factors have to be estimated. As already mentioned, these are pressure losses expressed as fractions of kinetic energy of the flow. They are the friction losses $K_f = f\frac{L}{D}$, the inlet losses K_i, and the outlet losses K_o. The Darcy friction factor for K_f is estimated with the same method used before to estimate losses in the experimental data (Serghide's solution). The Reynolds number is calculated by the simulative model at each timestep depending on the last calculated flow rate value. The K factors for the inlet and outlet can be estimated using tabled values of minor losses in pipe fittings. About the inlet loss factor, depending on the shape on the duct inlet, its value may vary a lot. For a sharp-edged inlet like the one designed for the Brouwersdam project and also the one of the experimental setup, $K_i = 0.5$ is suggested. Regarding K_o, by definition, in an outlet the whole amount of kinetic energy of the fluid exits the system, so $K_i = 1$ [26].

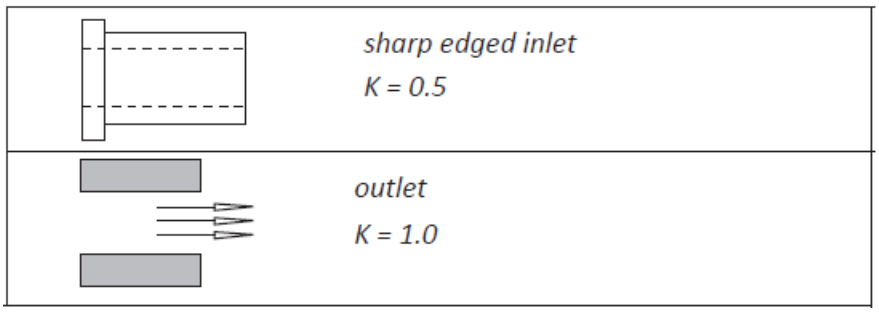

Figure 3.1: K values for inlet and outlet [26]

Regarding the efficiency of the system, the following efficiencies are defined:

- Hydro-mechanical efficiency, η_{mec}
- Electrical machine efficiency, η_{el}

Depending on the operation mode of the pump-turbine, the hydro-mechanical efficiency has two different definitions. In pump mode and pump-assisted drainage, it is defined as the hydraulic power expressed by the pump over the mechanical power acting on the shaft:

$$\eta_{mec,pump} = \frac{Q * H_p * \rho * g}{P_{sh}} \tag{3.5a}$$

In reverse turbine mode, it is defined as the mechanical power over the turbine hydraulic power. Therefore:

$$\eta_{mec,turb} = \frac{P_{sh}}{Q * H_p * \rho * g} \tag{3.5b}$$

The hydro-mechanical efficiency is calculated by the model at every timestep. The efficiency of the motor-generator is also defined in two different ways, according to the operating mode. In pump mode and pump-assisted drainage, it is the defined as the mechanical shaft power divided by the power fed to the electrical machine. In reverse turbine mode, it is the ratio between the electrical power generated over the mechanical power of the shaft.

$$\eta_{el,pump} = \frac{P_{sh}}{P_{el}} \tag{3.6a}$$

$$\eta_{el,turb} = \frac{P_{el}}{P_{sh}} \tag{3.6b}$$

Being all technical details about the machine missing at this stage of the Brouwersdam project, the motor/generator efficiency has been assumed. Usually, induction machines with higher rated power are more efficient than low power ones. This is due to the fact that in smaller machines the core length and diameter are smaller. In order to maintain a high magnetomotive force, generated by the current density, the number of windings has to be high. This increases the resistance in the windings, therefore affecting the efficiency of small electrical machines. The European Union is responsible for setting standards for the efficiency range of electrical machines. As shown in figure 3.2, the range of efficiency for high power machines (hundreds of kW) is in the order of 95% . Thus, this value has been assumed for the machine efficiency.

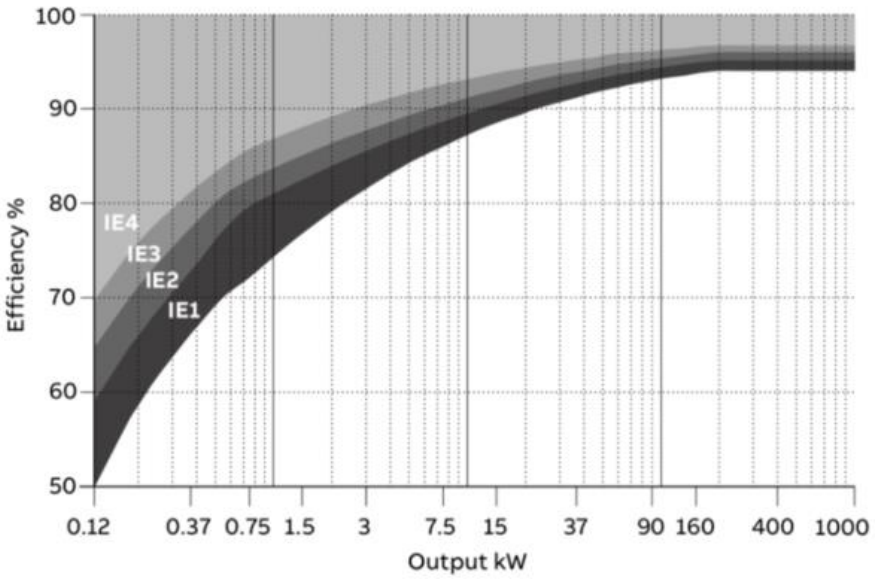

Rated output power P_N [kW]	Number of poles			
	2	4	6	8
11	89,4	89,8	88,7	86,9
15	90,3	90,6	89,7	88,0
18,5	90,9	91,2	90,4	88,6
22	91,3	91,6	90,9	89,1
30	92,0	92,3	91,7	89,8
37	92,5	92,7	92,2	90,3
45	92,9	93,1	92,7	90,7
55	93,2	93,5	93,1	91,0
75	93,8	94,0	93,7	91,6
90	94,1	94,2	94,0	91,9
110	94,3	94,5	94,3	92,3
132	94,6	94,7	94,6	92,6
160	94,8	94,9	94,8	93,0
200 up to 1 000	95,0	95,1	95,0	93,5

Figure 3.2: Efficiency standards for electrical machines [33]

The model also tracks the net energy balance of a single impeller/machine system during the first 30 seconds of operation, in order to better understand what the initial energy expense of the system is. In conclusion, in table 3.1 the geometrical and physical parameters of the model are summarized.

Table 3.1: Model geometrical and physical details

Model geometrical and physical details	
North Sea surface area	∞ km^2
Lake Grevelingen surface area	110 km^2
Conduit length	98 m
Conduit geometry	Square
Conduit cross sectional area	64 m^2, constant
Conduit material and surface roughness	Concrete, $\varepsilon = 3{,}048 * 10^{-3}$ m
Pump-turbine diameter	8 m
Pump-turbine moment of inertia	250000 $kg * m^2$
Added mass moment of inertia	33456 $kg * m^2$
Motor/generator moment of inertia	110000 $kg * m^2$

3.2 Hydraulic Torque and Inertia

3.2.1 Quasi-steady Hydraulic Torque

Assuming that system conditions change slowly, the hydraulic torque value for a certain shaft speed and flow rate can be obtained by the characteristic curves, which are drawn in steady-state conditions. This means that the variations in the system are to be considered quasi-steady. The evaluation of this assumption can be inspected studying the Strouhal number.

3.2.2 Unsteady Behaviour

It could be questioned if the results of the simulations, that are based on experimental data collected in steady-state conditions, could be suitable with the conditions of the real-case scenario. This can be investigated with the use of the Strouhal number. The Strouhal number is a dimensionless number that represents the ratio of inertial forces due to the local acceleration of the flow to the inertial forces due to the convective acceleration. As such, it is a measure of the rate of change of the flow rate relative to the convection of momentum within the pump:

$$St = \frac{du/dt}{u/\mathrm{T}} = \frac{du/dt}{u^2/\mathrm{S}} = \frac{\frac{1}{A}\frac{dQ}{dt}}{\frac{Q^2}{A^2 S}} \tag{3.7}$$

where:

- du/dt is the temporal acceleration of the flow at the pump-turbine section during the experiment.
- u is the axial flow velocity
- T is the residence time of the fluid in the pump
- S is the axial length of the pump
- A is the cross-sectional area

For Strouhal numbers higher than 0.1, the unsteady effects have a relevant influence on the flow, and the conditions have to be considered unsteady. Instead, for values lower than 0.1, the flow can be evaluated as quasi-steady [1]. In this case, the results of the validation experiments can be considered comparable to the model results.

3.3 Added Mass Moment of Inertia

The added mass moment of inertia represents the moment of inertia of the fluid entrained between the impeller blades, which obviously has a relevant effect on the dynamics of the system. This physical quantity is usually estimated experimentally inducing a known vibrational excitation on the shaft and the components connected to it, and then measuring the torque in response to it. The experimental setup available by HZ University was not equipped to perform this kind of experiments, so a model for the estimation of the added mass moment of inertia has been found in the literature. In particular, a model developed by the company HydroComp for marine propellers has been used. This model aimed to perfect previous models of added mass and added momentum estimations, mainly the one developed by Burrill and Robson in 1962 [30]. In fact, when reviewing the estimation formulas by Burrill, the authors found that they did not fit the experimental data really well, and some improvement could be made. The proposed new formula for added moment of inertia is [31]:

$$I_w = C_{IE} * \rho * D^5 \tag{3.8}$$

where:

$$C_{IE} = C_1 * EAR * \frac{P}{D} - C_2 \tag{3.9}$$

In addition:

- C_1 and C_2 are experimentally derived coefficients, which depend on the number of blades (Z).

- EAR is the expanded area ratio.
- $\frac{P}{D}$ is the pitch/diameter ratio.

The EAR is derived from the develop area ratio (DAR), which is the total area of the blades if they could be unattached from the hub and brought to zero pitch, divided by the whole area of the propeller disc. Moreover, the EAR is defined as the area obtained by flexibly distributing the DAR on a flat surface such that all sections would be parallel, divided by the propeller disc area. In other words, the EAR converts the propeller from its helix to a flat plane [32]. This is typically close in value to the DAR.

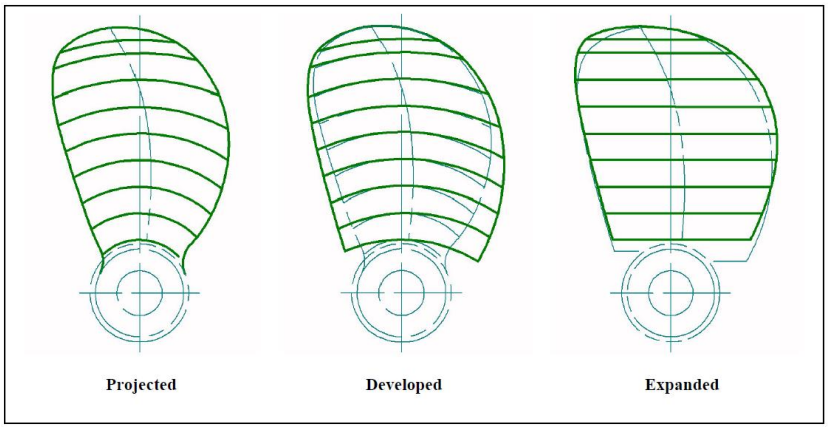

Figure 3.3: Graphical representation of PAR, DAR, EAR [32]

To calculate the EAR, the following conversion formula has been used [32]:

$$EAR = 0.34 * DAR * (2.75 + \frac{DAR}{Z}) \tag{3.10}$$

3.4 Electromagnetic Torque

Regarding the electromagnetic torque, at this moment there is no clear indication about the electrical machine that is expected to be used in the Brouwersdam project. Therefore, a number of assumptions have been made to model the electromechanical torque. In the model, an asynchronous machine has been represented. In figure 3.4 the typical torque curve for an asynchronous motor is shown (black curve), with respect to shaft speed. The y-axis represents the ratio of torque and rated torque. The region beyond the 100% of synchronous speed is the generator region, which mirrors exactly the motor region of the curve with respect to both axes.

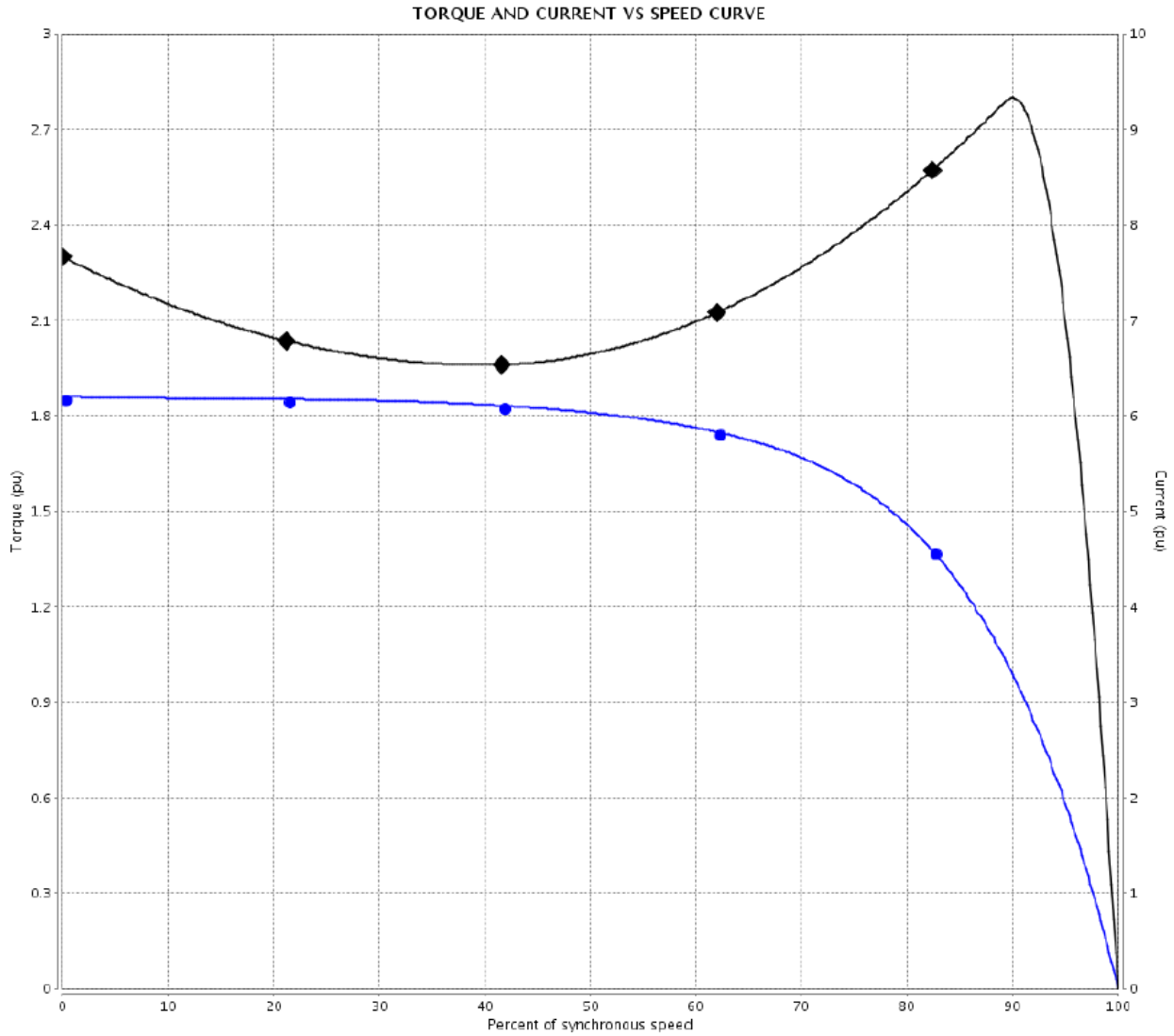

Figure 3.4: Typical torque (black) and current (blue) curves at varying shaft speed for an asynchronous motor

The torque curve of the electrical machine used in the model is different depending on the starting procedure. The results of three starting procedures will be analyzed in this thesis, in section 5:

- No kickstart
- Kickstart with constant synchronous speed
- Kickstart with varying synchronous speed

With no kickstart, the electric machine is used just as a generator, meaning that no mechanical torque is provided to the drivetrain by the motor at start-up, and the only torque accelerating the system is the hydraulic torque as a result of the free flow from high to low water level. Once the system surpasses the synchronous speed, the machine starts generating power.

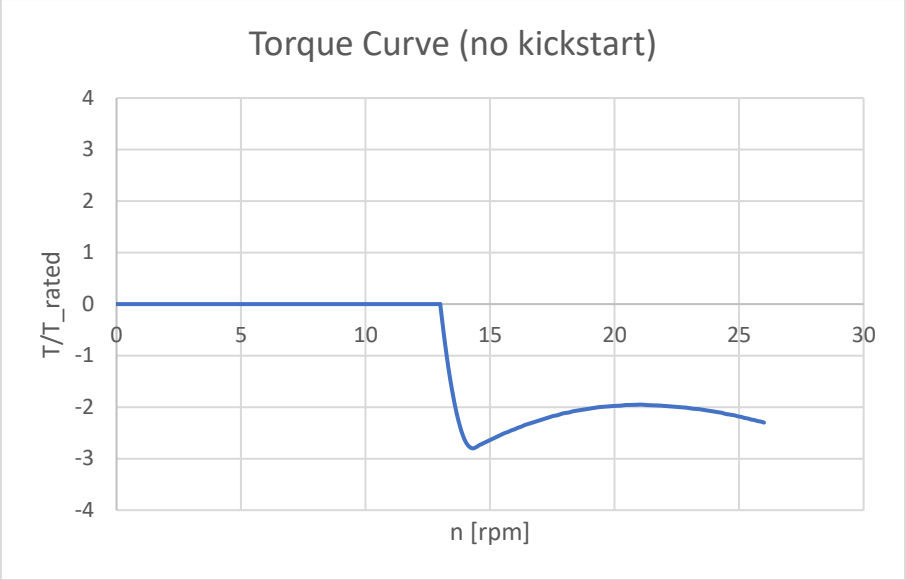

Figure 3.5: Torque curve for start-up procedure with no kickstart

In the kickstart procedure at constant synchronous frequency shown in figure 3.6, after the opening of the gate-valves, the motor supplies an electromechanical torque in order to speed up the drivetrain faster, and accelerate the flow in less time compared to the procedure with no kickstart. When the shaft speed becomes higher than the synchronous speed, the electric machine starts working as a generator. The issue with this strategy is that the system accelerates slowly when approaching synchronous speed, since the motor torque in this region is small. The equilibrium points of motor and generator operation lie in the central decreasing part of the curve, at shaft speed lower and higher than the synchronous speed respectively.

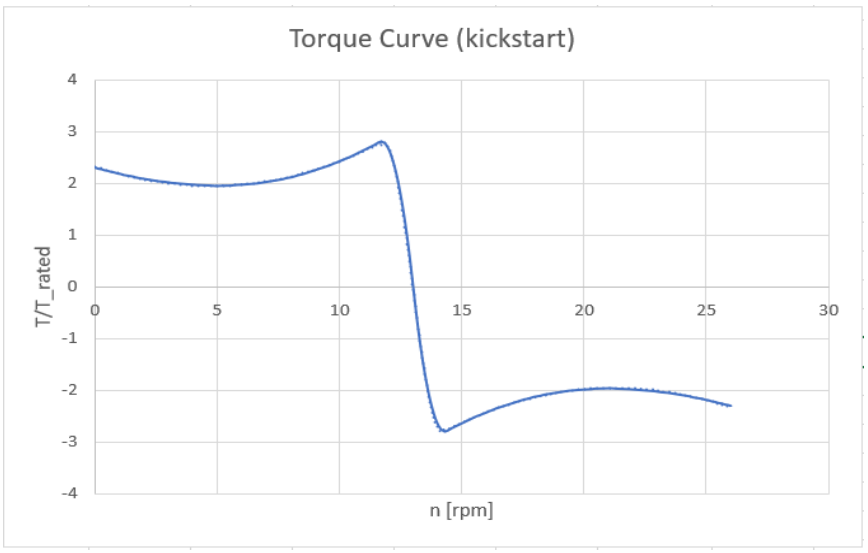

Figure 3.6: Torque curve of the machine in kickstart procedure

It is also possible to design a start-up procedure with varying frequency, using a frequency controller. The increase of the frequency of the current fed to the motor causes the torque curve to shift to the right, but it also causes a decrease of the torque magnitude. This is caused by the fact that the air-gap flux is

proportional to the ratio of the stator voltage to stator frequency. Hence, since the developed torque is dependent on the square of the air-gap flux, the torque-frequency relation in case of a constant stator voltage is stated by [27]:

$$T \propto \phi^2 = \left(\frac{V_s}{f_s}\right)^2 \tag{3.11}$$

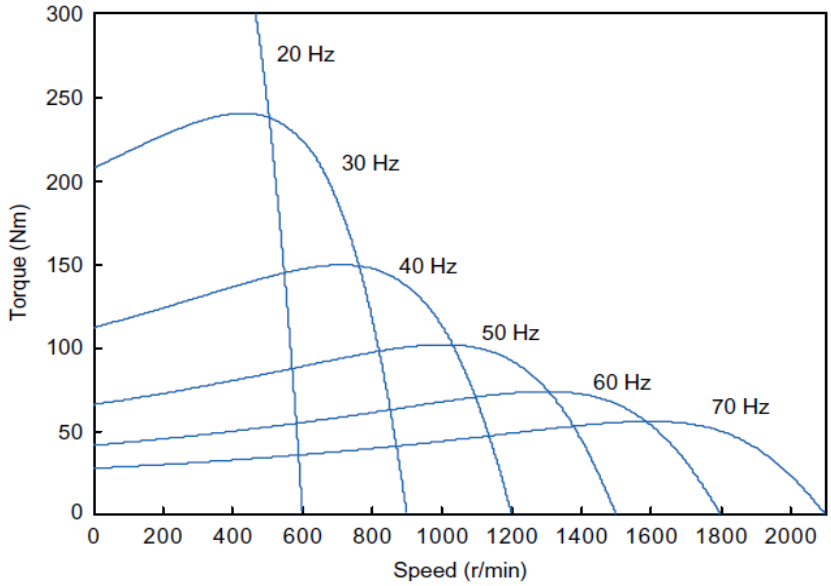

Figure 3.7: Effect of frequency variation on the torque curve [27]

To avoid this behavior and maintain a constant level of the torque for different frequencies, it is necessary to increase the voltage applied to the stator of the machine in such a way that:

$$\frac{V_s}{f_s} = const \tag{3.12}$$

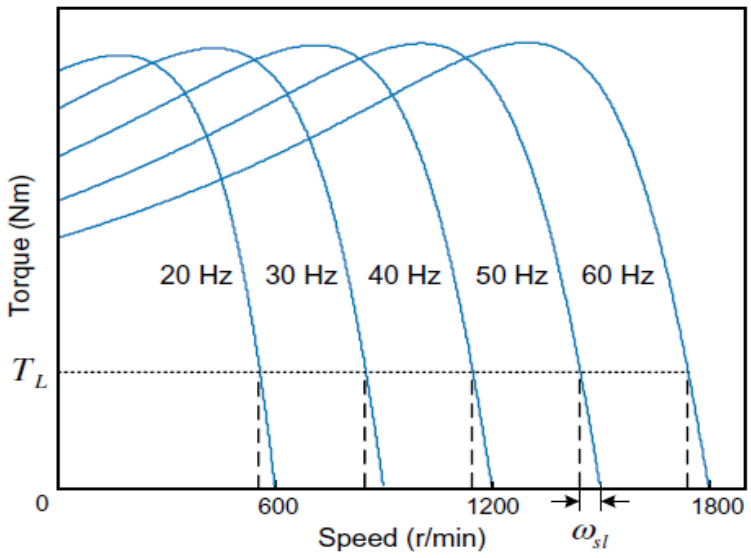

Figure 3.8: Torque curves with constant ratio of stator voltage and frequency [27]

This working region is called “constant torque region” as the constant ratio maintains a constant torque level. This linear increase of the voltage/frequency ratio is a viable strategy until the point where the voltage reaches the maximum value bearable by the stator. Surpassing this rated voltage value would compromise the integrity of the machine. Therefore, after this point an increase in frequency cannot be compensated by an increase in stator voltage, and the torque magnitude starts to decrease. This operating region is called “constant power region” as the torque and shaft speed variation are such that the power is maintained constant.

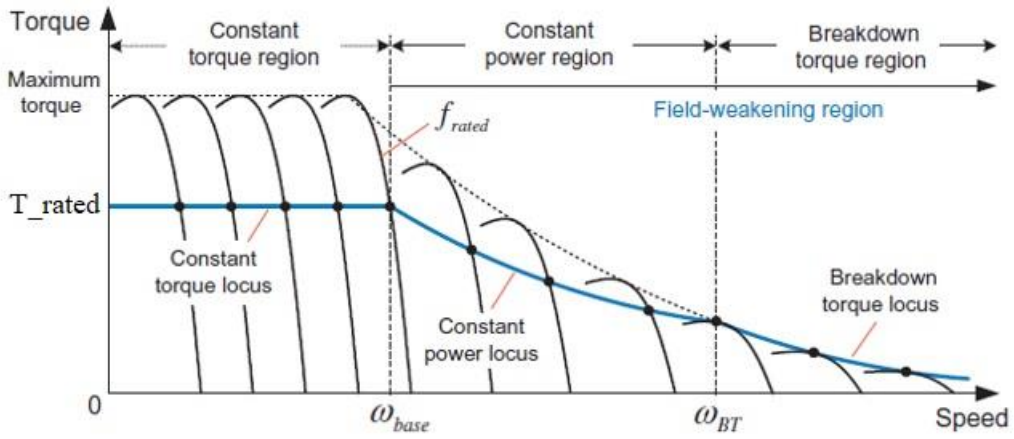

Figure 3.9: Torque dependency on frequency [27]

If the frequency is increased even more, the system reaches the “breakdown torque region”, where the rotor current decreases with $\frac{1}{f_s^2}$ and therefore the power starts decreasing. However, this region will not be investigated further as it is assumed that the system will work in constant torque and constant power regions only. In the constant torque region motors are usually working at torque values equal to the rated torque, as continuous operation at higher values could give overheating problems, compromising the integrity of the machine [28].

3.5 Frictional Torque

In equation (3.4), T_f represents the frictional torque exerted on the shaft rolling bearings and seals, which always opposes the angular velocity of the system. There are two kind of bearings frictional torque:

- Starting torque: it is defined as the frictional moment that the bearing must overcome to start rotating. It is composed of two terms, namely the sliding frictional moment and the frictional moment of seals, if present.
- Total frictional torque: it is defined as the frictional moment that opposes the bearing’s rotational while it is already rotating. It is composed of four terms, namely the rolling frictional

moment, the sliding frictional moment, the frictional moment of seals and the frictional moment due to drag losses in the oil bath of the bearing.

These two frictional torques are dependent on many variables, such as load, bearing radius, friction coefficient of the material, temperature, type of lubricant, and many others. None of these technical details are yet known, or even preliminarily investigated. For this reason, a generical evaluation of the order of magnitude of the frictional torque of the bearings through literature research has been performed. A research by Joshi et al. [29] aimed to introduce a new model that simplified previous ones for low speed applications, validating it experimentally. More precisely, it focuses on high load and low speed applications, which is the application field of the project at hand. A four-contact points ball bearing with 10 spheres was subject to different loads ranging from 0 to $2.5 * 10^4\ N$, and results were recorded and compared to the analytical model. No substantial effect of speed on the bearing torque was observed. Results for the mentioned ball bearing with cage are shown in figure 3.10.

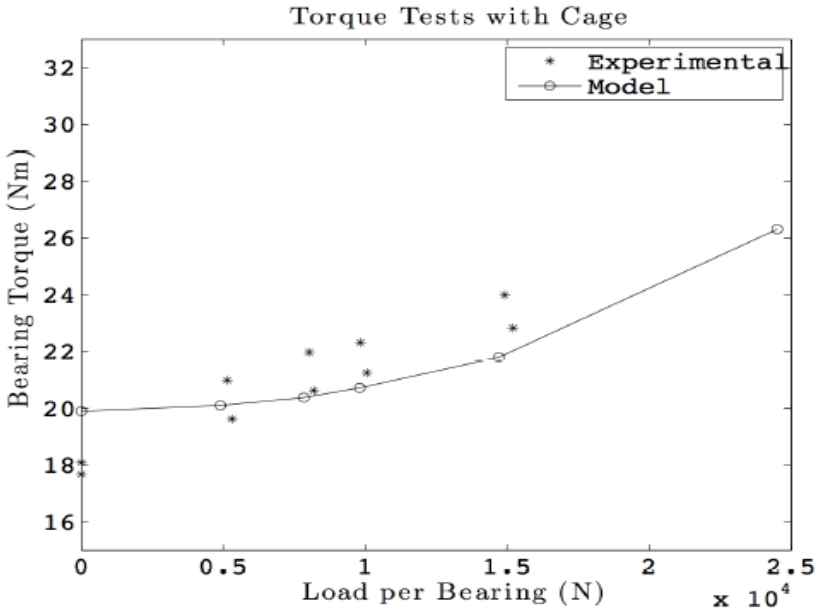

Figure 3.10: Bearing frictional torque at varying load [29]

Being the observed bearing torque in the order of tens of Nm, and being this value far smaller than those of the hydraulic and electromechanical torque (in the order of $10^5\ Nm$), the frictional torque on the drivetrain has been considered negligible in the model.

3.6 Pump-turbine and Electric Machine Inertia

As mentioned previously, as of today, there are no technical details about the motor-generator that would be used in the power plant. Because of this, a reasonable value for its moment of inertia had to be researched in the market. The machine's expected rotational speed of 13 rpm is compatible to that of large wind turbines' generators, so particular attention has been posed in this market sector.

3.7 Numerical Solver

The chosen simulation environment for the project at hand is Matlab-Simulink. Simulink is a graphical programming software, with a structure based on signals, representing variables and parameters, and blocks applying operations on said signals. Simulink is also able to integrate Matlab-based scripts and functions, introduced by specific Simulink blocks. The combination of Matlab's versatility and the accessibility of the graphical structure of Simulink makes them powerful and intuitive tools to simulate and analyze different multidomain dynamical systems. Simulink has also embedded a wide variety of numerical solvers, both continuous and discrete, with fixed-step and variable-step, to make the user able to choose the best suited method for the analysis of the system. In order to solve a differential equation on Simulink, its integral form has to be built in the simulation environment. For this project, the structure of the Matlab-Simulink environment is composed by three subsystems. Each of these subsystems evaluates one of the terms on the right-hand side of equation (3.2). The three outputs are then added/subtracted in accordance to their respective signs in equation (3.2), and the result $\frac{dQ}{dt}$ is then integrated in order to calculate the value of the flow rate, at each time-step. The numerical solvers provided by Simulink are differentiated based on two different aspects: step-size and model state.

- Fixed step/variable step solvers: fixed step methods solve the model using the same step size from the beginning to the end of the simulation. Generally, decreasing the step-size increases the accuracy of the simulation. Variable step methods solve the model varying the step-size during the simulation. The software automatically evaluates the adequate step size, reducing it during certain events like rapid changes in the system or zero-crossings, and increasing it when the state of a system changes slowly. While computing the optimal step-size increases the computational load, this can reduce the number of steps in the simulation, reducing the overall computational time.
- Continuous/discrete solvers: continuous solvers use numerical integration to compute continuous state of a model at the current time-step based on the states at previous time-steps and the state derivatives. They rely on blocks to compute the values of discrete states of the model. Discrete solvers are used to solve purely discrete models, and are not able to compute continuous models.

The choice of a continuous solver is mandatory, given the continuous nature of the problem. A variable step solver has also been considered not necessary, given that from preliminary simulations the computational time has been found very short, in the order of a few seconds. Moreover, the system state has been observed changing slowly, and results in section 4.1 show a very good accuracy when compared to the analytical solution, suggesting that the improved accuracy provided by variable-step solvers in fast changing systems is not necessary.

In the end, the fourth order Runge-Kutta method has been chosen. The Runge-Kutta methods are a family of numerical methods used to solve ordinary differential equations, developed by German mathematicians Carl Runge and Wilhelm Kutta. Of all these methods, the fourth order one is the most widely used. In our case, the problem to solve is an initial value problem. A generic initial value problem is in the form of:

$$y' = f(t, y), \quad y(t_0) = y_0 \tag{3.13}$$

where y(t) is the unknown function we want to approximate, and the function f and the initial conditions y_0, t_0 are known. For a given timestep dt, the method calculates the function y at the next timestep as:

$$y_{n+1} = y_n + \frac{1}{6} dt * (k_1 + 2k_2 + 2k_3 + k_4) \tag{3.14}$$

where:

$$k_1 = f(t_n, y_n) \tag{3.15a}$$

$$k_2 = f\left(t_n + \frac{dt}{2}, y_n + dt * \frac{k_1}{2}\right) \tag{3.15b}$$

$$k_3 = f\left(t_n + \frac{dt}{2}, y_n + dt * \frac{k_2}{2}\right) \tag{3.15c}$$

$$k_4 = f(t_n + dt, y_n + dt * k_3) \tag{3.15d}$$

Equation (3.14) is the fourth order approximation of $y(t_{n+1})$, where the next value y_{n+1} is equal to the present one y_n plus the weighted average of four increments k. These increments are the product of the size of the interval dt and an estimated slope defined by function f:

- k_1 is the slope at the beginning of the interval
- k_2 is the slope at the midpoint of the interval using y and k_1
- k_3 is the slope at the midpoint of the interval, but using y and k_2
- k_4 is the slope at the end of the interval

When doing the average of the slopes, those at the midpoint are given a weight double than the one at the beginning and end of the interval. Being a fourth-order method, the local truncation error (the error caused by one iteration) is in the order of $O(dt^5)$, and the total truncation error (the accumulated error of all iterations) is in the order of $O(dt^4)$. The solver uses the flow rate calculation at the previous timestep to calculate the new static head values of the two bodies of water, according to:

$$H_{s1,t+1} = H_{s1,t} + dH_{s1} \tag{3.16a}$$

$$H_{s2,t+1} = H_{s2,t} + dH_{s2} \quad (3.16b)$$

4 Verification and Validation

4.1 Numerical Verification

The goal of the numerical verification is to test the reliability of the numerical solver that will be used in the simulations. The results of a simplified version of the model, consisting in only the conduit and the two water columns, will be compared to the analytical solution of the differential equations representing the change in flow rate. Given the absence of the pump-turbine, the equation to be solved is equation (3.2) without the pump-turbine head term, and with a constant Darcy friction factor, derived from the equilibrium value:

$$\frac{dQ}{dt} = \frac{gA}{L}(H_{s1} - H_{s2}) - \frac{\left(f \cdot \frac{L}{D} + K_i + K_o\right)}{2AL} Q^2 = b - aQ^2, \qquad Q(0) = 0 \tag{4.1}$$

It is possible to derive the analytical solution of this non-linear differential equation (derivation fully described in appendix C). The analytical solution is:

$$Q(t) = \sqrt{\frac{b}{a}} * \frac{e^{2\sqrt{ab}t} - 1}{e^{2\sqrt{ab}t} + 1} + Q(0) \tag{4.2}$$

The equilibrium point of the solution is found introducing the limit of $Q(t)$ for $t \to +\infty$:

$$Q_\infty = \lim_{t \to +\infty} Q(t) = \sqrt{\frac{b}{a}} = 217.88 \frac{m^3}{s} \tag{4.3}$$

This numerical solution is compared with the simulations of the model in the configuration without the pump-turbine in figure 4.1, whereas their difference in absolute value is shown in figure 4.2.

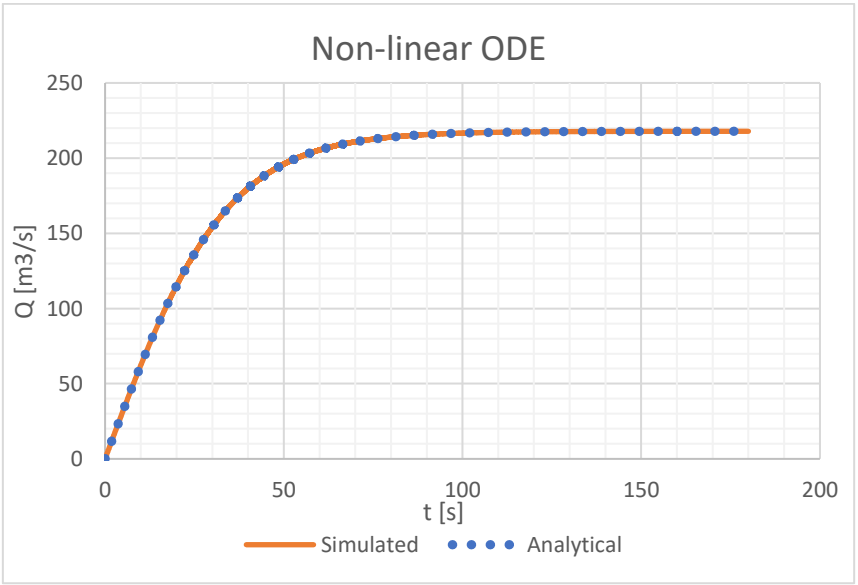

Figure 4.1: Comparison of simulation and analytical solution of the non-linear ODE

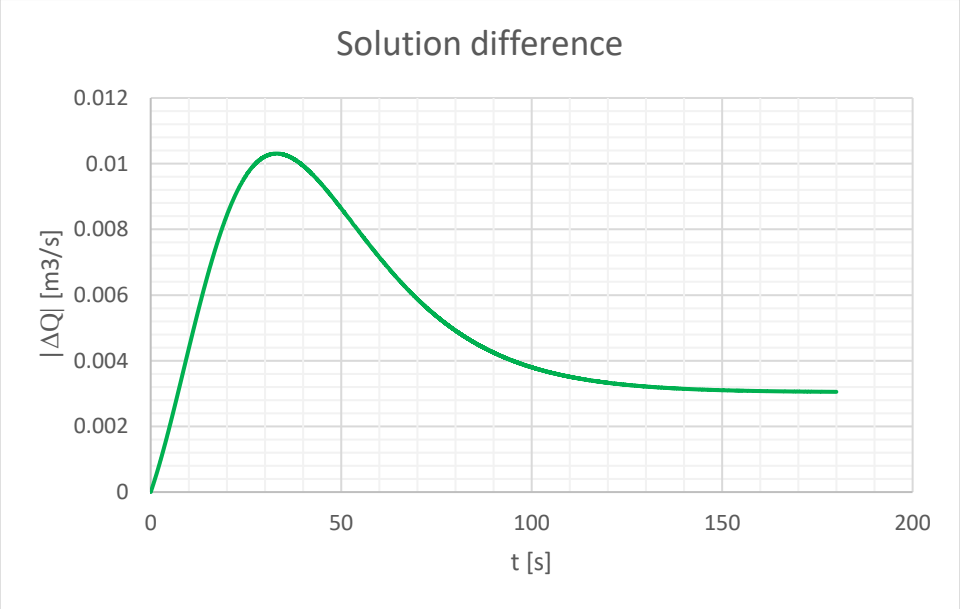

Figure 4.2: Difference between non-linear ODE analytical solution and simulation results, in absolute value

It is also possible to linearize equation (4.1) using a first order Taylor series around the equilibrium point Q_∞:

$$\frac{dQ}{dt} = f(Q_\infty) + \frac{df}{dQ}_{Q_\infty} * (Q - Q_\infty) = b - aQ_\infty^2 - 2aQ_\infty * (Q - Q_\infty)$$
$$\rightarrow Q' = b + aQ_\infty^2 - 2aQ_\infty Q, \qquad Q(0) = 0 \tag{4.4}$$

This equation can be rearranged in the form:

$$\frac{1}{2aQ_\infty} Q' + Q = \frac{b + aQ_\infty^2}{2aQ_\infty}, \qquad Q(0) = 0$$
$$\rightarrow \tau Q' + Q = F, \qquad Q(0) = 0 \tag{4.5}$$

This is a linear differential equation with a step response, where τ is called characteristic time, and represents the amount of time needed for the system to reach 63.2% of the equilibrium solution, and F is the step. Physically, this equation represents the variation of flow rate in a conduit due to a static head difference. The analytical solution of equation (4.5) is:

$$Q_{step}(t) = F * \left(1 - e^{-\frac{t}{\tau}}\right) \tag{4.6}$$

And the equilibrium value is:

$$Q_0 = \lim_{t \to +\infty} Q(t) = F \tag{4.7}$$

It is clear that the solution of equation (4.5) is different from the one of equation (4.1), them being two different kind of equations, but they share the same equilibrium value since the equation (4.5) has been linearized around the equilibrium value Q_∞. In fact, considering a static head difference of 1 meter, assuming a constant Darcy friction factor $f = 0.01575$ (which was found as the steady-state value in preliminary simulations), and utilizing the values already described for all the other parameters, we find:

- $a = 1.3496 * 10^{-4}\, m^{-3}$, $b = 6.407 \frac{\mathrm{m}^3}{\mathrm{s}^2}$
- $\tau = 17$ s, $F = 217.88 \frac{m^3}{s}$

The analytical solution of the linearized equation is compared, in figure 4.3, with the numerical results obtained applying the Runge-Kutta method, whereas their difference in absolute value is shown in figure 4.4.

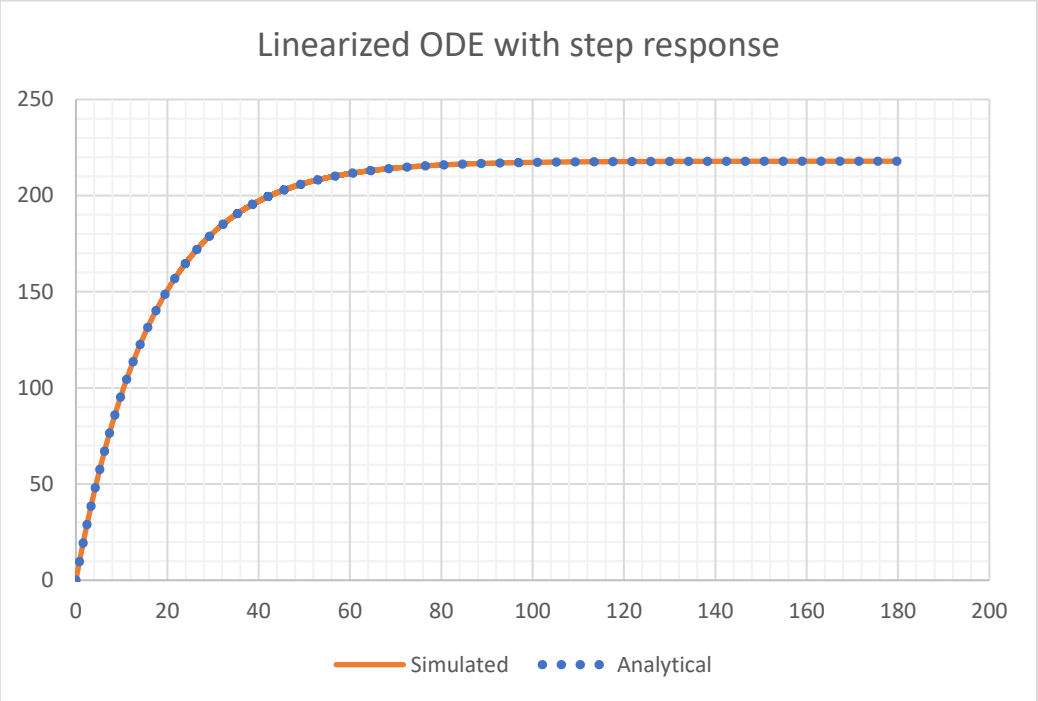

Figure 4.3: Comparison of analytical solution and simulation results of the linearized ODE with step response

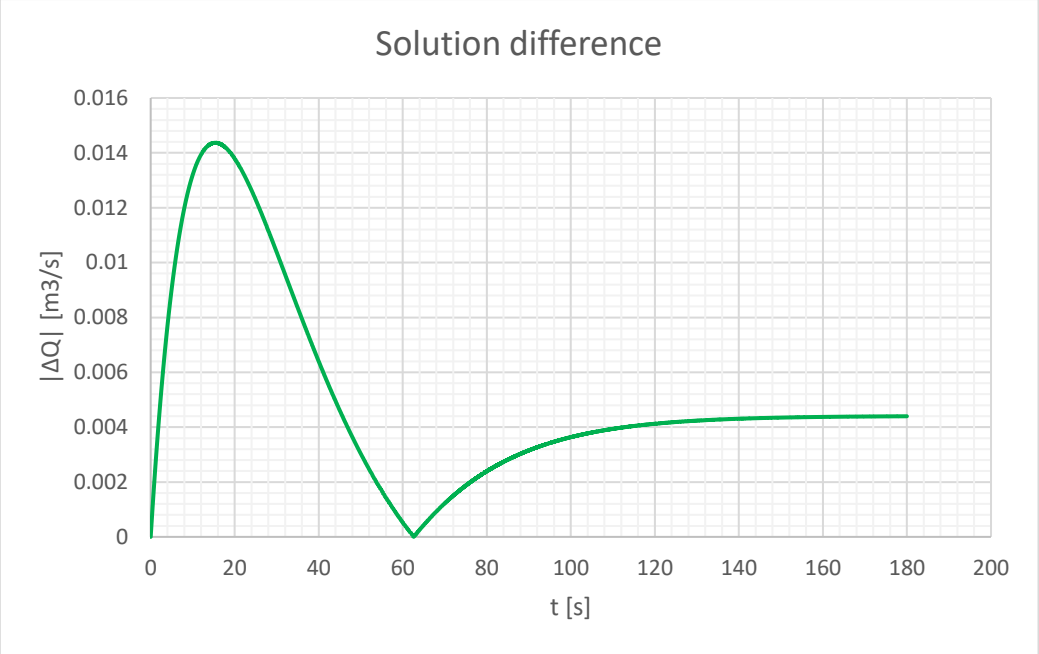

Figure 4.4: Difference between the linearized ODE analytical solution and simulation results, in absolute value

It could be interesting to see what happens introducing, in addition to a static head difference, a wavy perturbation on the side of the North Sea. This can be done adding an harmonic term to the right-hand side of equation (4.5).

$$Q' + 2aQ_0Q = (b + aQ_0^2) + Ksin(\omega t) \tag{4.8}$$

The solution to this equation is equal to the summation of the solutions of the single step response and harmonic response. Defining $\omega = 1$ and $c = 2aQ_0$, the solution is equal to:

$$Q_{harm}(t) = \frac{K(e^{-ct} + c * \sin(t) - \cos(t))}{c^2 + 1} \tag{4.9}$$

Therefore, the total solution of the linear equation with step plus harmonic response is:

$$Q_{tot}(t) = F * \left(1 - e^{-\frac{t}{\tau}}\right) + \frac{K(e^{-ct} + c * \sin(t) - \cos(t))}{c^2 + 1} \tag{4.10}$$

The analytical solution of equation (4.8) is compared, in figure 4.5, with the numerical results obtained applying the Runge-Kutta method, whereas their difference in absolute value is shown in figure 4.6.

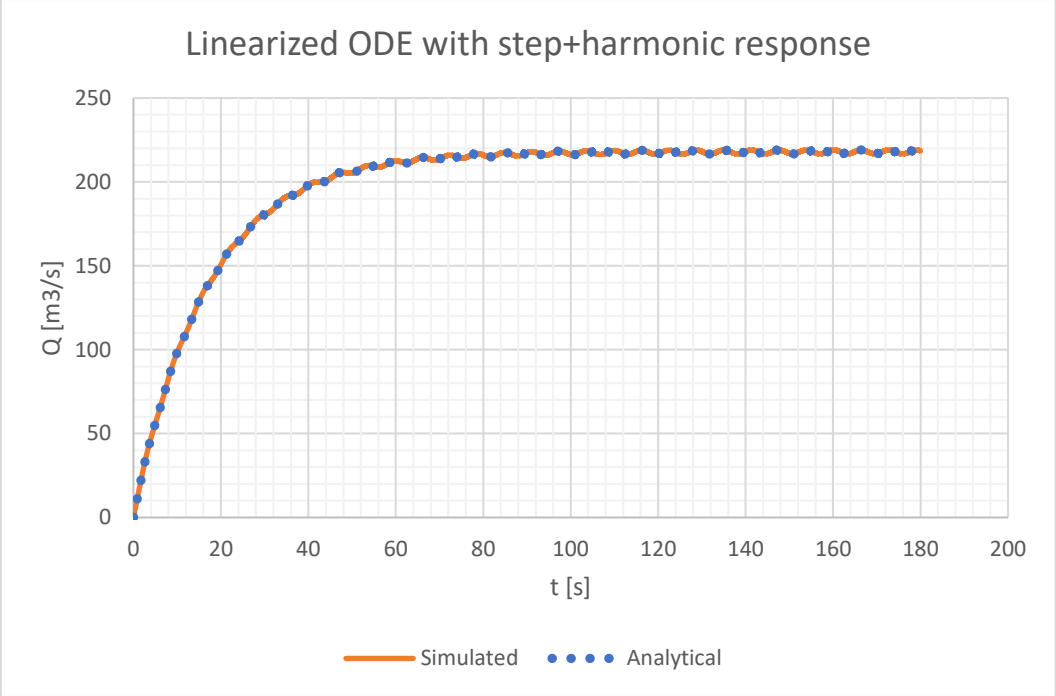

Figure 4.5: Comparison of analytical solution and simulation results of the linearized ODE with step plus harmonic response

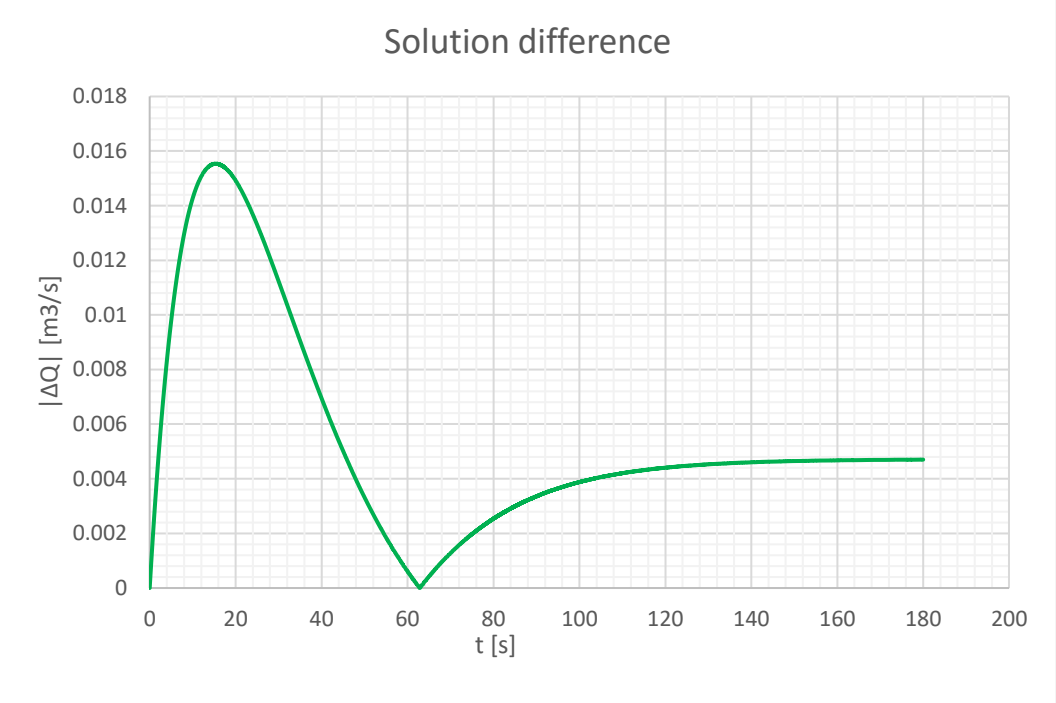

Figure 4.6: Difference between the analytical solution of linearized ODE with step plus harmonic response and simulation results, in absolute value

4.2 Validation

4.2.1 Experimental Setup

The model can also represent the experimental setup managed by HZ University, in order to compare the simulation results to the experimental result for model validation. The equations and the structure of the small-scale model are identical to the large-scale one, with differences lying in the geometry, dimensions, and in the moments of inertia. Regarding the added mass moment of inertia, the EAR for the impeller of the experimental setup (D=30 cm) has been calculated. The DAR has been calculated measuring the total blade area in the CAD files, and dividing it by the total disc area πR^2, returning a value of 0.63. The EAR calculation follows from equation (3.10), returning a value of 0.616. In addition, the pitch had also to be calculated, using measurements on the CAD file. The pitch is defined as the distance the impeller would advance in one rotation in a solid material. The blade width and the height difference between the leading and trailing edge of the blade have been measured at the section $r = 0.7 * R$. The pitch has been then calculated according to:

$$P = 0.7\pi D * \frac{Heigth}{Width} = 0.7\pi * 0.3\ m * \frac{0.045\ m}{0.12\ m} = 0.247\ m \tag{4.11}$$

The calculations for the added moment of inertia follow from equation (3.8) and (3.9):

$$C_{IE} = C_1 * EAR * \frac{P}{D} - C_2 = 0.00359 * 0.616 * \frac{0.247\ m}{0.3\ m} - 0.0008 = 1.021 * 10^{-3}$$

$$I_w = C_{IE} * \rho * D^5 = 1.021 * 10^{-3} * 1000 \frac{kg}{m^3} * (0.3\ m)^5 = 2.481 * 10^{-3} kg * m^2$$

Table 4.1 summarizes these values for the small-scale model. The main difference between the experimental setup and its modelling is the geometry of the duct. In fact, while the real duct is a converging-diverging pipe with different geometries (rectangular and circular) and varying cross-sectional area, in the 0-D model it has been only possible to assign a single type of geometry (circular) and a single value to the cross-sectional area for the entire length of the pipe.

Table 4.1: Details of the experimental setup representation in the simulation environment

Experimental setup representation	
High tank surface area	4.457 m^2
Low tank surface area	9.25 m^2
Conduit length	4.38 m
Conduit geometry	Circular
Conduit cross sectional area	0.0707 m^2, constant
Conduit material and surface roughness	Commercial steel, $\varepsilon = 4.572 * 10^{-5}$ m
Pump-turbine diameter	0.3 m
Pump-turbine moment of inertia	0.012 $kg * m^2$
Added mass moment of inertia	$2.481 * 10^{-3}$ $kg * m^2$
Motor/generator moment of inertia	0.126 $kg * m^2$

Figure 4.7: Experimental setup at HZ University

Model validation has been performed thanks to experimental data gathered at HZ University via use of the experimental setup of figure 4.7. This experimental setup presents some limitations. In fact, it is not possible to adjust the frequency with the frequency controller during an experiment, making it difficult to find a suitable strategy for validating the simulated results. The proposed solution was to perform a free-stream experiment. This consisted in opening the gate-valve in a situation where the high tank water level was sufficiently higher than the low tank one and let the water flow naturally, inducing a

rotation on the pump-turbine. The data about water levels, pump head and pump-turbine speed have been recorded with a frequency of 10 data points per second. The flow rate has been derived from the water level of the high tank as:

$$Q = \frac{dH_{s,high}}{dt} * A_{high} \tag{4.12}$$

where $H_{s,high}$ is the water level of the high tank and A_{high} is the surface area of the high tank. The equation $H_{s,high}(t)$ has been obtained via a third-order polynomial curve fitting. In order to obtain a better curve fitting, two different equations were used: one for the first 4 seconds, where the system conditions are changing rapidly, and one for the rest of the experiment, that lasted 38 seconds in total. The two equations are shown on the graph in figure 4.8. It has to be noted that due to a leakage of the valve in the experimental setup, the starting conditions of the experiment showed an initial flow rate and rotational speed of the pump-turbine different from zero. This has been taken into consideration when setting up the simulations, defining the same values as the initial conditions. Moreover, the electro-mechanical torque has been set to zero, given the fact that in the experiments the impeller was not driven by the electric machine.

This paragraph shows the results of the simulation of the small-scale model, compared with the free-stream experiments run at HZ University. Tank water levels, pump head and shaft speed have been measured, while the flow rate curves have been derived from the water level curves.

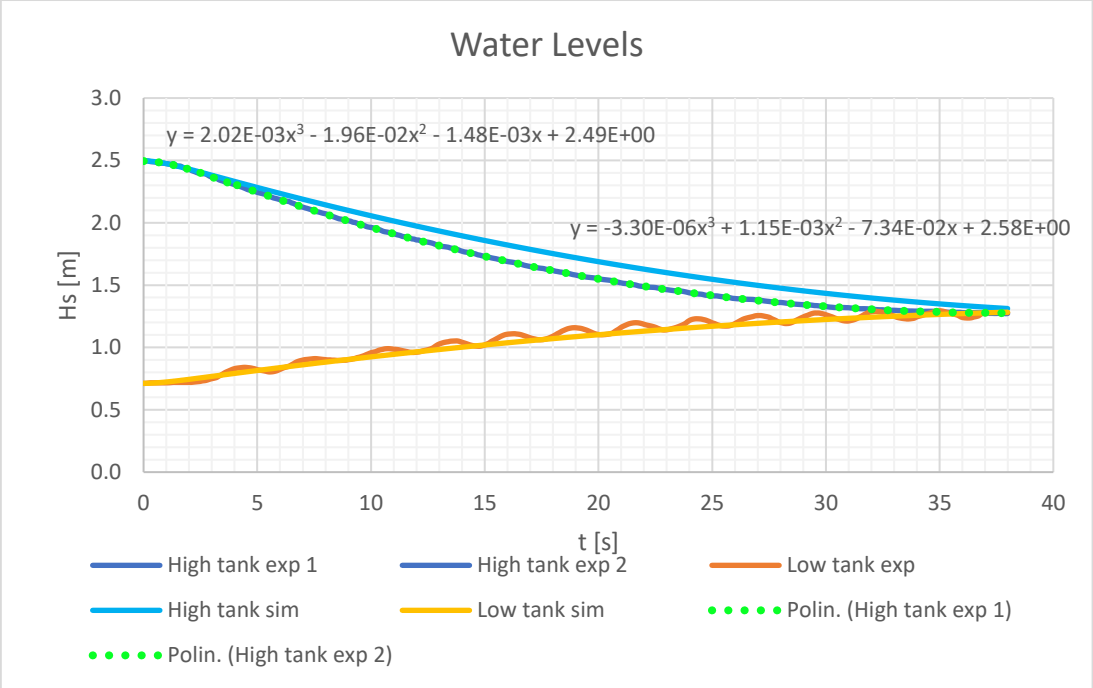

Figure 4.8: Tank water levels during the experiments and simulation

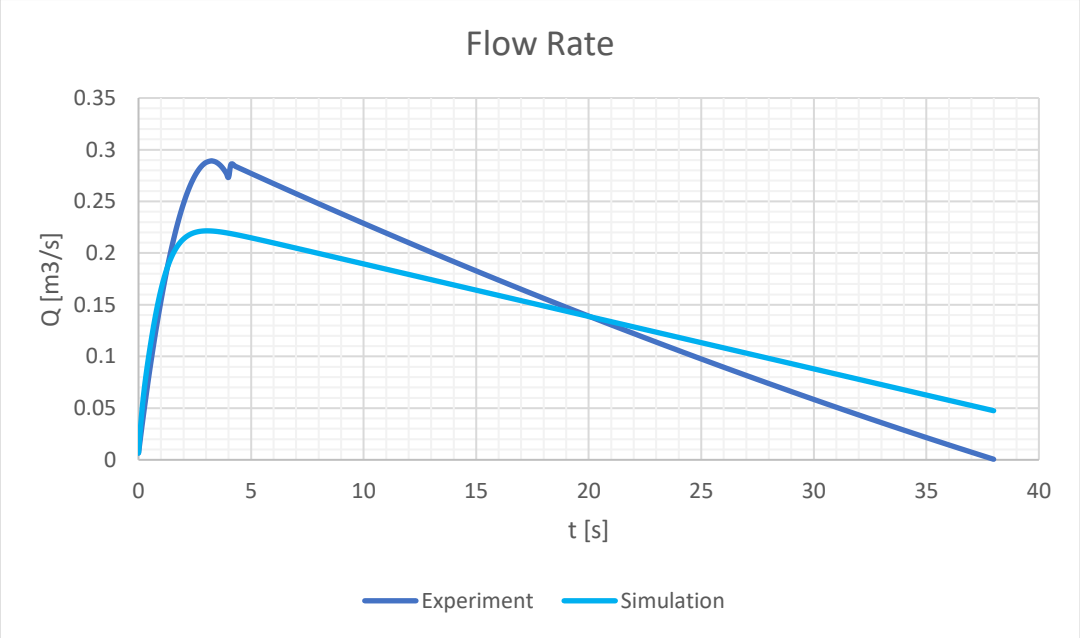

Figure 4.9: Flow rate during experiments and simulation

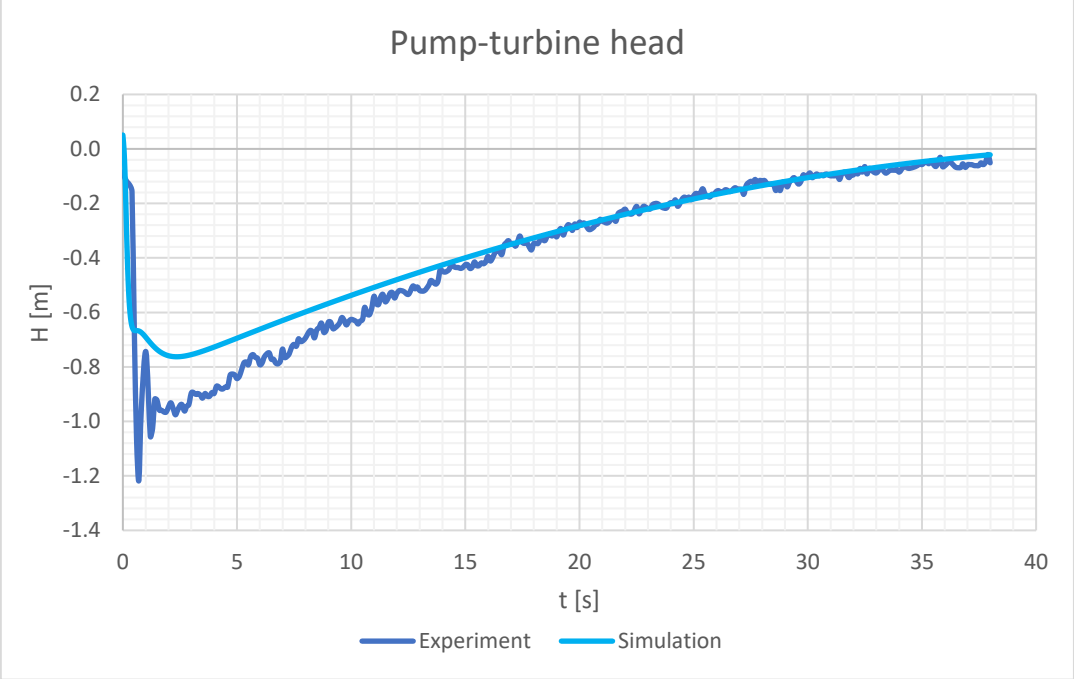

Figure 4.10: Pump-turbine head during experiments and simulation

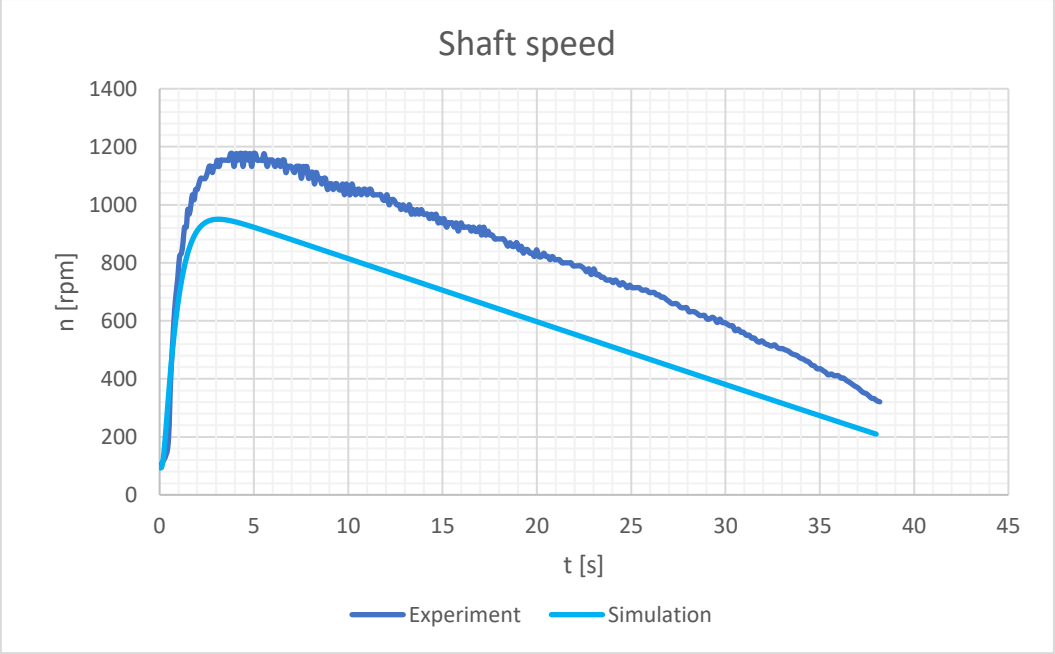

Figure 4.11: Shaft speed during experiments and simulation

The comparison graphs between the simulations of the small-scale model and the experimental results present some discrepancies. These have probably to be attributed to the geometrical differences between the two ducts. As discussed, while in the 0-D simulation environment a circular duct of constant diameter (30 cm) is modelled, the real experimental setup presents a complicated convergent-divergent geometry. Moreover, the average sectional area of the duct in the experimental setup is higher than the one modelled, since in the model the smaller section (the turbine section) was taken as the constant area. This leads, in the first phase of the experiment, to the experimental setup system reaching a higher flow rate compared to the modelled one. Moreover, there is uncertainty regarding the moment of inertia of the system. The other discrepancy lies in the fact that the flow rate in the experiments decreases with a faster rate than the one of the simulations. This is also noticeable in the water level curves of figure 4.8, especially those related to the high tank. In fact, a larger average cross-sectional area of the duct is able to deliver a higher flow rate at the beginning of the experiment, therefore reducing the static head difference faster compared to the simulated case. This causes a quicker reduction of the flow rate. This higher flow rate also induces a faster rotation of the impeller. Some difference in the flow rate trend could also be induced by the way it was approximated in the experiments, since it has been derived by a curve fit of the water level. In order to check the behavior of the system, simulations have been run with a constant duct diameter of 0.4 m and an increased inertia. The results for flow rate and shaft speed are shown in figure 4.12 and 4.13.

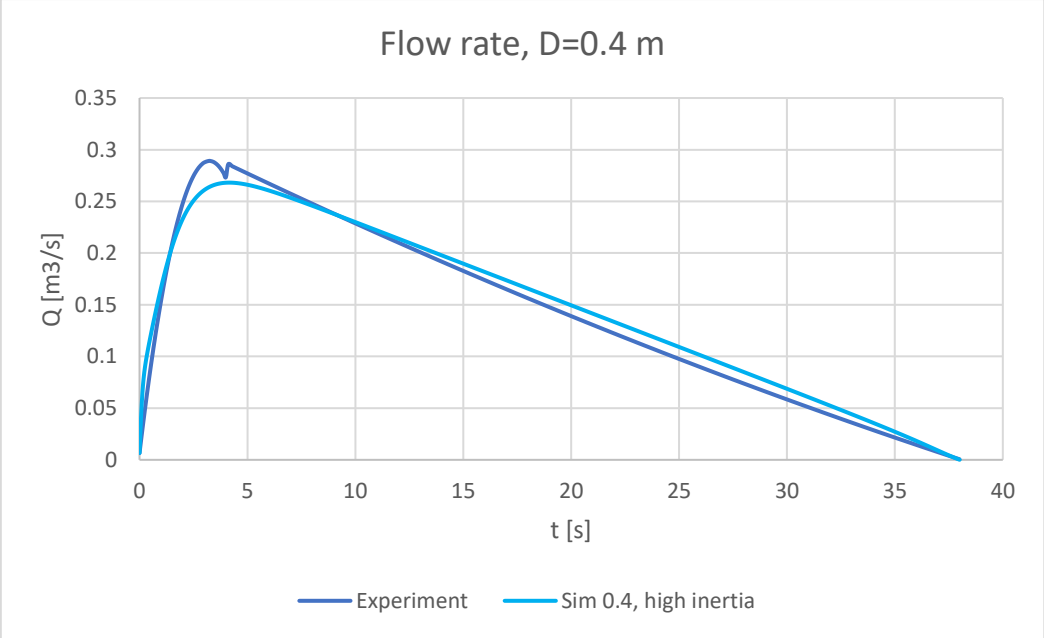

Figure 4.12: Flow rate as a function of time with increased pipe diameter (D=0.4 m)

The flow rate variation with time shows a better correspondence with the experimental results, suggesting that a duct diameter of 0.4 meters has a cross-sectional area (and therefore a pipe resistance) comparable to the average cross-sectional area of the experimental setup, and that an increased inertia better represents the real setup.

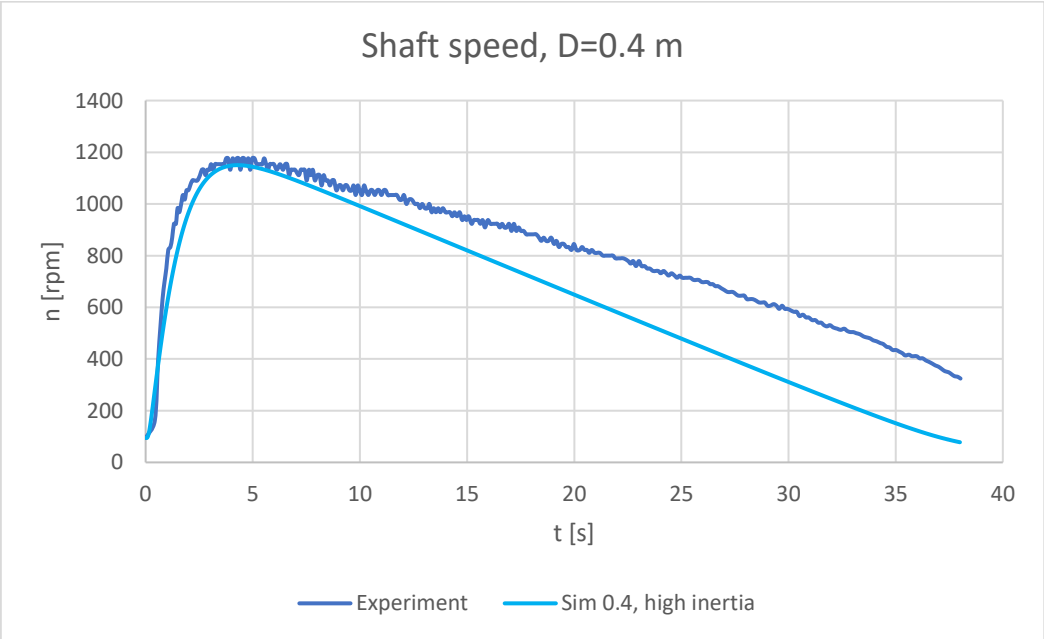

Figure 4.13: Shaft speed as a function of time with increased pipe diameter (D=0.4 m)

The shaft speed graph shows a better correspondence as well, despite a faster decrease compared to the experimental results. The calculations of the Strouhal number according to equation (3.7) for the validation experiment are shown in the figure below.

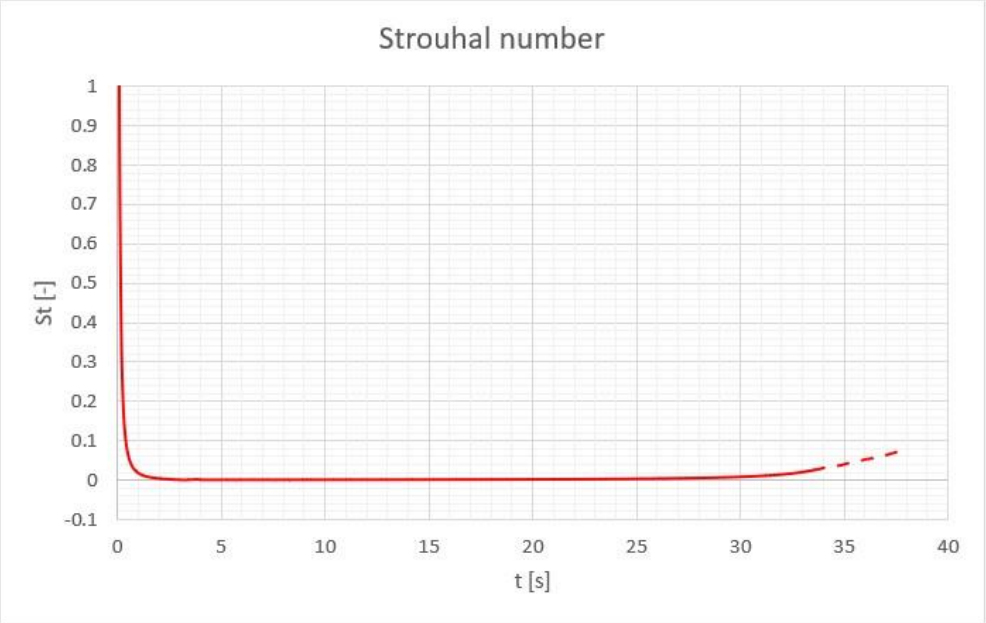

Figure 4.14: Strouhal number evaluation during the experiment

It is clear from the graph that the Strouhal number condition is respected for most of the 38-seconds experiment (specifically, from t=0.5). At the beginning of the experiment the Strouhal number reaches very high values, since the flow rate is close to zero, whereas its rate of change is significant. At the end of the experiment, the Strouhal number is ill-defined since both the flow rate and the flow rate variation assume values close to zero. These results allow to consider as quasi-steady the conditions during the validation experiments, meaning that they are comparable to the steady-state characteristics curves.

5 Results

The model has been simulated in two different configurations:

- Without the drivetrain, in order to compare the results to those of the analytical model and test the accuracy and robustness of the numerical method.
- With the drivetrain, consisting of pump-turbine, shaft and electrical machine, to represent the real scenario.

Regarding the moments of inertia of the motor-generator and impeller, members of the Finnish company "The Switch", part of the Yaskawa group, indicated as a suitable motor/generator their 4 MW electrical machine, which has a rated speed of 15.6 rpm. This machine has a total moment of inertia of 110'000 $kg * m^2$, and this value has been used in the model. The moment of inertia of the impeller designed by Nijhuis, calculated through CAD files, is 250'000 $kg * m^2$. Moreover, the added mass moment of inertia had also to be evaluated for the large-scale impeller. The EAR and the pitch/diameter ratio remain constant when the geometry is scaled up from a diameter of 30 cm to one of 8 meters. Thus, the factor C_{IE} remains constant, and the large-scale impeller added moment of inertia, according to equation (3.8) is:

$$I_w = C_{IE} * \rho * D^5 = 1.021 * 10^{-3} * 1000 \frac{kg}{m^3} * (8\,m)^5 = 33456\,kg * m^2$$

To test for different scenarios, simulations have been run with static head values of 0.5, 1 and 1.5 meters, for the case without drivetrain and with the drivetrain, and for all three start-up strategies: no kickstart, kickstart, kickstart with frequency controller (FC). This last strategy can be used to increase the shaft speed to values higher than those reached in the fixed synchronous speed start-up, by gradually increasing the frequency and stator voltage. Thus, with the impeller rotating at higher speed, a quicker development of the flow could be accomplished, reaching generating conditions faster than in the other two strategies. In the model, it is assumed that the boundary between the constant torque and constant power regions lies at 13 rpm. It has also been necessary to assume the rated torque of the machine in order to obtain values for the electromechanical torque in the torque curves. The starting assumption is that the system, during pump mode, should be able to deliver the same flow rate as in turbine mode with a static head of one meter. From preliminary simulations of a single conduit with pump-turbine, a steady-state flow rate of about 80 $\frac{m^3}{s}$ has been observed in those conditions. According to the characteristic curves derived from the data provided by Nijhuis, this amount of flow rate is obtained in pump mode at 25 rpm, with an electrical power need of 1276 kW. This value is assumed to be the power during the operation in the constant power region. The torque for all the points in this region is then calculated via the usual relation between torque and power (2.7). In the constant torque region, the torque is equal to the one at 13 rpm, which is:

$$T(13\ rpm) = \frac{P(13\ rpm)}{13 * \frac{\pi}{30}} = 937\ kNm \tag{5.1}$$

As stated before, the torque at which the machine operates in the constant torque region is the rated torque, therefore it will be assumed as such. This gives the following torque curve for the start-up strategy with frequency controller:

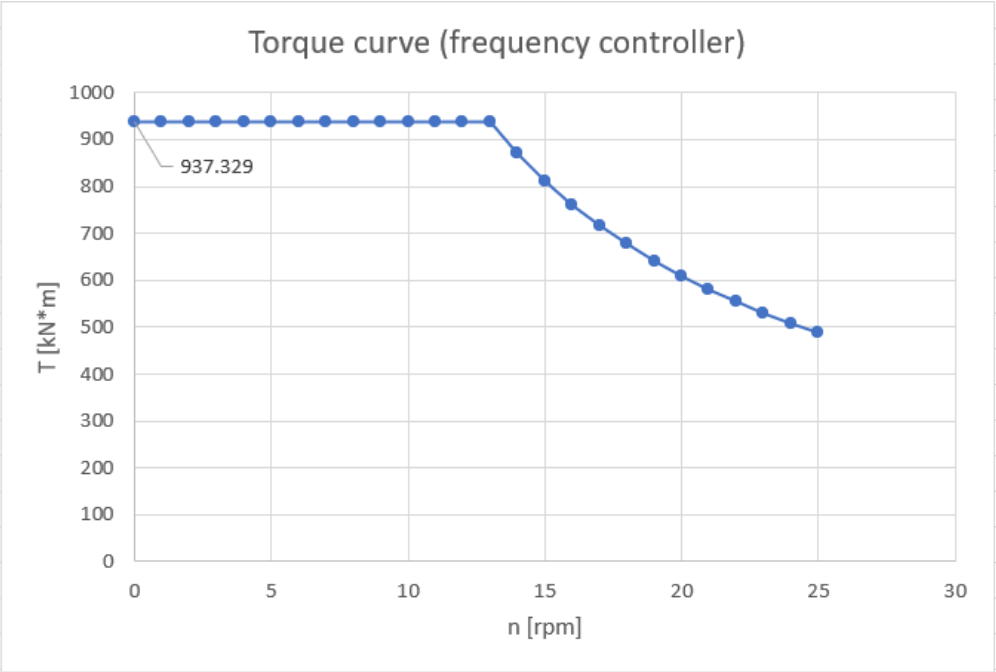

Figure 5.1: Starting torque for the frequency controller strategy

In this starting procedure, once the flow rate reaches a value close to the equilibrium one, the frequency is set to a value that grants a synchronous speed slightly higher than 13 rpm. This difference is called slip. This leads to the system working on the same torque curve shown in figure 3.6. When the frequency switch happens, the electrical machine will be working in the generator region of this curve, and will gradually settle to shaft speed values slightly higher than the synchronous speed.

5.1 No pump-turbine

The following graphs show the development of flow rate with a static head difference of -0.5, -1, and -1.5 meters respectively, in a configuration with no pump-turbine. The simulation covers the first 3 minutes after the opening of the gate-valves, to let the system reach steady-state conditions.

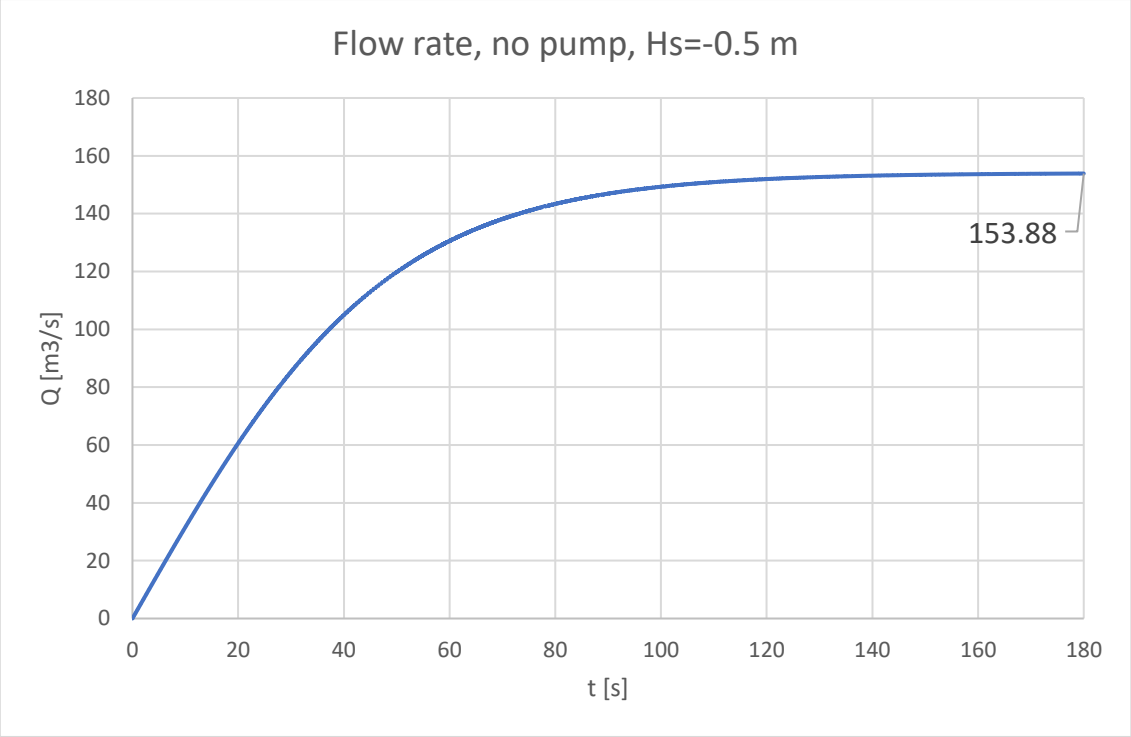

Figure 5.2: Flow rate development, static head = -0.5 m, no pump-turbine

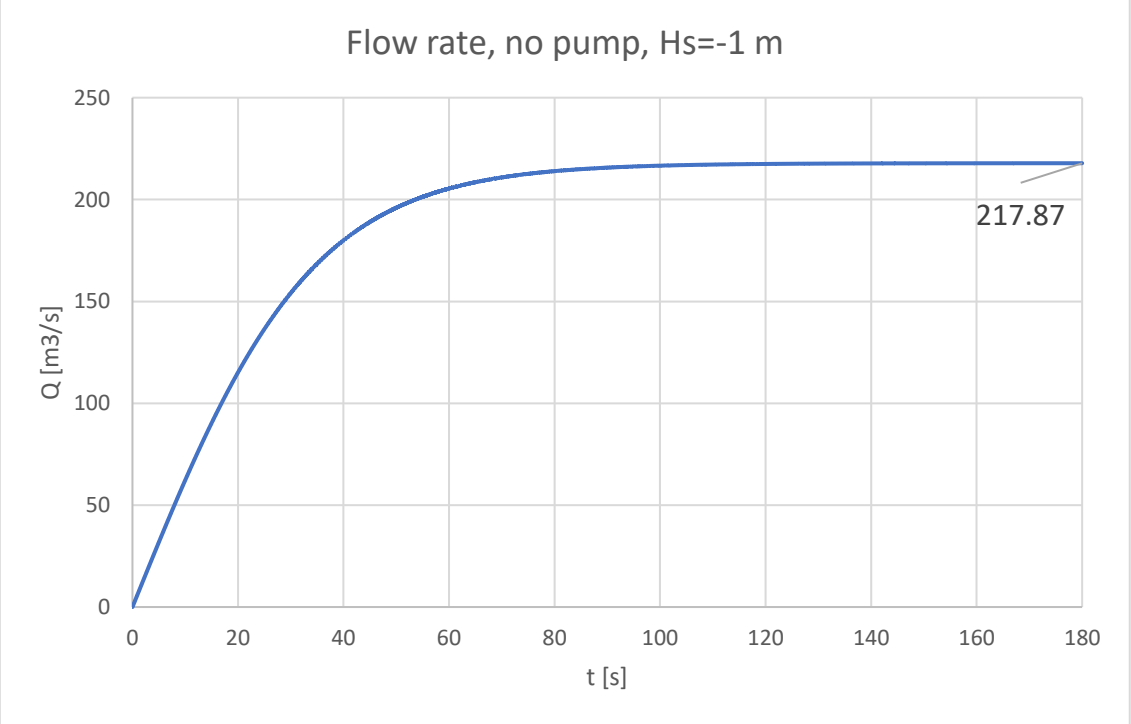

Figure 5.3: Flow rate development, static head = -1 m, no pump-turbine

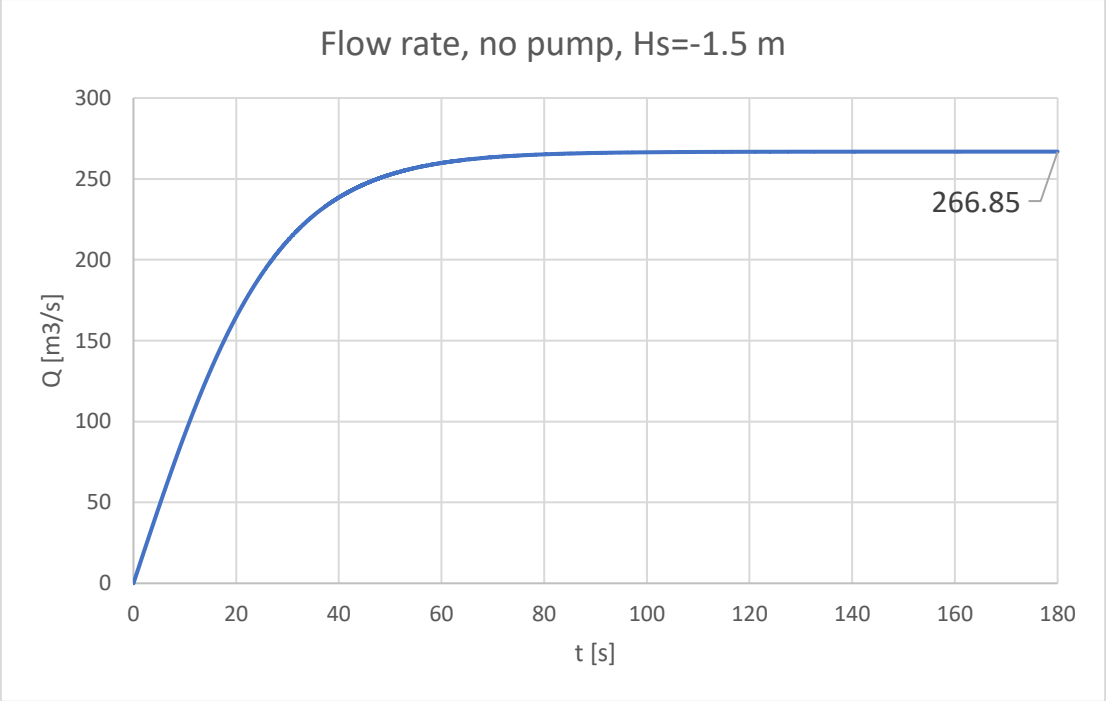

Figure 5.4: Flow rate development, static head = -1.5 m, no pump-turbine

5.2 Static head = -0.5 m

The following graphs show flow rate, shaft speed, electrical power (consumed if positive, generated if negative), mechanical efficiency and net energy balance for the three different start-up strategies, with a static head of -0.5 meters. Moreover, the net energy balance for the two kickstart strategies is shown. The simulation covers the first 30 seconds after the opening of the gate-valves.

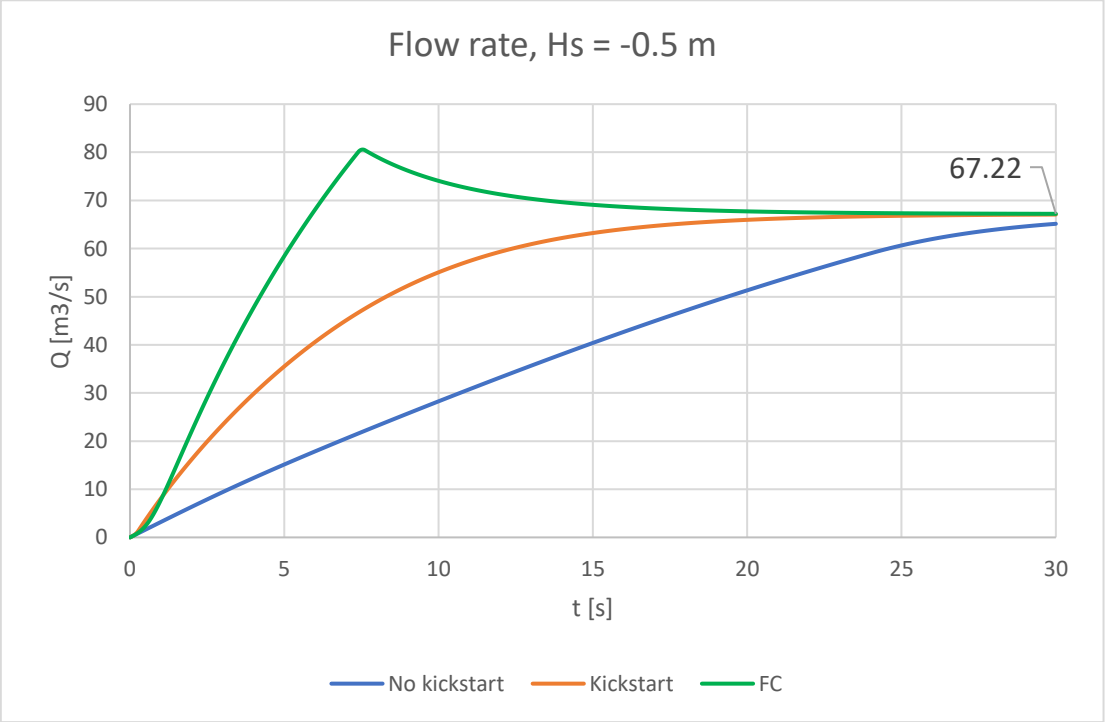

Figure 5.5: Flow rate in function of time, static head = -0.5 m

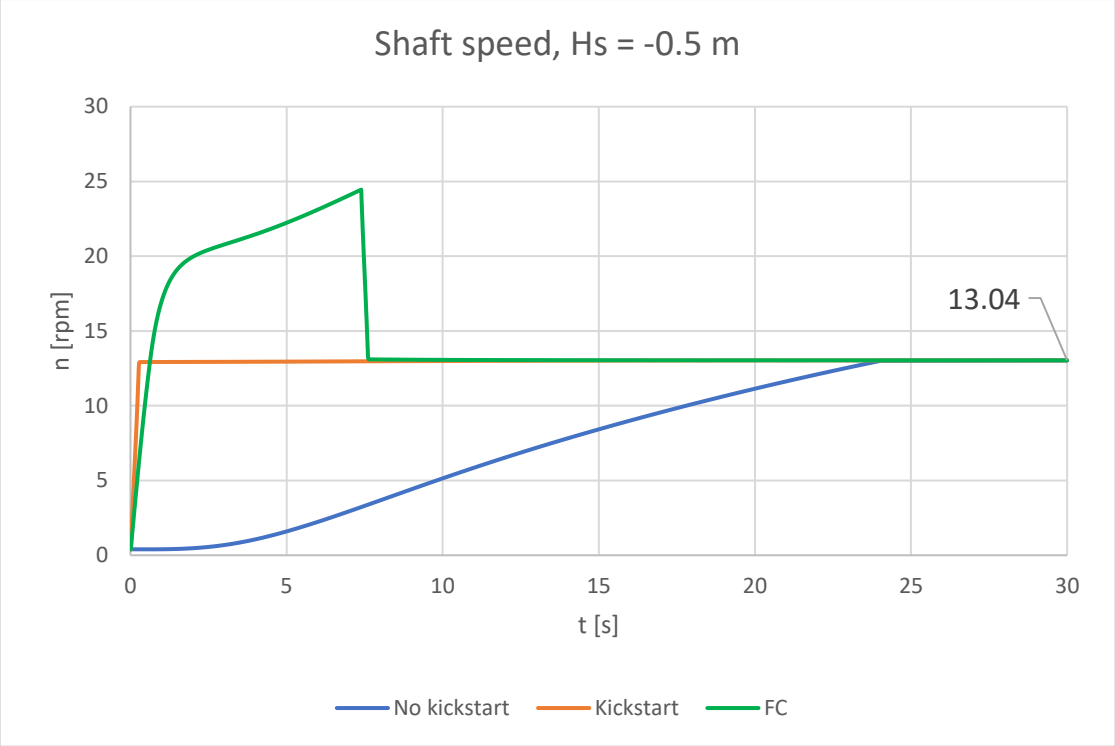

Figure 5.6: Shaft speed in function of time, static head = -0.5 m

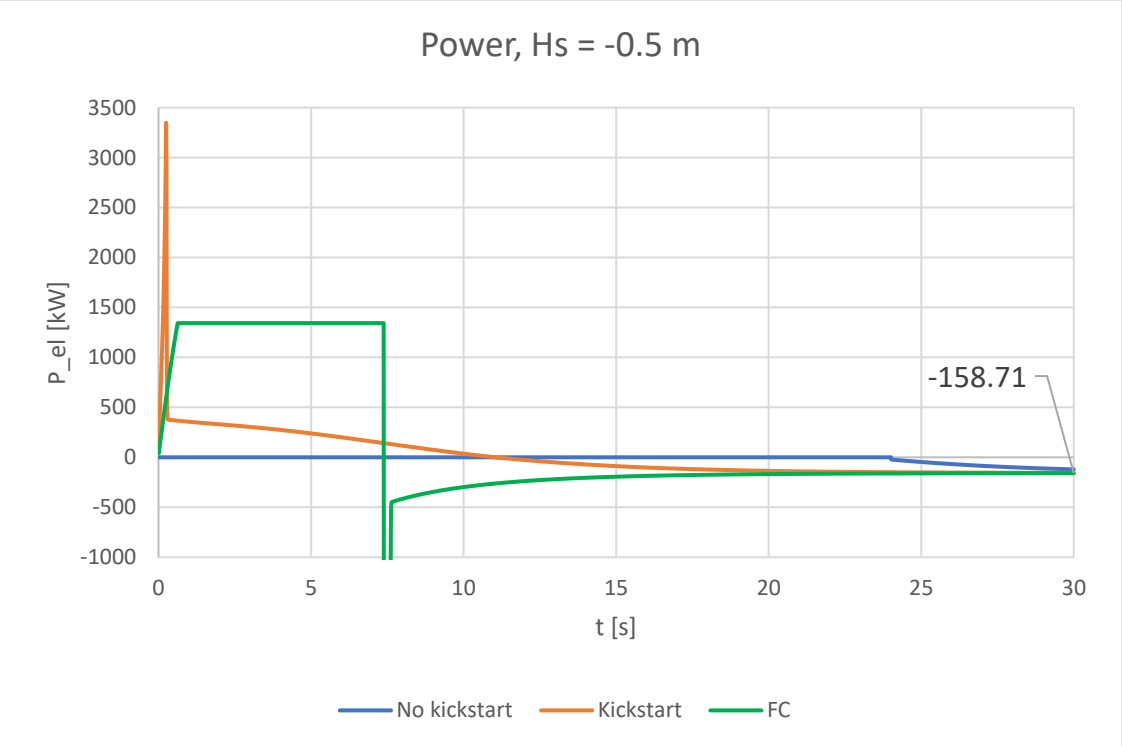

Figure 5.7: Electrical power in function of time, static head = -0.5 m

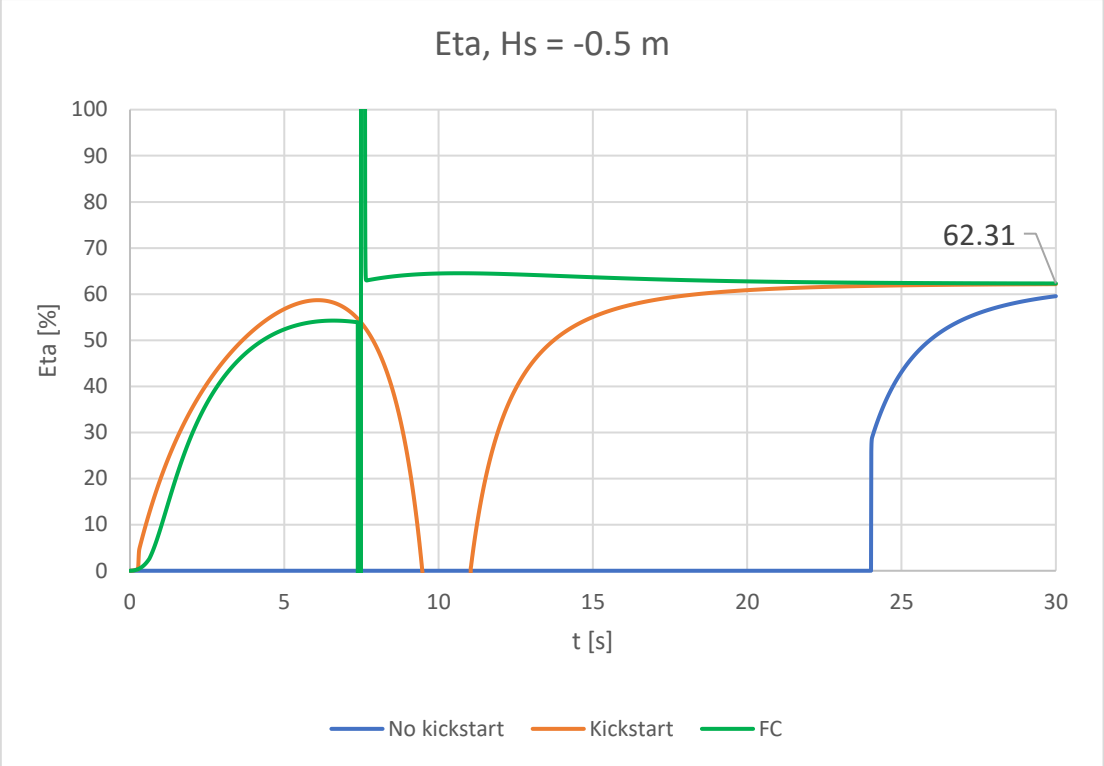

Figure 5.8: Mechanical efficiency in function of time, static head = -0.5 m

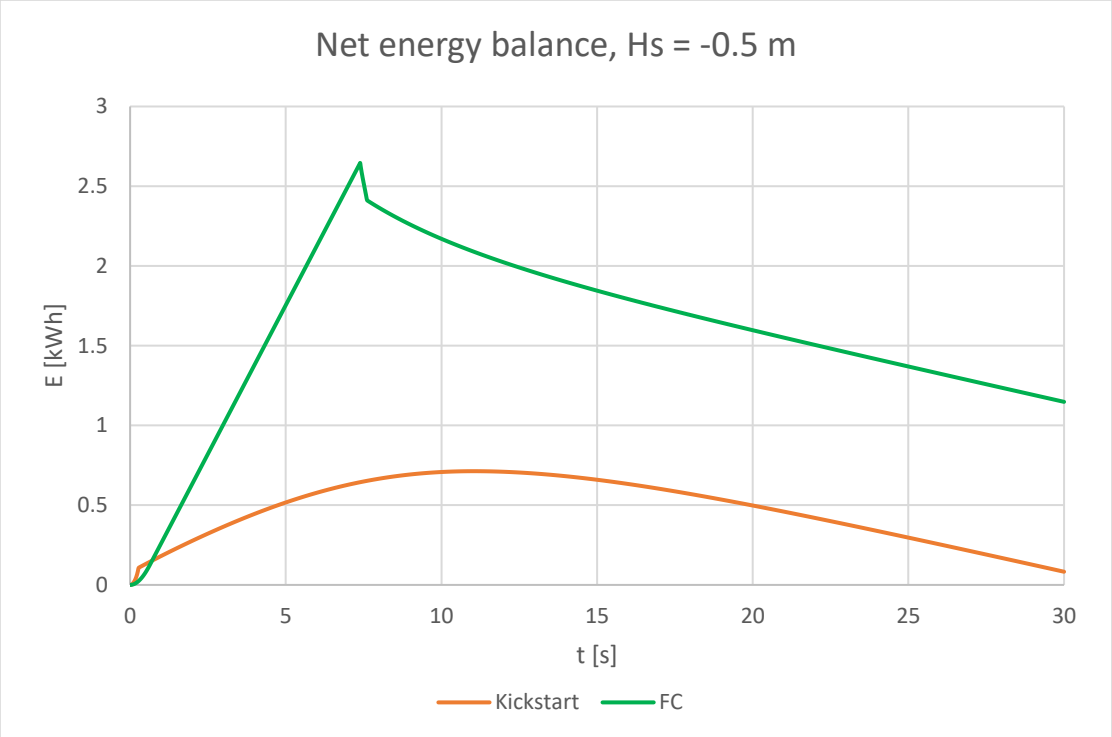

Figure 5.9: Net energy balance during start-up, static head = -0.5 m

In addition, the model records the Q-H and Q-P points of the pump-turbine during the simulations, in order to draw the following system graphs. In the Q-H graph, the first quadrant represents the pump

mode, the region between the x-axis and the runaway curve represents the pump-assisted drainage mode, and the region below the runaway curve represents the reverse turbine mode.

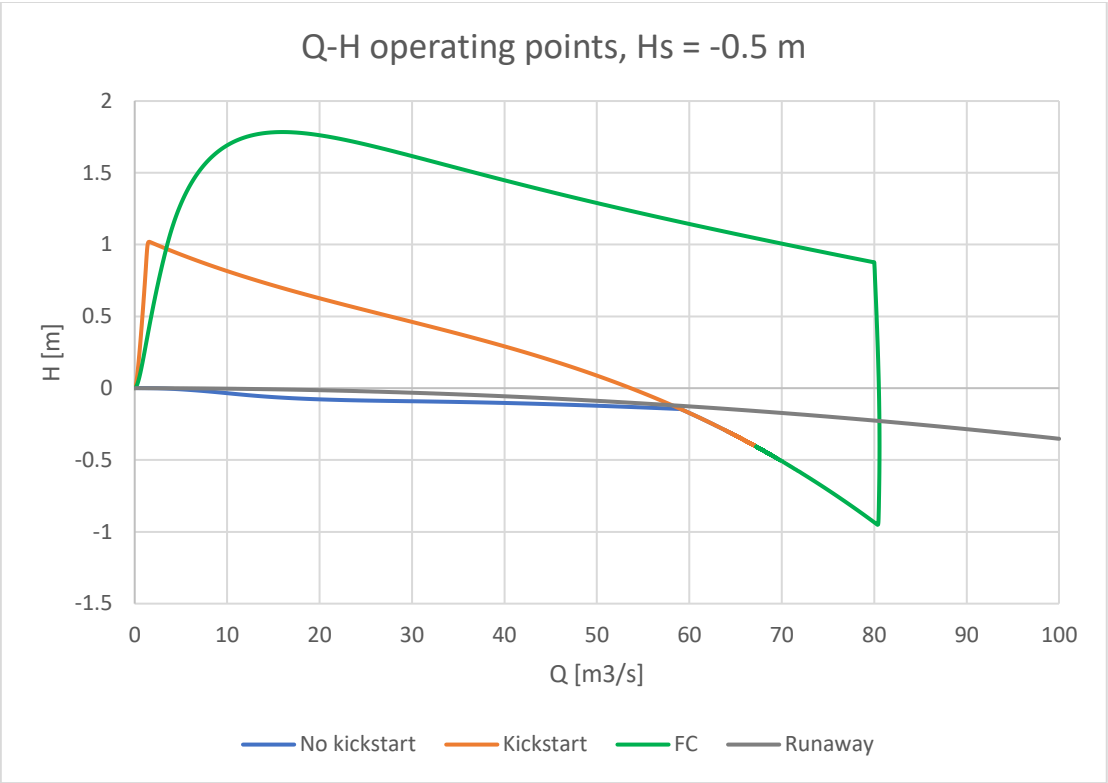

Figure 5.10: Q-H curves of the three different strategies, static head = -0.5 m

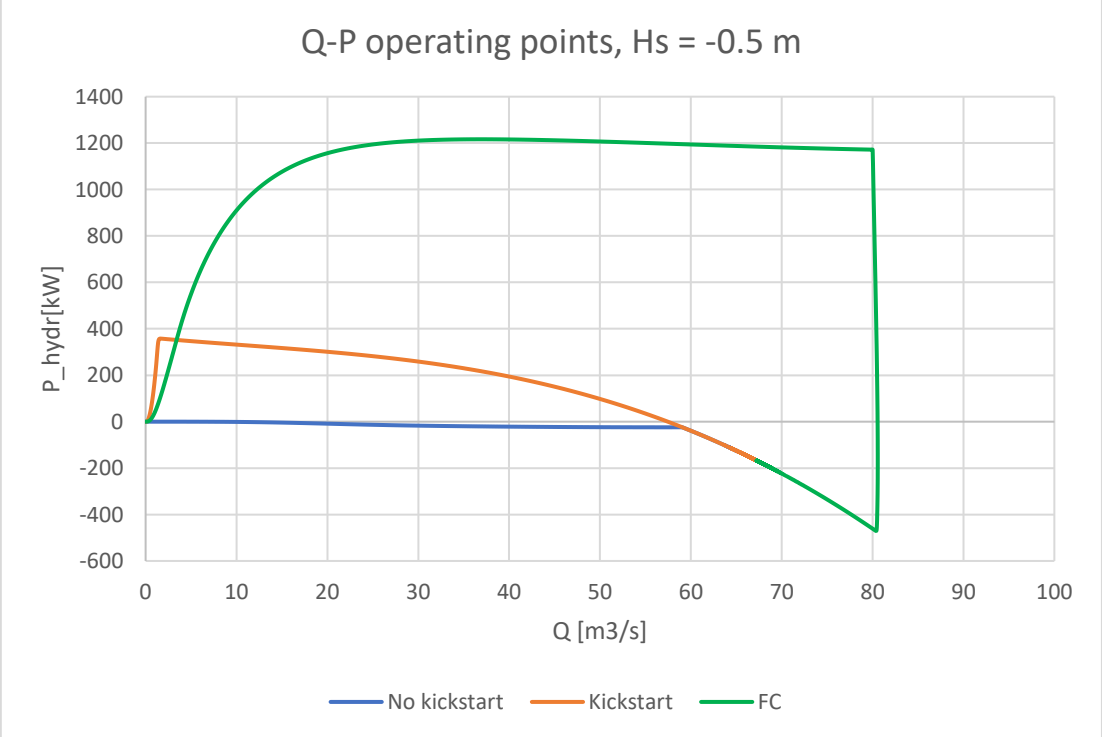

Figure 5.11: Q-P curves of the three different strategies, static head = -0.5 m

5.3 Static head = -1 m

The following graphs show flow rate, shaft speed, electrical power (consumed if positive, generated if negative) and mechanical efficiency for the three different start-up strategies, with a static head of -1 meter. Moreover, the net energy balance for the two kickstart strategies is shown. The simulation covers the first 30 seconds after the opening of the gate-valves.

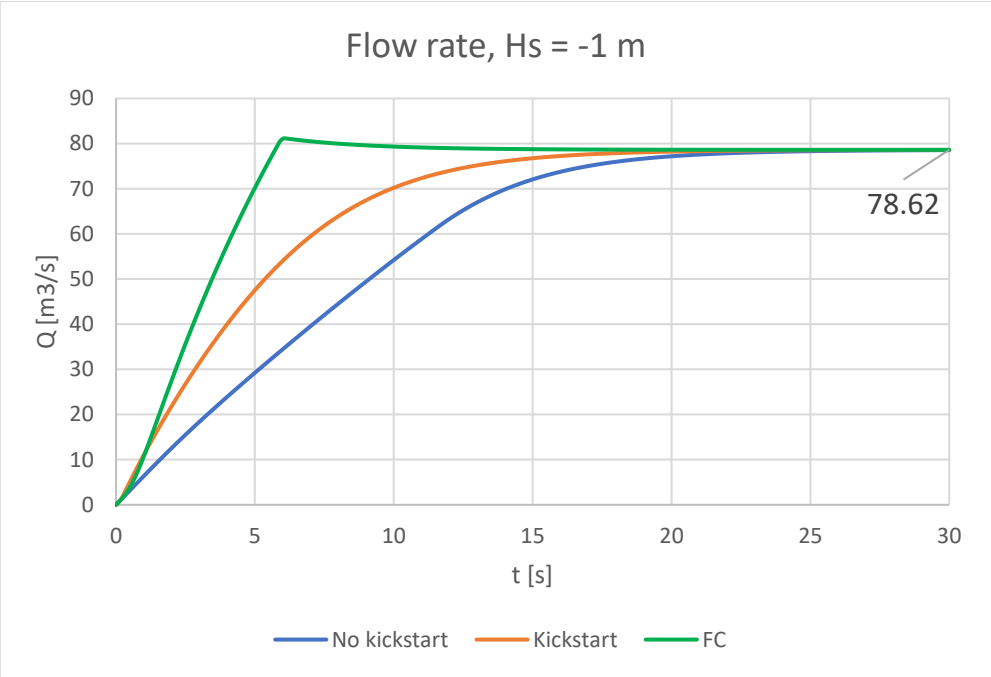

Figure 5.12: Flow rate in function of time, static head = -1 m

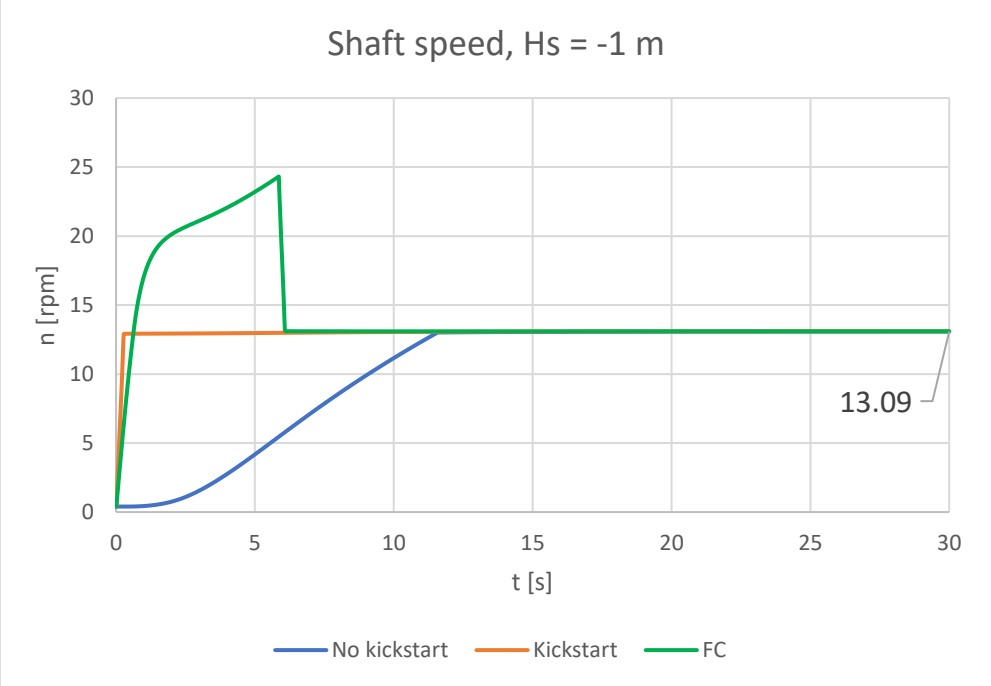

Figure 5.13: Shaft speed in function of time, static head = -1 m

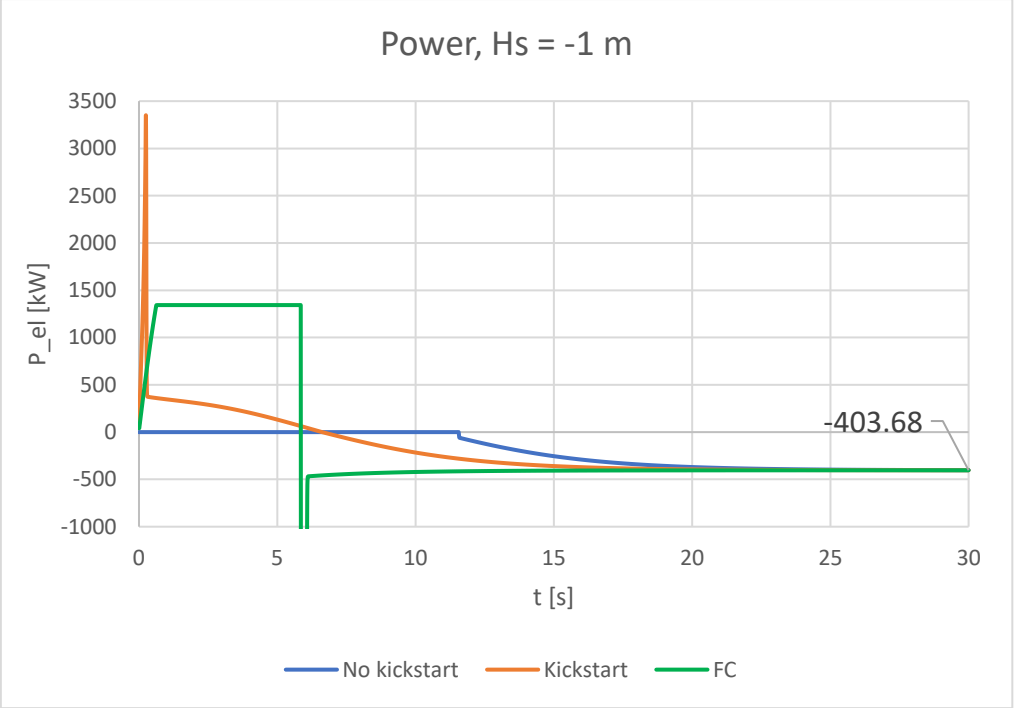

Figure 5.14: Electrical power with function of time, static head = -1 m

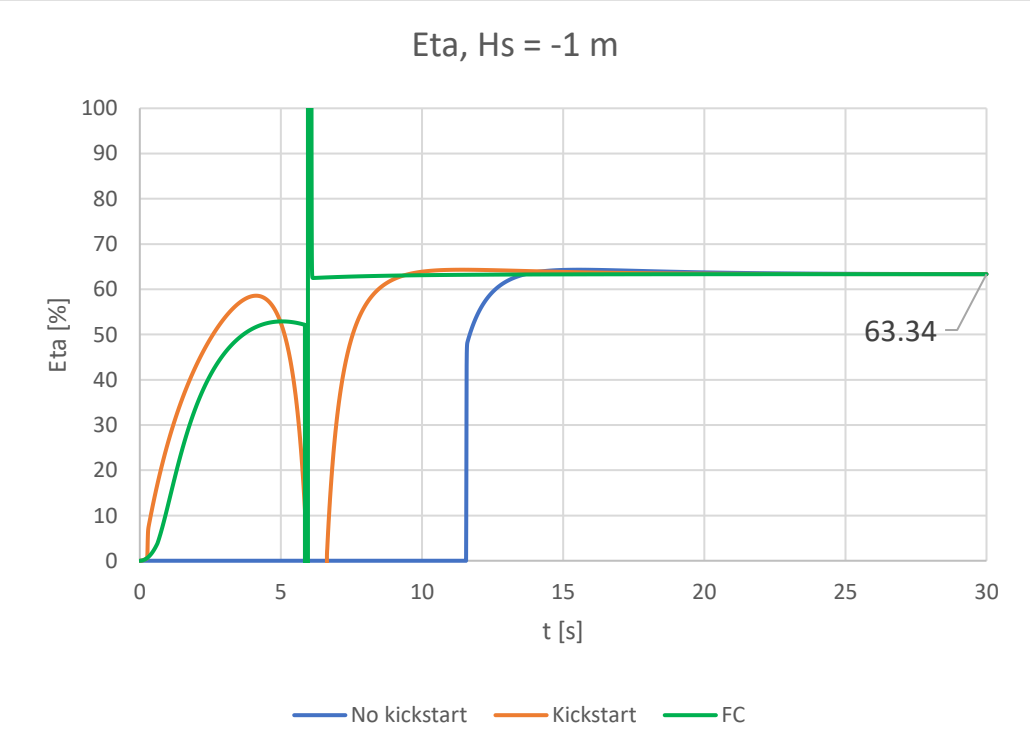

Figure 5.15: Mechanical efficiency in function of time, static head = -1 m

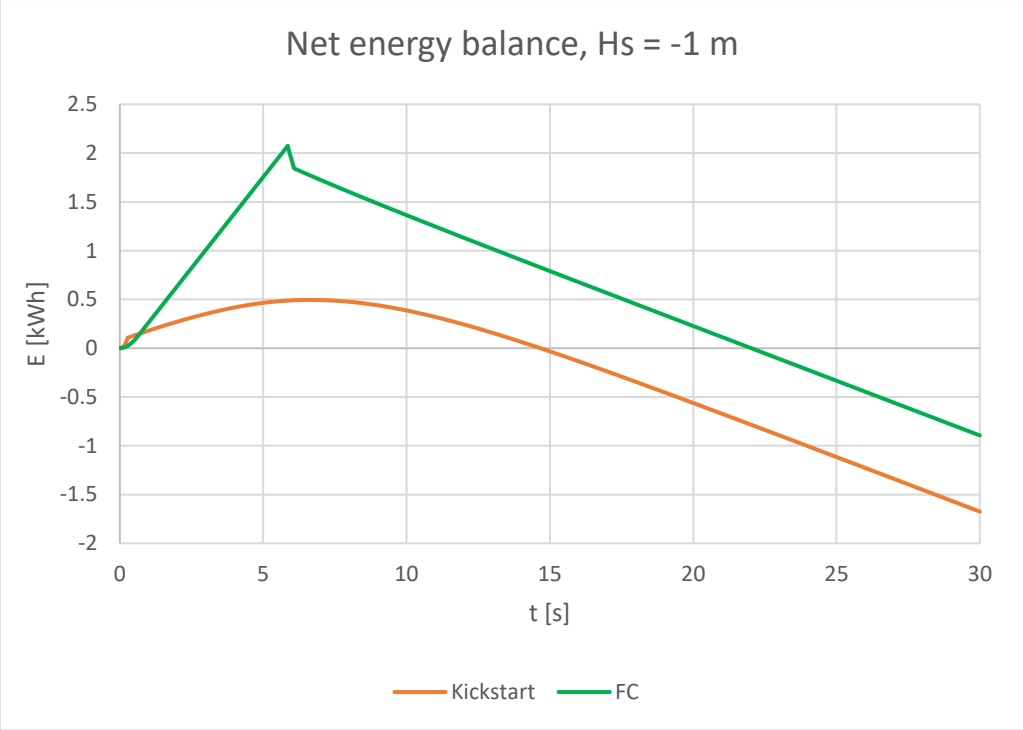

Figure 5.16: Net energy balance during start-up, static head = -1 m

In addition, the model records the Q-H and Q-P points of the pump-turbine during the simulations, in order to draw the following system graphs.

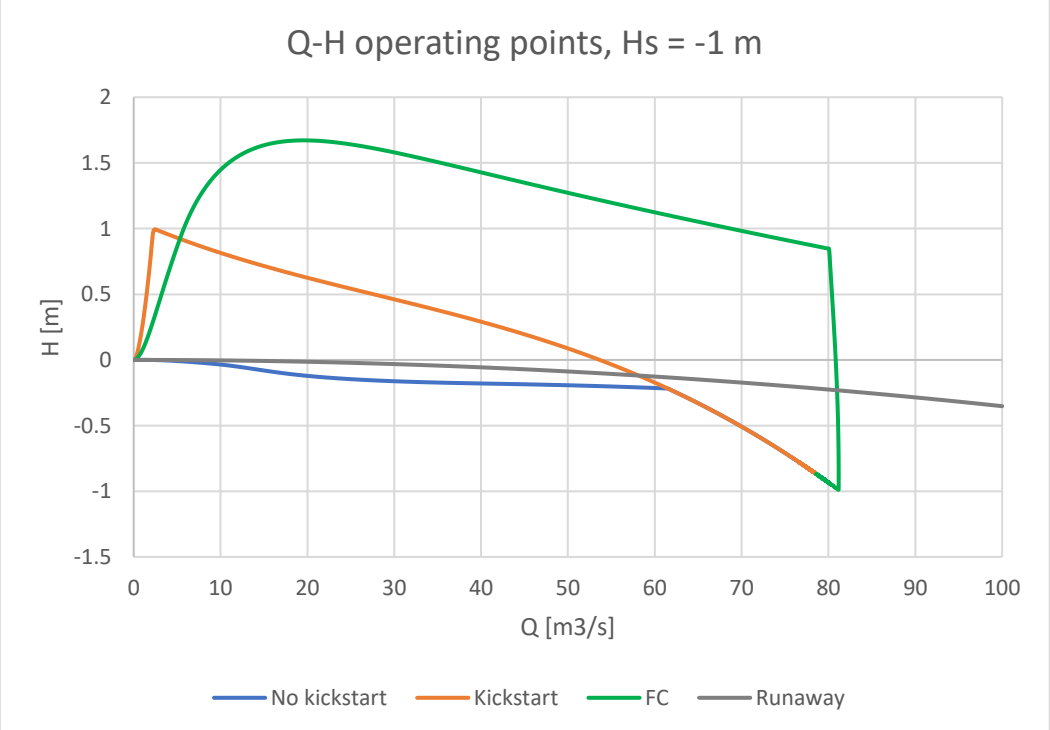

Figure 5.17: Q-H curves of the three different strategies, static head = -1 m

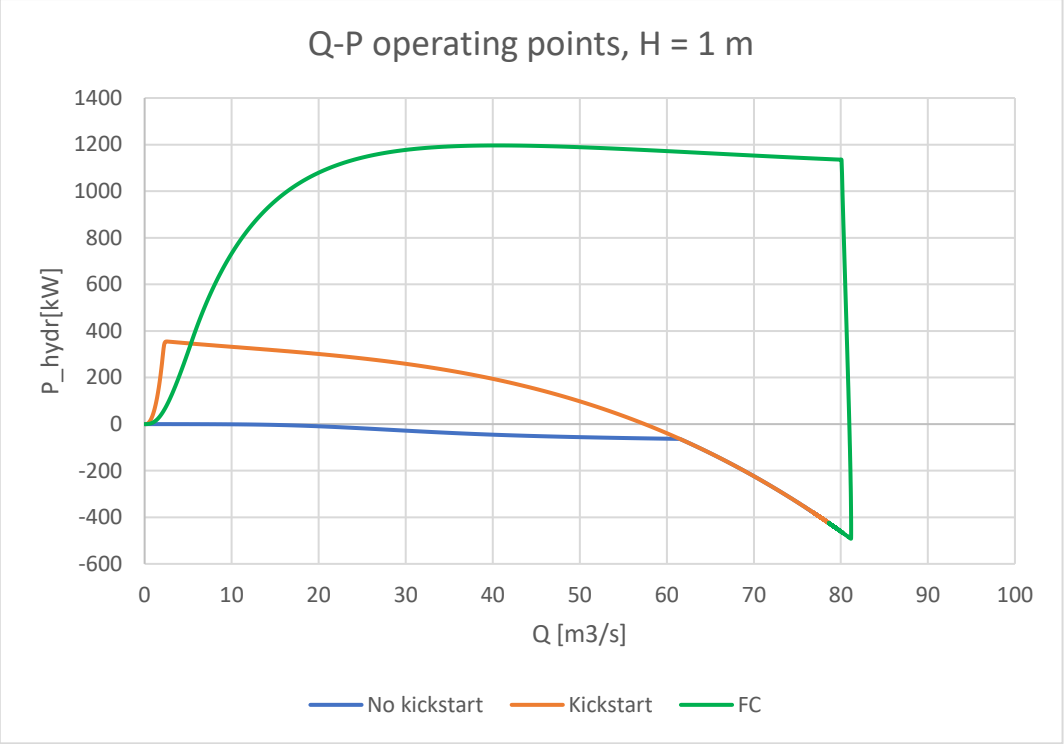

Figure 5.18: Q-P curves of the three different strategies, static head = -1 m

5.4 Static head = -1.5 m

The following graphs show flow rate, shaft speed, electrical power (consumed if positive, generated if negative) and mechanical efficiency for the three different start-up strategies, with a static head of -1.5 meter. Moreover, the net energy balance for the two kickstart strategies is shown. The simulation covers the first 30 seconds after the opening of the gate-valves.

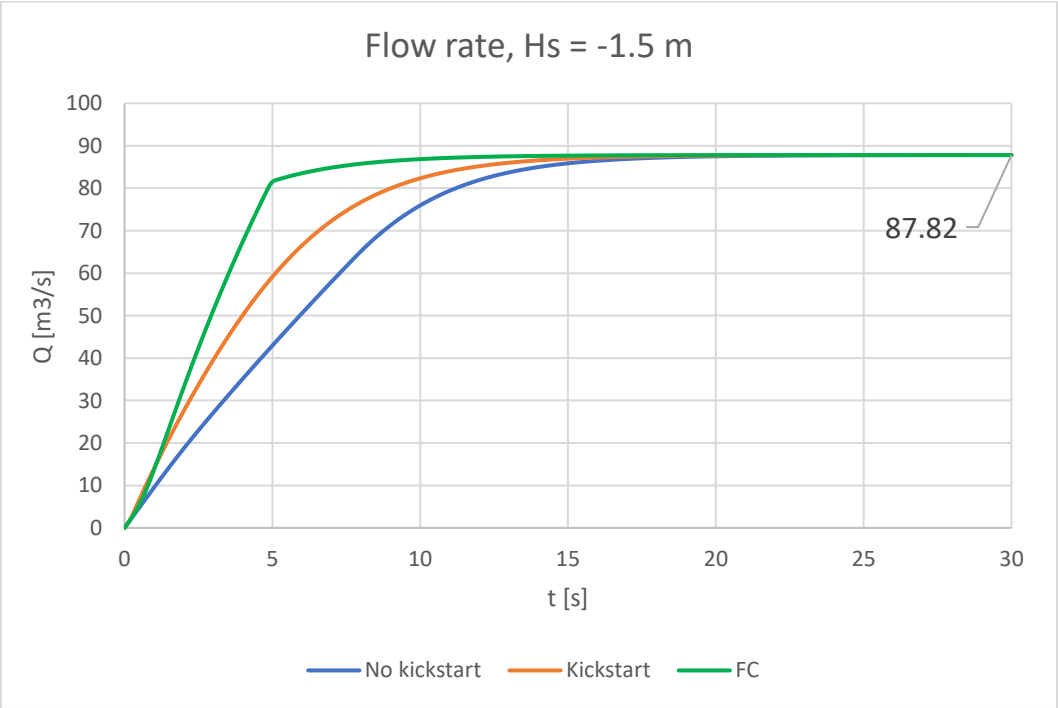

Figure 5.19: Flow rate in function of time, static head = -1.5 m

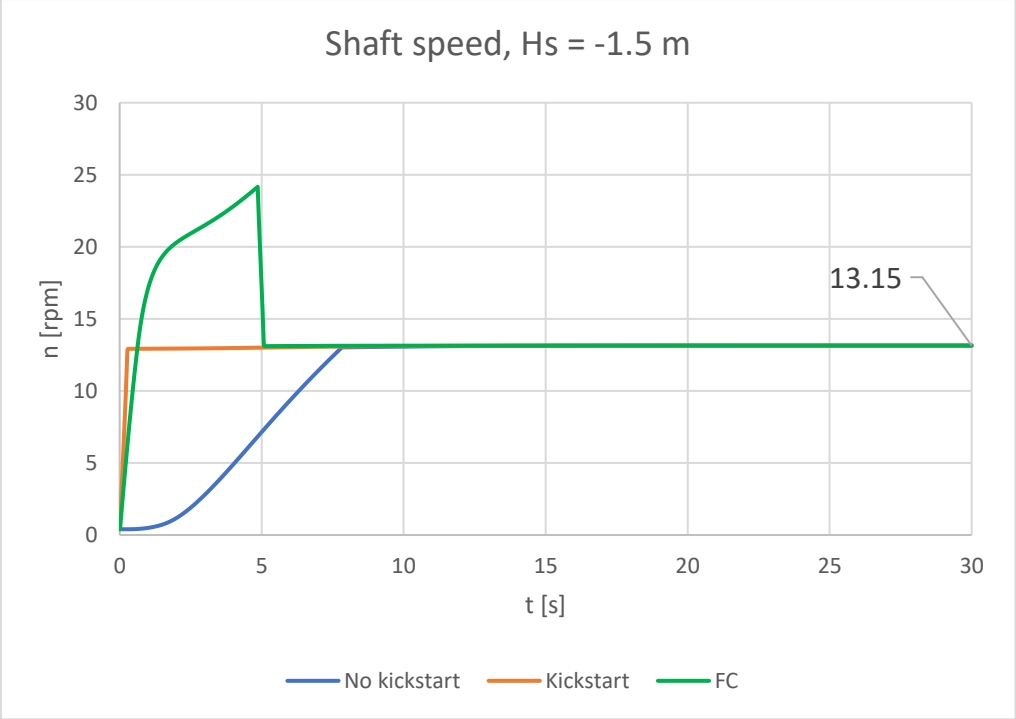

Figure 5.20: Shaft speed in function of time, static head = -1.5 m

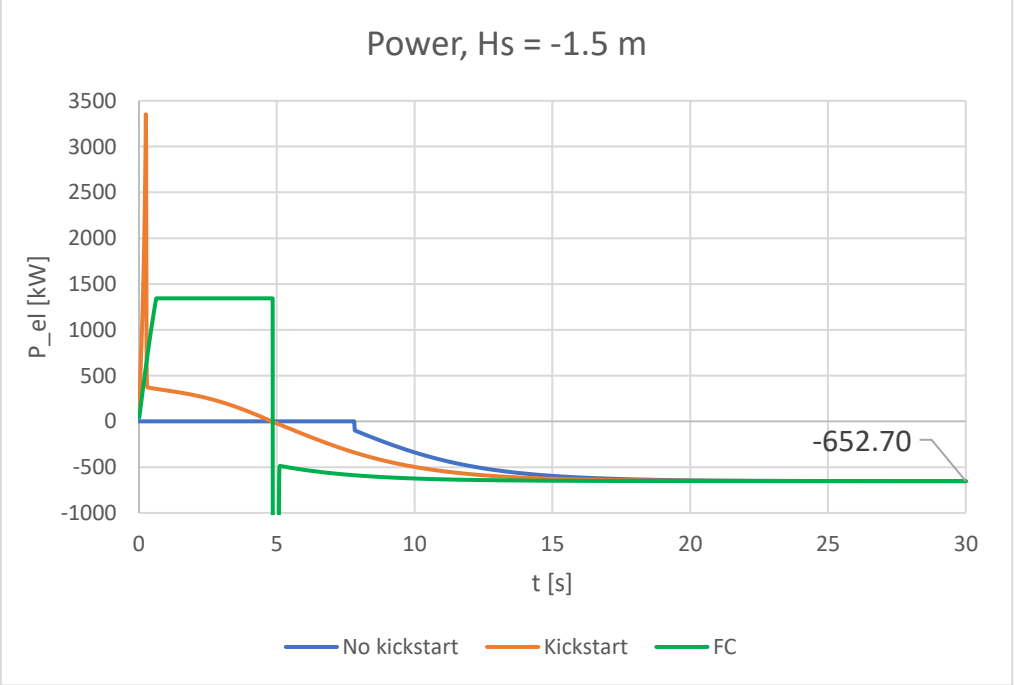

Figure 5.21: Electrical power in function of time, static head = -1.5 m

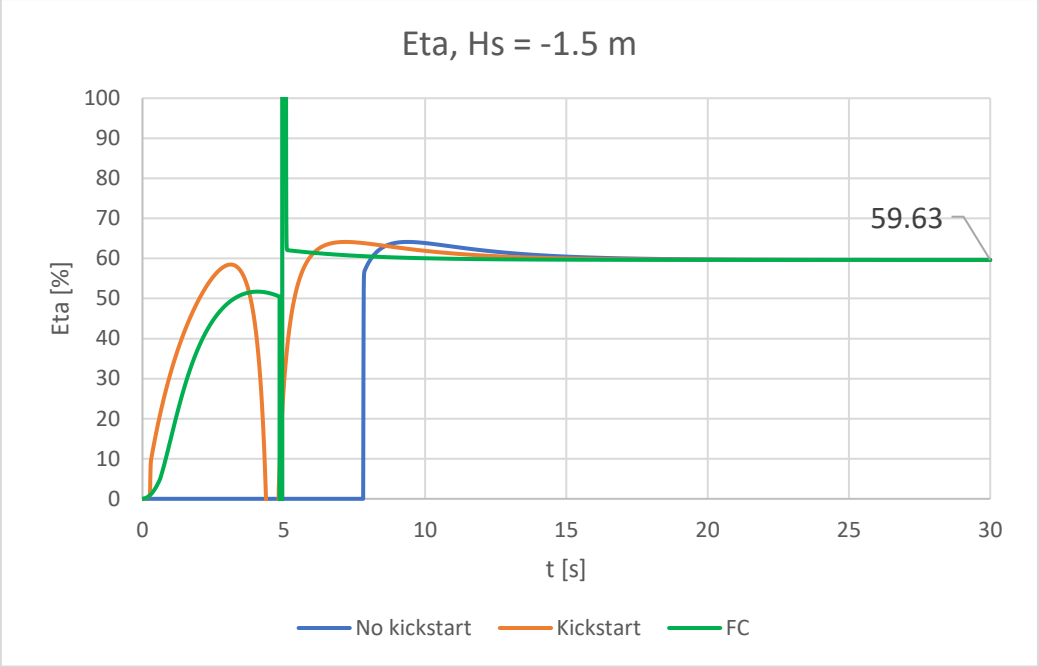

Figure 5.22: Mechanical efficiency in function of time, static head = -1.5 m

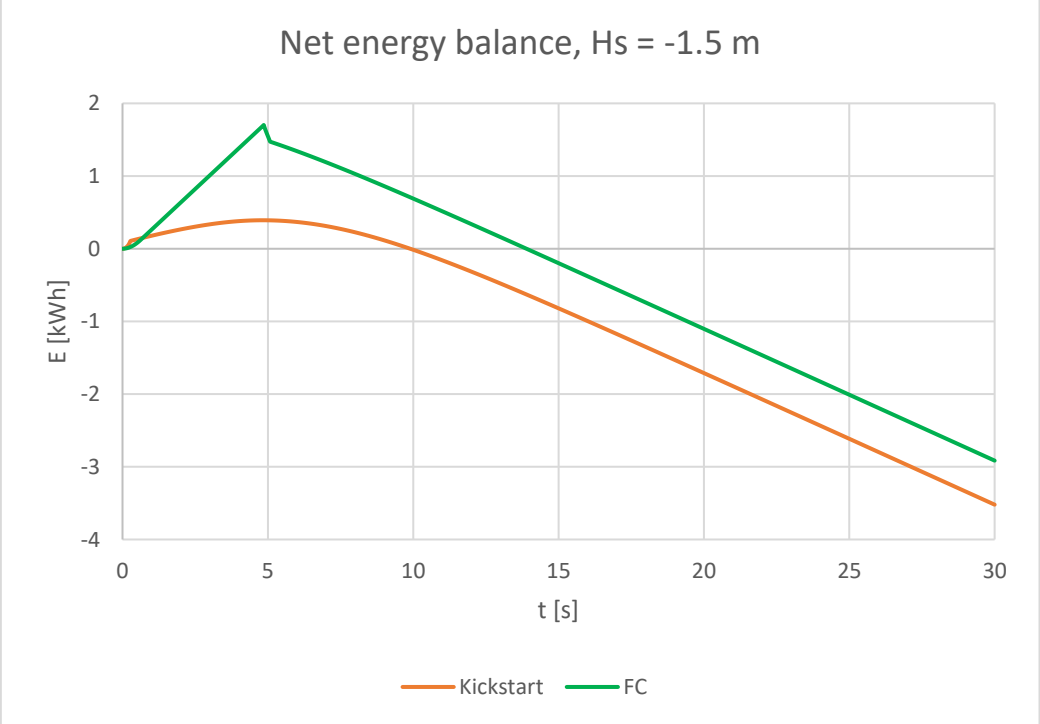

Figure 5.23: Net energy balance during start-up, static head = -1.5 m

Moreover, the model records the Q-H and Q-P points of the pump-turbine during the simulations, in order to draw the following system graphs.

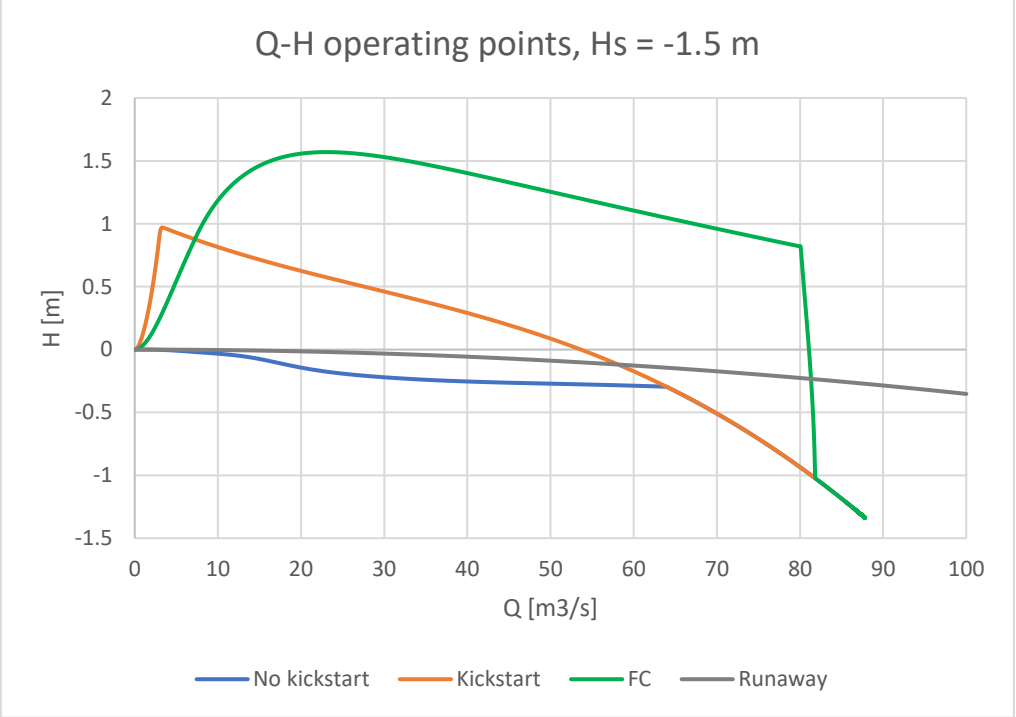

Figure 5.24: Q-H curves of the three different strategies, static head = -1.5 m

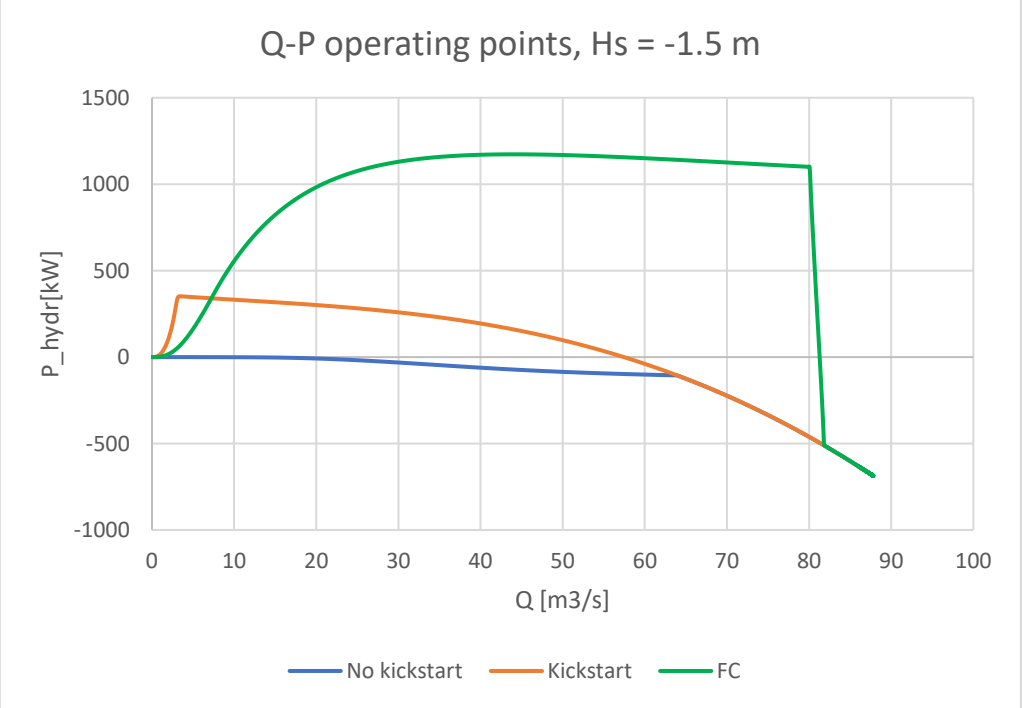

Figure 5.25: Q-P curves of the three different strategies, static head = -1.5 m

5.5 Power Plant with 15 Pump-Turbines

The large-scale model has been modified to also return the flow rate and energy generation of the entire power plant, consisting in 15 conduits with one pump-turbine each. With the total flow rate managed by the power plant it is possible to estimate the volume of water flowing in the lake in one flood tide, therefore calculating the variation of water level. This can give an idea on the impact of the re-opening of the Brouwersdam and the start of the operations of the power plant, especially regarding the desire of bringing back a tidal range of 40 cm in lake Grevelingen. The water level of the North Sea is subject to the tide, and it has been modelled with a sinusoidal curve.

$$H_{sea} = 1.25 * \sin\left(\frac{\pi}{6} * (t + 0.1)\right) + 10 \tag{5.2}$$

This represents a sinusoidal tide of period equal to 12 hours, with an amplitude of 1.25 meters. The last term added to the equation has only a numerical stability purpose, as a negative value of the static head would return errors in the simulation. This value will be subtracted before the model constructs the result graphs. The initial static head value is 0.0654 m NAP while the initial value of the lake static head is set to -0.3 m NAP. The model simulated for a time span of 5 hours after the opening of the gate-valves. The graphs show the change in water level of the North Sea and lake Grevelingen, the total water discharge of the power plant and the total energy generation during a flood tide.

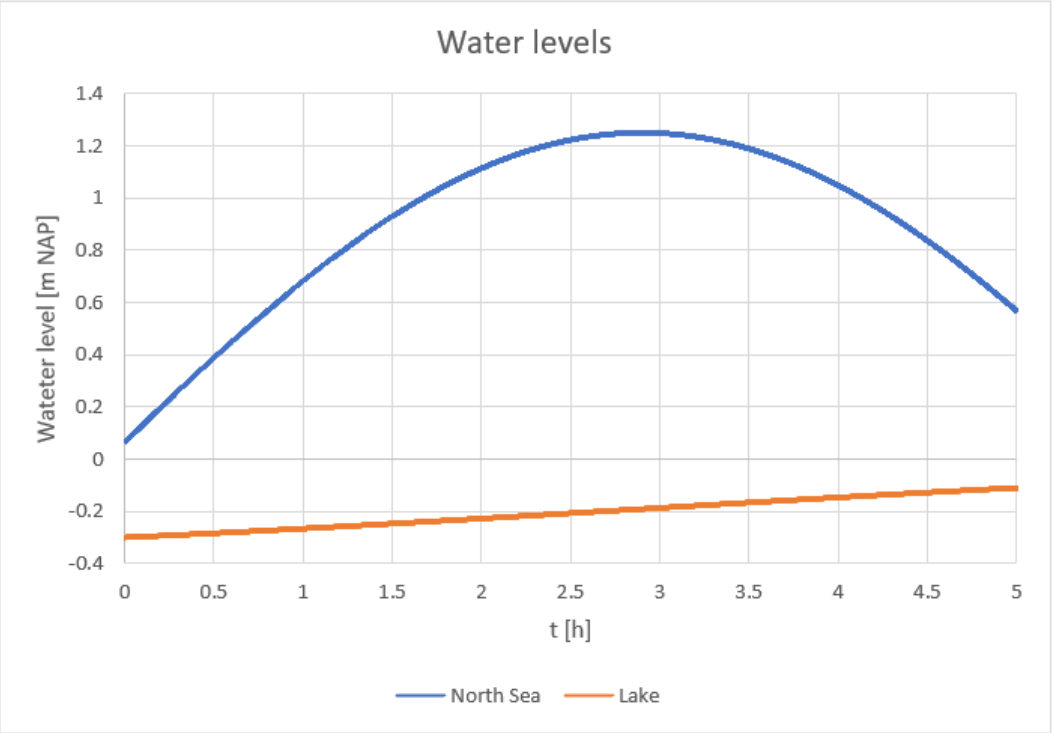

Figure 5.26: Water levels of North Sea and lake Grevelingen

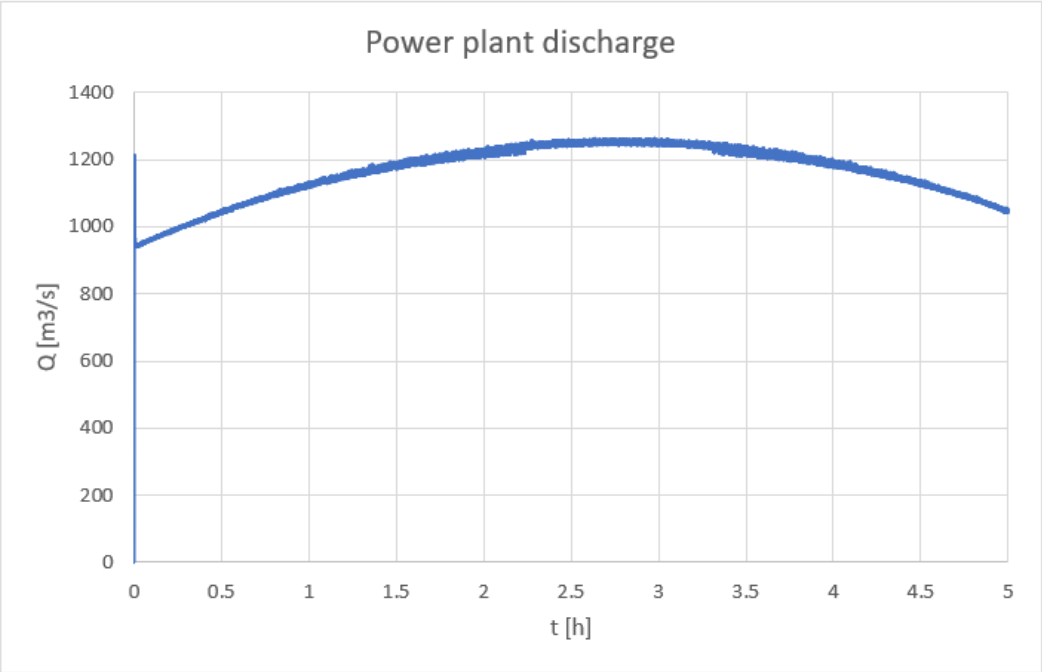

Figure 5.27: Total discharge of the power plant

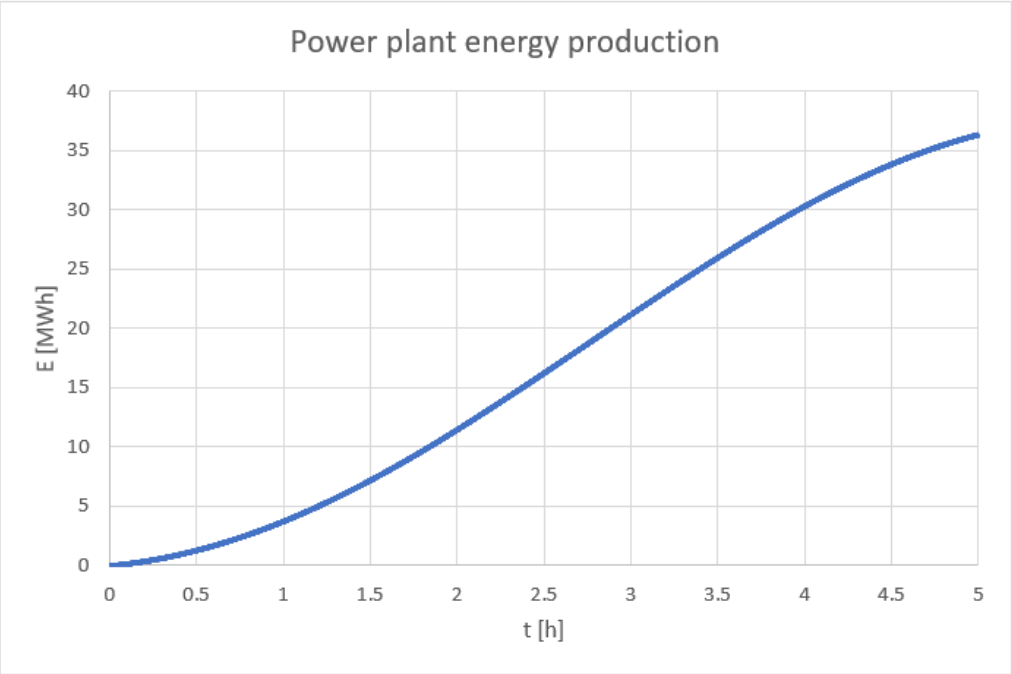

Figure 5.28: Energy production of the Brouwersdam in five hours of flood generation

6 Discussion of Results

It is possible to observe a few common trends in the experimental results, for all three static head differences. In fact, as expected, the flow rate increases faster adopting the two kickstart strategies, with and without frequency controller, with the frequency-controlled one being the faster of the three. This is due to the ability of the system to accelerate the drivetrain faster, as shown in the shaft speed graphs. In addition, it can be noted how, for the frequency-controlled strategy, the flow rate condition of $80\frac{m^3}{s}$ to switch the system to generation mode is probably not suited in the case of a static head of 0.5 m. In fact, the flow rate tends to "overshoot", trying to reach a higher equilibrium value, due to the higher shaft speed the system is rotating at. Once the frequency is switched back to the one with a synchronous speed of 13 rpm, the flow rate drops to a lower equilibrium value. The speed with which the system slows down is dependent on its total inertia. This suggests that it could be preferable to implement different flow rate conditions, depending on the static head value, when the system has to be started. It can also be observed how, with the kickstart strategy, the system struggles to accelerate around the synchronous speed. This is due to a drop in the mechanical torque provided by the motor after the shaft speed reaches 11.7 rpm, reaching values close to 0 when approaching 13 rpm. This has been the main reason to implement the kickstart strategy with the frequency controller. Indeed, working at higher frequency, the frequency-controlled system accelerates faster and up to higher speeds. Another thing to note about the kickstart strategy is that it presents a power demand peak during the start-up. This is caused by the high increase in mechanical torque in the speed range that goes from 0 to 11.7 rpm, where the system reaches the breakdown torque, which is equal to 2.8 times the rated torque. For pumps that are coupled to a motor without a frequency controller, this problem is usually solved with the use of a "soft starter", an electronic device that reduces the current surge at start-up. This in turn reduces the torque, which leads to a slower start. However, this approach has not been considered in this research. The kickstart procedure with frequency controller shows a first phase where the electrical machine works in the constant torque region at the rated torque (increasing power with shaft speed), and then a second phase where it works in the constant power region (horizontal power curve). Regarding the regular starting procedure, it can be observed how, for static head values of 0.5 and 1 meter, the system does not reach generating conditions in the first ten seconds after the opening of the gate-valves. Moreover, although it is able to do it for a static head of 1.5 meters, it does not reach a generation output close to the equilibrium value in the ten seconds threshold.

As expected, the higher the static head difference, the quicker the start-up of the system, and the higher the yielded power. The time needed for the flow rate to develop and for the system to reach the generating conditions, for the three static head scenarios and for the three starting strategies, has been resumed in the following tables. Since the equilibrium values of flow rate and power are reached

asymptotically, they will be considered reached at 90% of their equilibrium values. The values of the kickstart with frequency controller procedure at $t = 30\ s$ are used as equilibrium values.

Table 6.1: Flow rate and power data, Hs = -0.5m

Static head = -0.5 m				
	$Q_{t=30s}$	Time to reach 90% Q_{eq}	$P_{t=30s}$	Time to reach 90% P_{eq}
No kickstart	$65.1\frac{m^3}{s}$	$24.9\ s$	$121.1\ kW$	$> 30\ s$
Kickstart	$67.1\frac{m^3}{s}$	$12.7\ s$	$155.9\ kW$	$21.6\ s$
Kickstart with FC	$67.2\frac{m^3}{s}$	$5.2\ s$	$158.7\ kW$	$7.4\ s$

With a static head of $0.5\ m$ the only strategy able to reach nominal generating condition in less than 10 seconds is the frequency-controlled strategy. This is something worth of consideration, since usually tidal barrage power plants operation is started at the beginning of the tidal cycle, when the built static head is still small, as showed in figure 6.1.

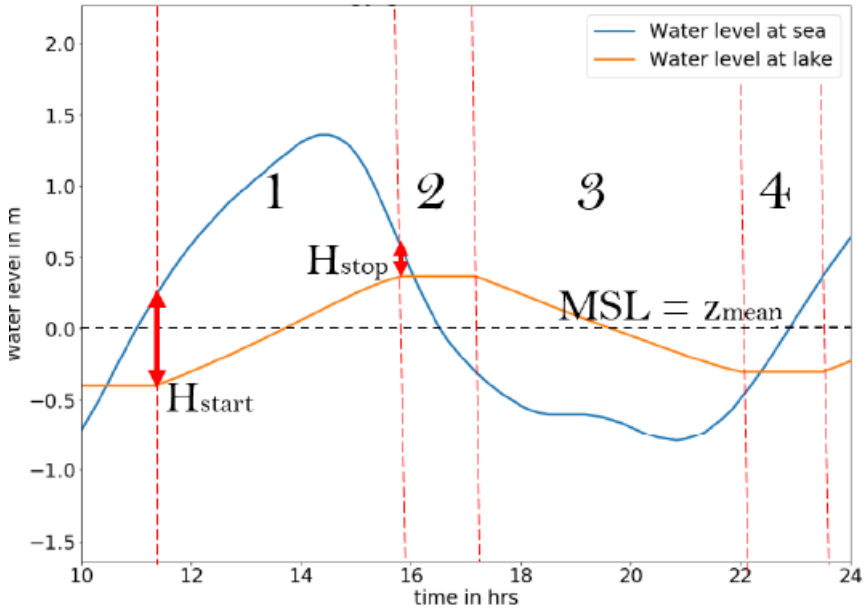

Figure 6.1: Hypothetical two-sided generation scheme for the Brouwersdam power plant [34]

Table 6.2: Flow rate and power data, Hs = -1 m

Static head = -1 m				
	$Q_{t=30s}$	Time to reach 90% Q_{eq}	$P_{t=30s}$	Time to reach 90% P_{eq}
No kickstart	$78.6\frac{m^3}{s}$	14.3 s	402.2 kW	19.5 s
Kickstart	$78.6\frac{m^3}{s}$	10.2 s	403.2 kW	15.4 s
Kickstart with FC	$78.6\frac{m^3}{s}$	5 s	403.7 kW	5.9 s

Even in the 1-meter static head case, the only viable strategy to reach nominal generation in less than 10 seconds is the one with frequency controller.

Table 6.3: Flow rate and power data, Hs = -1.5 m

Static head = -1.5 m				
	$Q_{t=30s}$	Time to reach 90% Q_{eq}	$P_{t=30s}$	Time to reach 90% P_{eq}
No kickstart	$87.8\frac{m^3}{s}$	10.9 s	652.5 kW	14.6 s
Kickstart	$87.8\frac{m^3}{s}$	8.7 s	652.6 kW	12.5 s
Kickstart with FC	$87.8\frac{m^3}{s}$	4.8 s	652.7 kW	4.9 s

For a static head of 1.5 meters, despite the simple kickstart strategy was able to reach generating conditions in the 10 seconds window, it was found to generate only 76% of the equilibrium value. Therefore, even for the last scenario, it is confirmed that the only strategy able to reach nominal generating conditions in less than 10 seconds is the kickstart with frequency controller. The power output is in line with other commercially used bulb turbines of similar size. For example, a single turbine in use at La Rance power plant (diameter 5.35 m) produces an average output of 4 MW with an average head of 8 meters [35]. According to simulations, a static head difference of 8 meters for the Brouwersdam case would yield about 7.7 MW with an 8-meters diameter turbine. However, it appears

that in all these scenarios the system is not working at the point with the highest power. This condition is realized when the system operates with a rate of reaction of 66.6%, meaning that the head jump across the impeller is 66.6% of the static head difference [25].

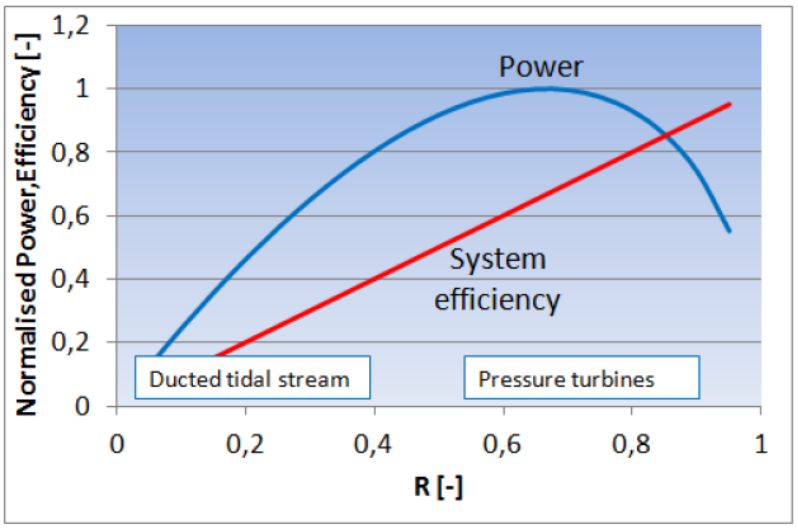

Figure 6.2: Normalized power and efficiency in function of the rate of reaction [25]

Knowing the rate of reaction R for the maximum power condition and the equilibrium flow rate in the configuration without the impeller it is possible to calculate the flow rate obtained in that condition, according to:

$$H_{net} = H_s * \left(1 - \left(\frac{Q_{pump}}{Q_{no\ pump}}\right)^2\right) \tag{6.1a}$$

$$\rightarrow\ Q_{pump} = \sqrt{(1-R)} * Q_{no\ pump} \tag{6.1b}$$

Once the Q-H point for the maximum power condition is known, it is possible to derive the equilibrium shaft speed from the characteristic curves of the pump-turbine. The table below resumes the maximum power conditions for the three static head scenarios.

Table 6.4: Conditions for maximum yielded power

Maximum Power Conditions				
H_s	$H_{pump,Pmax}$	Q_{Pmax}	n_{Pmax}	P_{max}
-0.5 m	-0.333 m	89 m3/s	19.5 rpm	290.73 kW
-1 m	-0.666 m	126 m3/s	28 rpm	823.21 kW
-1.5 m	-1 m	154.2 m3/s	34 rpm	1510.74 kW

This table shows that, despite the shaft speed of 13 rpm initially suggested by the project stakeholders as the rated speed of the turbines, a much larger power generation could be achieved adapting the shaft speed of the impeller to the values shown in the table, depending on the static head conditions. In addition, increasing the frequency of the motor/generator in order to increase the shaft speed of the system would probably allow the regular kickstart procedure to reach nominal generating condition faster, maybe even respecting the starting time constraint. On another note, the 10 second constraint for power generation has been set in order to design a starting procedure that would allow the power plant to quickly answer to rising demand coming from the grid. Although, using the two kickstart strategies, during the first few seconds the power plant would actually ask for energy from the grid in order to accelerate the water in the conduit. This could prove to be a problem from a grid balance point of view. If that would be the case, a possible solution could be the installation of batteries, in which the energy needed for the kickstart could be stored during turbine operation. The simulations showed the energy needed for the two kickstart procedures, at the three different static heads, which are summed up in the following table.

Table 6.5: Energy demand at start-up

Energy needed at start-up (single turbine)			
Static Head	0.5 m	1 m	1.5 m
Kickstart	0.71 kWh	0.5 kWh	0.39 kWh
Kickstart with FC	2.64 kWh	2.08 kWh	1.7 kWh

Given the short time the system has to operate in pump mode, the energy it would need to be started is rather low. Regarding efficiency, the mechanical efficiency was tracked during the simulations. The spikes/drops of the curves represent the system operation passing from the pump-assisted drainage to reverse turbine mode. In this intersection point the mechanical efficiency switches from definition (3.5a) to (3.5b), and since the mechanical power values are close to 0 the efficiency shows large spikes.

Table 6.6: Mechanical efficiencies for different static heads

Equilibrium Mechanical Efficiency	
Hs = -0.5 m	62.3%
Hs = -1 m	63.3%
Hs = -1.5 m	59.6%

As mentioned in section 2.2, the efficiency's low values could be explained with their derivation from the small impeller data.

6.1.1 Complete Power Plant

The simulation of the fifteen conduits gives some insight of the consequences of the power plant operation. The water level of lake Grevelingen increased by 20 cm during the first flood tide. This is still not the 40 cm oscillation that the Dutch government aims to reintroduce in the lake, but operating at higher shaft speeds as suggested in the previous paragraph could grant a higher total flow rate, allowing to restore the desired tidal range in lake Grevelingen. In 5 hours, the net energy balance shows a generation of 36 MWh, with an average of 7.2 MWh in one hour. This energy production would be able to power about 15000 households, according to an average household consumption in the Netherlands of 11.5 kWh per day [36]. The total flow rate reached a maximum value of 1220 $\frac{m^3}{s}$.

7 Conclusions and Recommendations

A 0-D model has been constructed to simulate the behavior of flow, its effects on the drive train, and the performance of a symmetrical pump-turbine in the ducts of a hypothetical power plant constructed in the Brouwersdam. In particular, it was of major interest to analyze the time needed by the system to start generating power, and see if it was at all possible to reach nominal generating conditions in less than 10 seconds. In order to find the better strategy to achieve this result, three different start-up procedures were designed: natural flow start, kickstart and kickstart implementing a frequency controller. The simulation results of a simplified configuration of the system were compared to the analytical solution of flow equations in order to test the solidity and accuracy of the solver used in the simulation environment (Matlab-Simulink). A simple free-flow test was run at the laboratories of HZ University of Applied Sciences to compare and validate the results of the simulative model. In conclusion, the large-scale model showed the key role of the kickstart strategy with frequency controller. If the 10 seconds time window for the start of power generation needs to be respected, the acceleration of the flow given just by the water level difference, and the shaft acceleration consequently generated just by the flow/impeller interaction, are not sufficient. Moreover, for most of the static head ranges that are generated at the Brouwersdam location, the kickstart procedure at fixed frequency would also be not sufficient. It is clear how, if the power plant should start operating when the built static head difference is still low, the use of the frequency-controlled start-up would be unavoidable. In addition, the use of a frequency controller would be required anyway because of the variable-speed nature of this application. According to the simulations, the strategy with frequency controller grants a start-up time of 7.4, 5.9 and 4.9 seconds at static head differences of 0.5, 1 and 1.5 meters respectively. The power generation in these scenarios is of 159, 403 and 652 kW respectively. These values are in the order of magnitude of the expected output of a turbine of this size, at a low static head difference. Although, these values are still far from the point of maximum power generation. The conditions for maximum power yield have been calculated, and the suggestion would be to operate the system at these conditions, despite the initial suggestion of a rated speed given by the project stakeholders. The higher shaft speed values could allow the normal kickstart procedure to respect the 10 seconds time limit for nominal power generation.

It is evident that a 0-D model has to deal with a relevant approximation, especially when comparing its results with the experimental setup of HZ University, given the complex geometry of the duct. In order to have a better insight of the topic and to be able to compare the model results to the experimental setup, generating 3-D geometries of the Brouwersdam conduits and the experimental setup pipe is suggested. Moreover, upgrading the setup of HZ University with more accurate sensors and a bypass duct with a pump would guarantee the performing of steady-state experiments and more precise results. In addition, more detailed information about the electric machine to be used in the Brouwersdam power plant would allow to model the power/generator more accurately, yielding more realistic results.

8 Bibliography

[1] J. van Berkel, J. Maas, S. van Schaick, A. Heutink, "*Climate Power Plant for Water Safety and Renewable Energy*", 2019

[2] L. Angelova, F. de Groen, "*Export Potential of the Brouwersdam Tidal power station*", Deltares, 2019

[3] J. T. Houghton et al., "*International Panel on Climate Change*", Climate change 1995, Cambridge University Press, 1996

[4] US, NREL, "*Climate change technology program, technology options: for the near and long term*", DOE/PI-0002; 2005.

[5] R. Mazumder, M. Arima, "*Tidal rhythmites and their implications*", Earth–Science Rev 2005

[6] F. O. Rourke, F. Boyle, A. Reynolds, "*Tidal energy update 2009*", Applied Energy Volume 87, pp. 398-409, Elsevier, Department of Mechanical Engineering, Dublin Institute of Technology, 2010

[7] R. H. Clark, "*Elements of tidal-electric engineering*", John Wiley and Sons, 2007

[8] R. F. Nicholls-Lee, S. R. Turnock, "*Tidal energy extraction: renewable, sustainable and predictable*", Science Progress 91, pp. 81-111, 2008

[9] I. G. Bryden, "*Tidal energy"*, Encyclopedia of energy, vol. 6, 2004

[10] L. Mooyaart, T. van den Noortgaete, "*Getijcentrale in de Brouwersdam Variantenstudie", Haskoning Nederland BV, 2010*

[11] V. Ramos, R. Carballo, M. Sanchez, M. Veigas, G. Iglesias, "*Tidal stream energy impacts on estuarine circulation*", Energy Conversion and Management, Volume 80, pp. 137-149, Elsevier, 2014

[12] F. T. Vriese, J. van Berkel, B. P. M. van Esch, A. W. Breukelaar, "*Evaluation of Fish Injury and Mortality Associated with scale models of the Pentair Fairbanks Nijhuis Modified Bulb turbine and the Water2Energy Cross Flow turbine*", Adviesbureau voor Bodem, Water en Ecologie, 2015

[13] M. H. van Saase, "*The Conceptual Design of a Tidal Power plant in the Brouwersdam",* Faculty of Civil Engineering and Geoscience, TU Delft, 2018

[14] J. van Berkel, T. Kraassenberg, P.Paulus, MIRT Grevelingen "*Tidal Power plant Brouwersdam: Project Outline"*, 2011

[15] Projectbureau Getijdencentrale Brouwersdam, "*Verslag van de precompetitieve fase*", 2015

[16] T. Wright, P. M. Gerhart, "*Fluid Machinery. Application, Selection and Design*", CRC Press, 2009

[17] D. Z. Haman et al., "*Selection of Centrifugal Pump Equipment*", University of Florida, 2021

[18] O. D. Thapar, "*Modern Hydroelectric Engineering Practice in India, Electro-Mechanical Works",* Indian Institute of Technology, 2020

[19] T. Ma, H. Yang, L. Lu, J. Peng, "*Pumped Storage-Based Standalone Photovoltaic Power Generation System: Modelling and Techno-Economic Optimization*", Applied Energy, Volume 137, pp. 649-659, Elsevier, 2015

[20] R. Jiang, J. Wang, Y. Guan, "*Robust Unit Commitment with Wind Power and Pumped Storage Hydro*", IEEE Transactions on Power Systems, Volume 27, pp 800-810, IEEE, 2012

[21] B.P.M. van Esch, "*Lecture 9 - Pumped Storage 1*", 4BM10 Hydraulic Turbomachines Course, TU/e, 2019

[22] Z. Zhang, "*Hydraulic Transients and Computations",* Springer, 2019

[23] M. Stewart, "*Surface Production Operations, Volume 3: Facility Piping and Pipeline System*", Elsevier, 2016

[24] D. J. Zigrang, N.D. Sylvester, "*A Review of Explicit Friction Factor Equations*", Journal of Energy Resources Technology, Jun 1985, 107(2), pp. 280-283, 1985

[25] J. van Berkel, "*Best Available Technique for Ultra Low Head Tidal and River Hydropower",* EWTEC, 2015

[26] B.P.M van Esch, "*Thermal and Fluid Engineering Reader*", Department of Mechanical Engineering, TU/e, 2017

[27] K. Sang-Hoon, "*Electric Motor Control*", Elsevier, 2017

[28] G. Musgrove et al., "*Compression Machinery for Oil and Gas*", Elsevier, 2019

[29] A. Joshi et al., "*Running Torque of Slow Speed Two-Point and Four-Point Contact Bearings*", Lubricants, MDPI, 2015

[30] L. C. Burrill, W. Robson, "*Virtual Mass and Moment of Inertia of Propellers*", TU Delft, 1962

[31] D. M. MacPherson, V. R. Puleo, M. B. Packard, "*Estimation of Entrained Water Added Mass Properties for Vibrational Analysis*", HydroComp Inc., 2007

[32] D. M. MacPherson, V. R. Puleo, M. B. Packard, "*Blade Area Ratio Defined",* HydroComp Inc. Technical Report 135, 2007

[33] European Commission, "*Commission Regulation 2019/1971*", Official Journal of the European Union, 2019

[34] A. Rijnink, "*A new generation flood defences: dam with tidal power station including pumping capacity*", TU Delft, 2020

[35] Tethys, "*OES Environmental Metadata: La Rance Tidal Barrage",* Tethys.pnnl.gov

[36] Environment central and RVO, 2017

Appendix A - Nijhuis Experimental Data

The experimental data collected by Nijhuis is used to construct the Q-H and Q-P characteristic curves of the pump-turbine for different shaft speeds. All the measurements relative to flow rate, manometric head, and power have been scaled to different shaft speed values, from 100 rpm to 900 rpm in both directions, with intervals of 100 rpms (while the impeller diameter is kept constant) according to the scaling laws for pumps.

The Q-H characteristic curves are shown in the picture below:

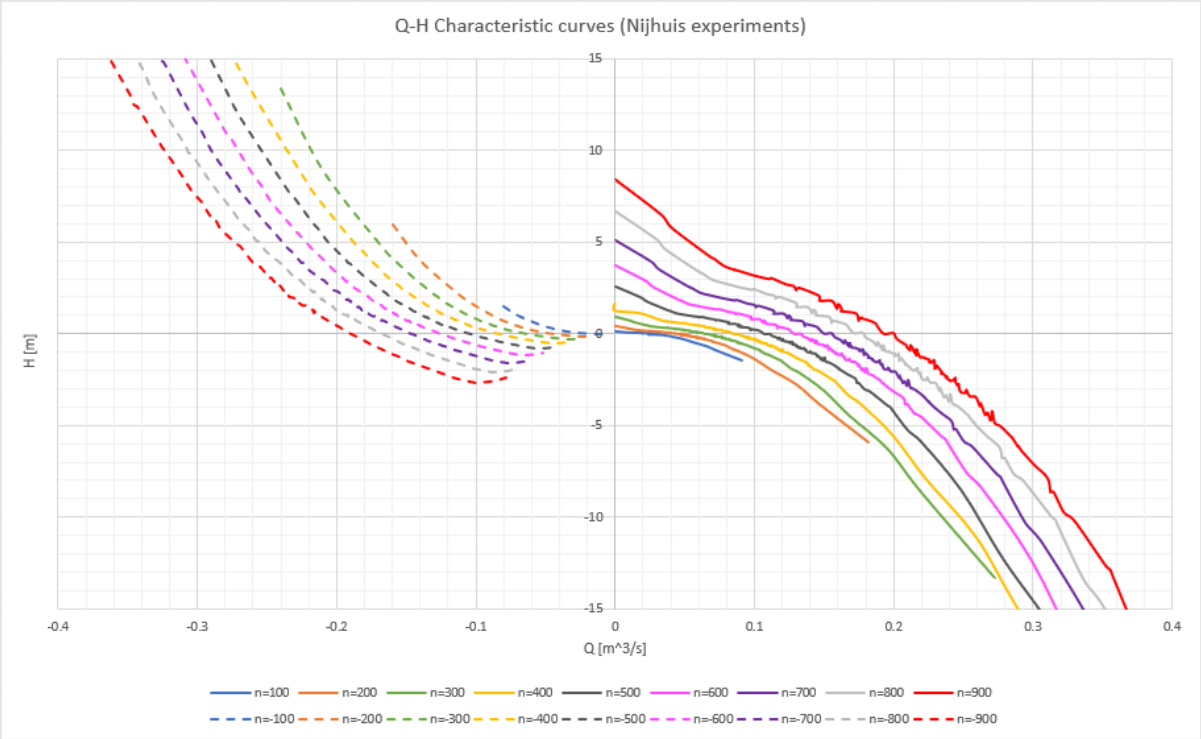

Figure A.1: Q-H characteristic curves of the pump-turbine (Nijhuis experimental setup)

The visible fluctuations in the curves are due to small inaccuracies in the measurements of head and flow rate. These inaccuracies become more noticeable once they are scaled up to higher shaft speed curves. The curves are not exactly symmetrical, as the pump-turbine housing (bulb) and connecting pipes introduce some asymmetries. The Q-P curves are also shown in the picture below.

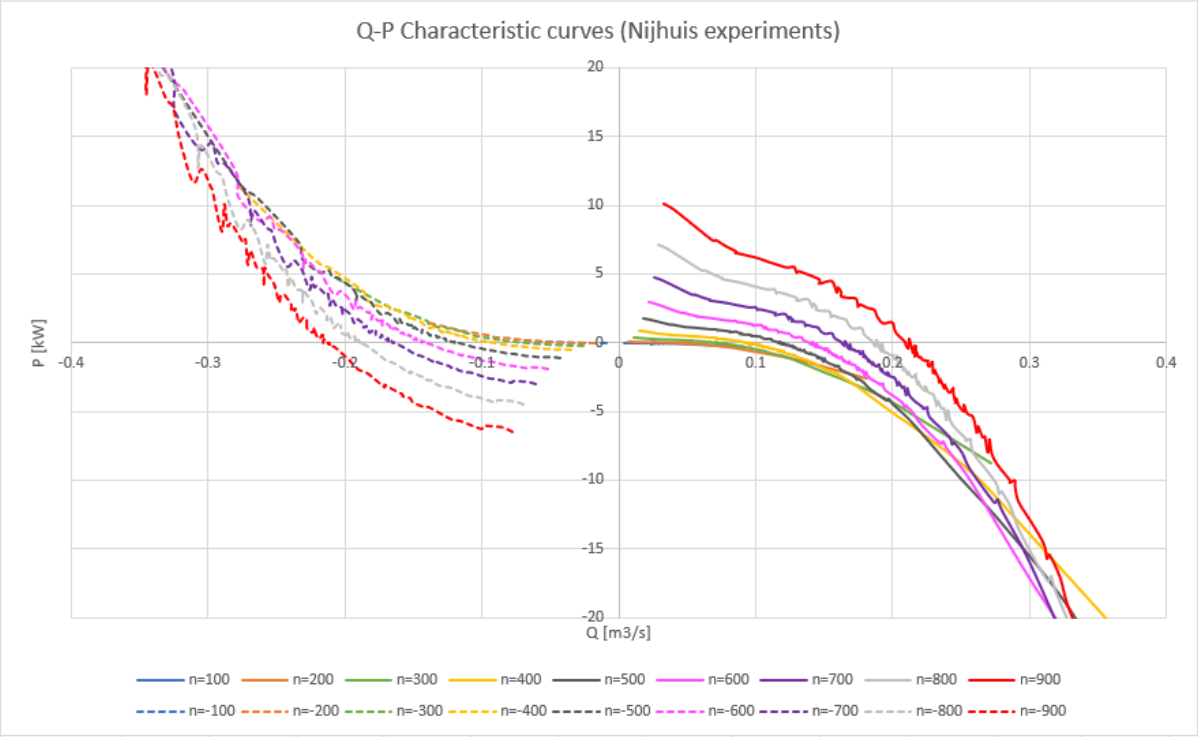

Figure A.2: Q-P characteristic curves of the pump-turbine (Nijhuis experimental setup)

Appendix B – EWTEC 2021 Paper

Kickstart Procedure of a Tidal Power Plant

M. Capozucca, Dr. ir. J. van Berkel, Dr. B. P. M. van Esch

Abstract—**1 Barrage type tidal power plants can provide flexibility to the electricity grid thanks to the ability of hydraulic machines to be operated both as pumps and turbines. The added value of a fast switching tidal power plant is investigated within the project "Playing with Current(s)" (PwC), which is executed by universities, national knowledge institutes, utility companies and turbine manufacturers in The Netherlands.**

Necessary condition for grid-stabilisation is that a power plant can come on-line, from zero to full power within a very short time span. As in The Netherlands power dispatching is done every 15 minutes, within the PwC project the maximum spin-up time is set ambitiously at 10 seconds.

This paper covers the investigations of the transient behaviour of a tidal pump-turbine during start-up. The governing equations for the ramping-up of the turbine are outlined. The drive train equation of motion involves the hydrodynamic torque exerted by the water flow on the impeller and the electromagnetic torque of the motor/generator. The hydrodynamic torque has been derived from measurements of a prototype pump-turbine under laboratory conditions, in four quadrants (pump and turbine mode, forward and reverse). The head-flowrate-power curves are scaled for the case of an 8-m diameter tidal pump-turbine. This kind of hydraulic machine may be used for a 25-MW tidal power plant application in the Brouwersdam (Region of Zeeland, Western Netherlands). Special attention is given to inertia effects of the moving water column inside the 98-meters long turbine duct and to the rotating turbine impeller, shaft and to the electrical machine.

As preliminary tests have shown that the full-load, passive ramping-up time of the tidal power plant is in the range of 20-30 seconds, two "kickstart" procedures have been proposed and investigated. During kickstart, the turbine is first operated as a pump to accelerate the water mass inside the duct to the desired full-load speed, and then switched from pump to turbine operation.

The paper covers the theory of the kickstart tidal turbine and the non-linear model calculations. Results are compared with the analytical solution of a simplified flow differential equation and with tests done with the Tidal Turbine Test Setup at HZ University of Applied Sciences.

Results show that a kickstart with a frequency controller may reduce the ramping-up time to less than 10 seconds, which is sufficiently fast to operate the tidal power plant as a grid stabilisation facility. This could allow a utility company to use the tidal power plant for electricity trading purposes, which is particularly interesting given its predictability. It results in tidal power offering a 10% added value over less predictable renewable energy sources like wind and solar power.

Keywords—**Grid balancing, Kickstart, Tidal power.**

I. Introduction

IN 1954 the Dutch government started the "Deltawerken" program, a series of civil engineering projects aimed at protecting the coastal area of South-Holland and Zeeland from North Sea floods, like the disastrous flood that hit the area in 1953. One of the artificial basins created in this instance was lake Grevelingen, separated from the North-Sea by the Brouwersdam. Completed in 1965, this dam contributed to the

This work was initiated by the HZ University of Applied Sciences and supported by the Dutch RAAK PRO program under SiA grant. In addition, the work was supported by the experimental data collected by the turbine manufacturer Nijhuis Pompen, the Ministry of Infrastructure and Water Management, the regional energy and network companies, infrastructure companies and environmental research institutes.

M. Capozucca is Master student at Eindhoven University of Technology, Faculty of Mechanical Engineering, The Netherlands, email: m.capozucca@student.tue.nl

J. van Berkel is Professor Renewable Energy in Delta Area's at HZ University of Applied Sciences, Vlissingen, The Netherlands, email: berk0018@hz.nl

B.P.M. van Esch is Associate Professor at Eindhoven University of Technology, Faculty of Mechanical Engineering, The Netherlands, email: B.P.M.v.Esch@tue.nl

water safety management of the area. However, its ecological conditions have been deeply affected since the water recirculation has been hindered by the dam, and therefore the quality of life of flora and fauna of the area has been negatively influenced. Consequently, the touristic and economic appeal of the region has been affected as well. For all these reasons, the Dutch government decided to reintroduce a dampened tide in the lake via new openings in the dam, and this intervention could be coupled with the installation of reversible bulb pump-turbines. These hydraulic machines would have the primary role of managing the water safety of the area by regulating the water level in the lake. In fact, the sea level rise expected in the next decades would slowly but surely make it more difficult to drain water from the lake back to the sea, since the static head difference between the North Sea and Lake Grevelingen during flood tides will tend to increase, while the one during ebb tide will decrease instead. The use of pump-turbines would also give the possibility to recover some of the energy spent during pump operation, working as tidal turbines. The analyzed configuration considers 98-meters long conduits with 8-by-8 meters square cross-sectional area. The project framework "Playing with current(s)" is using this research as a case study to evaluate this technical solution for different applications in many locations around the globe. The power plant could also play an important role in the stabilization of the energy grid, being able to operate as an energy sink, storing energy in form of water head (pumped storage), or energy producer (turbine operation). It is of utmost importance that, in order to be able to be competitive on the energy market and respond to the grid instabilities, the power plant is able to start operating in turbine mode as quickly as possible. In particular, a 10 seconds window has been established. In the usual start-up procedures of such systems, the flow and shaft accelerations rely just on the static head difference between the two water columns, but in order to comply with the mentioned time restriction, it could be important to "kickstart" the system, accelerating the flow with pump operation to reach generating conditions faster than with just natural flow. This can be done at constant frequency, or varying the frequency during the start-up with the use of a frequency converter. All of these strategies have been investigated, with the use of a 0-D, time dependent model.

II. MODEL DESCRIPTION

A. *Governing equations*

The system behavior is modelled by a 0-D, time-dependent numerical model (fourth rank Runge-Kutta method) in a Matlab-Simulink environment. The water inertia is described by the following equation, derived from Newton's second law of motion [1].

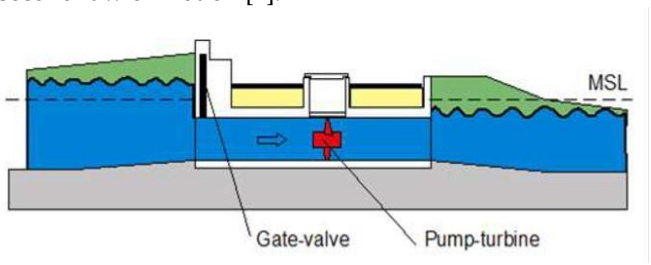

Fig. 1. Sketch of the duct, pump-turbine and water bodies.

$$\frac{dQ}{dt} = \frac{gA}{L}\left(\Delta H_s + H_p\right) - \frac{\frac{fL}{D_h} + K_i + K_o}{2AL} Q^2 \qquad (1)$$

where:

- Q — Volumetric flow rate [m^3/s]
- g — Acceleration of gravity [m/s^2]
- A — Duct cross-sectional area [m^2]
- ΔH_s — Static-head difference [m]
- H_p — Pump-turbine head [m]
- f — Darcy friction factor [-]
- L — Conduit length [m]
- D_h — Hydraulic diameter [m]
- K_i, K_o — Inlet and outlet K factors [-]

The first term on the right-hand side of the equation (1) represents the acceleration of the flow rate due to the static head difference and pump-turbine head, whereas the second term represents the flow rate variation due to friction, inlet and outlet losses.

The water levels are adjusted at each timestep according to:

$$\frac{dH_s}{dt} = \frac{Q}{A_s} \qquad (2)$$

where A_s is the surface area of the body of water considered.

The drivetrain dynamics is modelled via the following equation.

$$T_h + T_m - T_f = \left(I_p + I_m + I_w\right) * \dot{\omega} \qquad (3)$$

where:

- T_h Hydraulic torque [Nm]
- T_m Electric machine torque [Nm]
- T_f Bearings friction torque [Nm]
- I_p Pump moment of inertia [kg*m²]
- I_m Elec. motor moment of inertia [kg*m²]
- I_w Added mass mom. of inertia [kg*m²]
- $\dot{\omega}$ Angular acceleration [rad/s²]

Equations (1), (2) and (3) are coupled and solved for the variables Q, H_s, and $\dot{\omega}$ (T_h in equation (3) is a function of Q and shaft speed).

To evaluate H_p in equation (1), experimental data has been used. The pump-turbine used during the experiments is an impeller with five symmetrical blades, meaning that the blades have a symmetrical profile at each section.

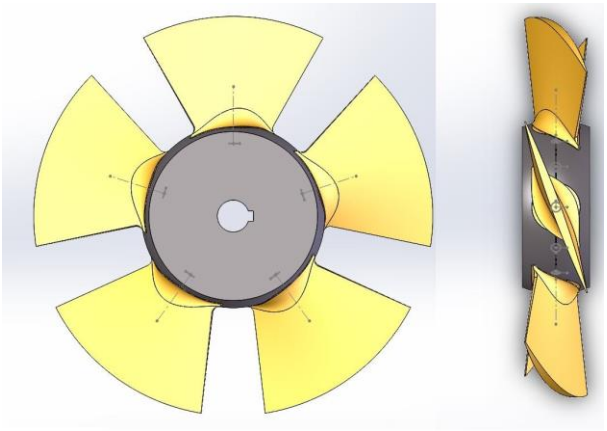

Fig. 2. Front and side view of the experimental setup impeller.

Symmetrical impellers represent a compromise between pump and turbine operation, theoretically providing the same efficiency between pump and reverse pump mode, and turbine and reverse turbine mode. The pump-turbine 4-quadrant characteristics curves have been drawn (shown in the figure below for different shaft speeds).

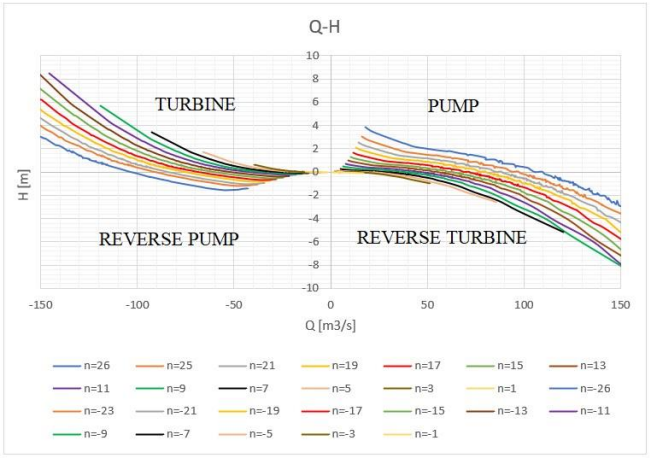

Fig. 3. Characteristic curves for different shaft speeds (1 rpm to 26 rpm) for the 8-m diameter pump-turbine.

The curves in Figure 3 are not exactly symmetrical, as the pump-turbine housing (bulb) and connecting pipes presented some asymmetries.

The different characteristics are scaled by the model for the case of an 8-meters in diameter pump-turbine. and according to the simulated shaft speed, following the pump scaling laws:

$$Q_2 = Q_1 * \left(\frac{n_2}{n_1}\right) * \left(\frac{D_2}{D_1}\right)^3 \quad (4a)$$

$$H_2 = H_1 * \left(\frac{n_2}{n_1}\right)^2 * \left(\frac{D_2}{D_1}\right)^2 \quad (4b)$$

$$P_2 = P_1 * \left(\frac{n_2}{n_1}\right)^3 * \left(\frac{D_2}{D_1}\right)^5 \quad (4c)$$

$$T_2 = T_1 * \left(\frac{n_2}{n_1}\right)^2 * \left(\frac{D_2}{D_1}\right)^5 \quad (4d)$$

Since the measurements of the manometric head in the experiments could not be used, it has been calculated as

$$H_p = H_s + H_{loss} \quad (5a)$$

for positive flow rate, and as

$$H_p = H_s - H_{loss} \quad (5b)$$

for negative flow rate. The losses term H_{loss} has been estimated using [2]:

$$H_{loss} = f\frac{L}{D_h} * \frac{\left(\frac{Q}{A}\right)^2}{2g} \quad (6)$$

The Darcy friction factor has been estimated using Serghide's solution to Colebrook's equation, stating [3]:

$$f = \left[A - \frac{(B-A)^2}{C - 2B + A}\right] \quad (7)$$

The coefficients A, B and C are defined as

$$A = -2\log\left(\frac{\varepsilon}{3.7 * D_h} + \frac{12}{Re}\right) \quad (8a)$$

$$B = -2\log\left(\frac{\varepsilon}{3.7 * D_h} + \frac{2.51A}{Re}\right) \quad (8b)$$

$$C = -2\log\left(\frac{\varepsilon}{3.7 * D_h} + \frac{2.51B}{Re}\right) \quad (8c)$$

where ε is the pipe surface roughness and Re is the Reynolds number defined as:

$$Re = \frac{\rho\frac{Q}{A}D_h}{\mu} \quad (9)$$

The Darcy friction factor term of equation (1) has been evaluated with equation (7) as well. The K factors in the losses term of equation (1), representing the fraction of kinetic energy lost at the sharp inlet and outlet sections, have been evaluated as 0.5 and 1 respectively. In conclusion, the model is able to evaluate the flow rate from equation (1) at each timestep and adjust the water levels of the two water columns accordingly.

The hydraulic torque has again been estimated using the scaled experimental result. For the evaluation of the electro-mechanical torque, three starting procedures have been studied:

1. Natural flow start
2. Kickstart with fixed frequency
3. Kickstart with frequency controller

As the precise electrical machine has not been defined yet, the characteristics of an asynchronous (induction) motor/generator have been modelled. In case of natural flow start, the motor torque has been set to 0 until the system reaches the synchronous speed, assumed as 13 rpm. After the synchronous speed, the machine starts working as a generator and the torque is derived from the following curve.

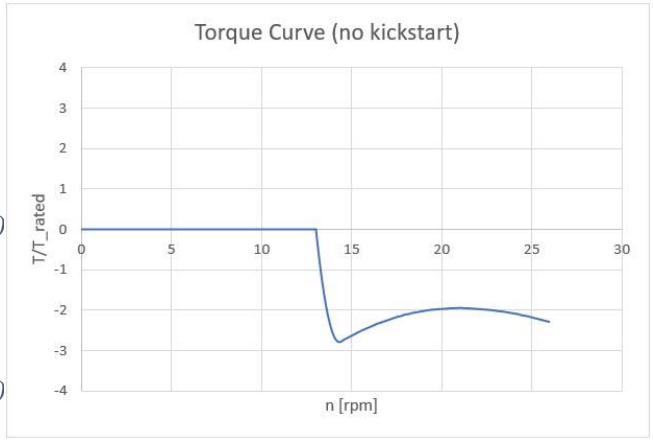

Fig. 4. Scaled mechanical torque curve for the natural flow start in function of shaft speed.

In the kickstart with fixed frequency, the machine starts working as a motor to speed up the shaft. The motor region curve mirrors exactly the generator region of Figure 4.

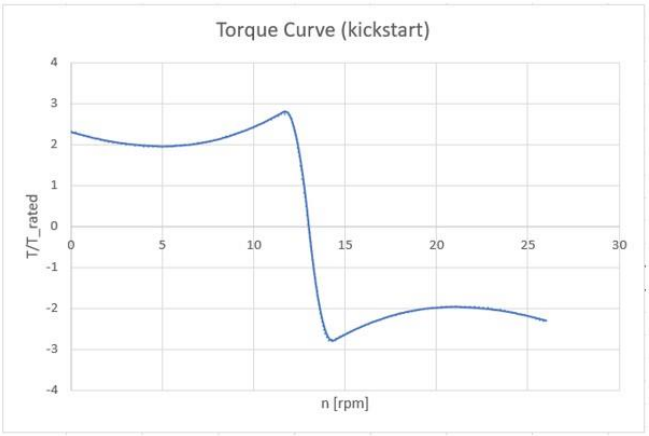

Fig. 5. Scaled mechanical torque curve for the fixed-frequency kickstart procedure in function of shaft speed.

The third starting strategy involve a frequency controller, able to continuously vary the frequency of the current fed to the machine along with the shaft speed of the drivetrain. This allows to reach higher shaft speeds and therefore accelerate the system faster. Once the flow rate reached values comparable to those of the generating conditions (about 80 m^3/s) the frequency is switched back to the same frequency of the normal kickstart procedure, hence the system starts generating energy. Increasing the frequency alone would reduce the torque magnitude of the machine, so it is necessary to also increase the stator voltage of the machine according to [4]:

$$\frac{V_s}{f_s} = const. \tag{10}$$

This can be done until the rated voltage of the machine is reached (constant torque region). Increasing the frequency even more would cause the torque to drop in magnitude (constant power region). The resulting graph for the torque is shown in Figure 6.

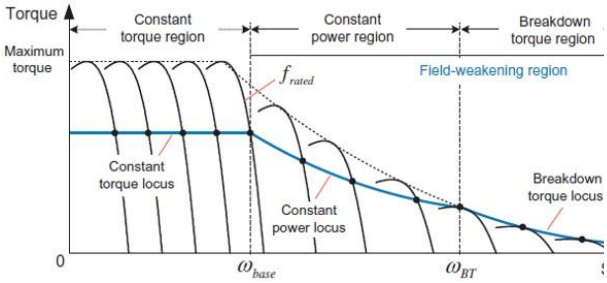

Fig. 6. Motor torque curve as a function of speed for operation with frequency controller [4].

In the constant torque region, the machine is assumed to work at the rated torque, since continuous operation at higher values would cause overheating problems. In order to obtain a proper value for the rated torque, it has been assumed that the system in pump mode should handle the same flow rate it would handle in turbine mode with a 1-meter head. From preliminary simulations has been found that this flow rate would be around 80 m^3/s. From the characteristics curve of the pump, it emerges that this condition is verified at 25 rpm, with a power need of 1276 kW. This value has been assumed as the power in constant power region, and the torque in all the points of this region have been calculated via the toque-power relation:

$$T = \frac{P}{n} \tag{11}$$

The value of the speed at ω_{base} is assumed to be at 13 rpm. The torque in that point, assuming that the grid frequency is equal to the one of the motor, is equal to:

$$T_{13} = \frac{1276\ kW}{13 * \frac{\pi}{30}} = 937.33\ kNm \tag{12}$$

Therefore, this value has been assumed as the rated torque for the torque curves of all three strategies.

Regarding the frictional torque of the bearings, as of today there are no details about technical specifications that deeply influence it (such as loads, dimensions of the shaft, type of lubricants, etc.). Consequently, information to evaluate the order of magnitude of the bearings torque has been taken from literature. It has been found that this usually is in the range of tens or hundreds Nm [5], whereas the system has been showing total torque values on the shaft in the order of 10^5 Nm from preliminary simulations. For this reason, the frictional torque of bearings in equation (3) has been assumed negligible.

Regarding the inertia of the drivetrain, the moment of inertia of the impeller has been calculated through CAD files, and is equal to 250000 $kg \cdot m^2$. The electrical machine moment of inertia has been estimated via a market research. Tidal applications usually utilize electrical machines similar to the wind power applications. In particular, the Finnish company The Switch produces a 4 MW electrical machine with a rated speed of 15.6 rpm and a moment of inertia of 110000 $Kg \cdot m^2$. This value has been assumed as the moment of inertia of the electrical machine of the model. The last term to be evaluated is the added mass moment of inertia. This term represents the moment of inertia of the fluid entrained between the impeller blades, which obviously has a relevant effect on the dynamics of the system. A model developed by the company HydroComp for marine propellers has been used to estimate this term. This model aimed to perfect previous models to estimate the added mass moment of inertia, mainly the one developed by Burrill and Robson in 1962 [6]. The proposed formula for the estimation of the added mass moment of inertia is [7]:

$$I_w = C_{IE} * \rho * D^5 \tag{13}$$

where:

$$C_{IE} = C_1 * EAR * \frac{P}{D} - C_2 \tag{14}$$

In addition:

- C_1 and C_2 are experimentally derived coefficients dependent on the number of blades (Z)
- EAR is the expanded area ratio
- P/D is the pitch/diameter ratio

The pitch of the impeller is defined as the distance the impeller would advance in one

rotation in a solid material. It is calculated according to the following formula:

$$P = 0.7\pi * D * \frac{x}{y} \quad (15)$$

where x is the blade width and y is the height difference between the leading and trailing edges. Both of these are measured at the blade section corresponding to 70% of the total radius.

The EAR is derived from the DAR, which is the total area of the blades if they could be unattached from the hub and brought to zero pitch, divided by the whole area of the propeller disc. The DAR is measured from the CAD files. The EAR is defined as the area obtained by flexibly distributing the DAR on a flat surface such as all sections would be parallel, divided by the propeller disc area. It is calculated from the DAR according to [8]:

$$EAR = 0.34 * DAR * \left(2.75 + \frac{DAR}{Z}\right) \quad (16)$$

Initially, the moment of inertia of added mass has been evaluated for a small-scale impeller which will be used for experimental validation of the model. This is a 5-bladed impeller of 30 cm in diameter with symmetrical blades. The pitch has been measured using the CAD files. This geometry is then scaled up to the 8 m diameter one, maintaining geometric similarity. This means that the EAR and the pitch/diameter ratio would remain constant, therefore C_{IE} is unaffected by the scaling of the impeller. The resulting value for I_w is 33456 kg·m².

In conclusion, the angular acceleration is calculated by the model from equation (3) at each timestep.

B. *Numerical solver*

The fourth order Runge-Kutta method has been chosen as the numerical method to solve equations (1), (2) and (3) in their integral form, for the variables Q, $\dot{\omega}$, and H_s. The problem to solve is an initial value problem in the form of:

$$y' = f(t, y), \quad y(t_0) = y_0 \quad (17)$$

Where y(t) is the unknown function of time we want to approximate, and the function f and the initial conditions y_0 and t_0 are known. For a given timestep dt, the method calculates the function y at the next timestep as [9]:

$$y_{n+1} = y_n + \frac{1}{6} dt * (k_1 + 2k_2 + 2k_3 + k_4) \quad (18)$$

Where:

$$k_1 = f(t_n, y_n) \quad (19a)$$

$$k_2 = f\left(t_n + \frac{dt}{2}, y_n + dt * \frac{k_1}{2}\right) \quad (19b)$$

$$k_3 = f\left(t_n + \frac{dt}{2}, y_n + dt * \frac{k_2}{2}\right) \quad (19c)$$

$$k_4 = f(t_n + dt, y_n + dt * k_3) \quad (19d)$$

Being a fourth-order method, the local truncation error (the error caused by one iteration) is in the order of $O(dt^5)$, and the total truncation error (the accumulated error of all iterations) is in the order of $O(dt^4)$.

III. MODEL VALIDATION

C. *Numerical validation*

In order to check the solver's accuracy and partially the reliability of the model, the analytical solution of a simplified version of equation (1), excluding the pump head term, has been compared to the simulation results of the model in the same configuration (no pump-turbine, shaft and motor-generator). The simplified version of equation (1) is:

$$Q' = \frac{gA}{L}\Delta H_s - \frac{\frac{fL}{D_h} + K_i + K_o}{2AL} Q^2 = b - aQ^2 \quad (20)$$

with a and b constants.

This equation represents the case of a flow through a duct with constant water level difference of 1 meter and constant friction factor f=0.0158, derived from the equilibrium value.

The analytical solution of the initial value problem with the initial condition Q(0)=0 of equation (20) is in the form:

$$Q(t) = \sqrt{\frac{b}{a}} * \frac{e^{2\sqrt{ab}t} - 1}{e^{2\sqrt{ab}t} + 1} \quad (21)$$

The analytical solution of the non-linear ODE and the simulation results are compared in

Figure 7, whereas their difference in absolute value is presented in Figure 8.

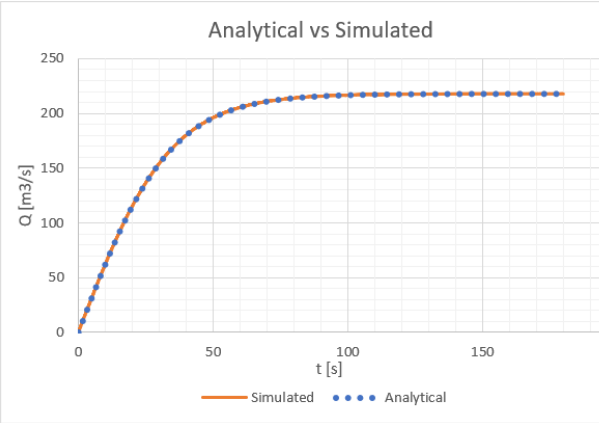

Fig. 7. Analytical solution of equation (20) compared with simulation results.

As presented, the model generates a very good approximation of the analytical solution for the flow development in a conduit between two water columns of different head.

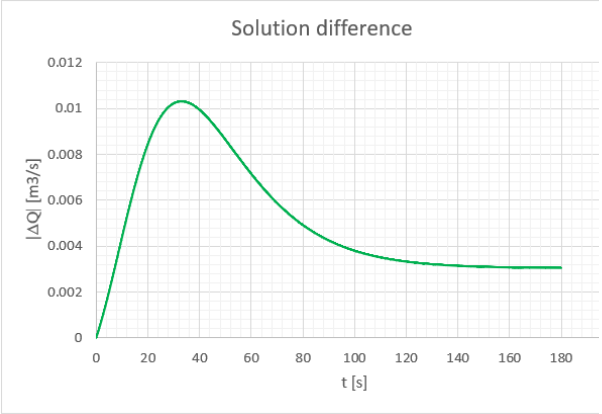

Fig. 8. Difference between analytical solution and simulation results, in absolute value.

D. *Experimental validation*

Experimental validation has been performed with the use of the experimental setup managed at HZ University of Applied Sciences. It consists of two water tanks connected by a convergent-divergent duct. A model-scale pump-turbine is placed at the section with smallest cross-sectional area. The results of this model have been compared to a small-scale version of the model presented in section II. The dimensions and inertias of the small-scale model are:

- Constant duct diameter D=0.3 m
- Duct length L=4.38 m
- Impeller moment of inertia I_p=0.012 kg·m²
- Added mass moment of inertia I_w=2.481*10^{-3} kg·m²
- Motor-generator moment of inertia I_m=0.126 kg·m²

The moment of inertia of the impeller has been provided by the manufacturer, whereas the moment of inertia of the motor-generator has been read from the technical specifications of the machine used for the experimental setup. The added mass moment of inertia has been calculated with formula (13)

In order to compare the results of the simulations, that are derived from steady-state experiments, to the unsteady ones of the experimental setup of HZ University, the Strouhal number has to be evaluated. This non-dimensional number is the ratio between the inertia effects due to the local acceleration of the flow and those due to the convective acceleration [10]. As such it is a measure of the rate of change of the flow rate relative to the convection of momentum within the pump:

$$St = \frac{du/dt}{u/T} = \frac{du/dt}{u^2/S} = \frac{\frac{1}{A}\frac{dQ}{dt}}{\frac{Q^2}{A^2 S}} \qquad (22)$$

where:

- u is the axial flow velocity
- T is the residence time of the fluid in the pump
- S is the axial length of the pump
- A is the cross sectional area

If the Strouhal number is smaller than 0.1, the effects of the local acceleration are considered negligible, and the pump-turbine operation can be considered quasi-steady, therefore comparable to the model results. The Strouhal number as a function of time for the model validation experiment is reported in the graph below.

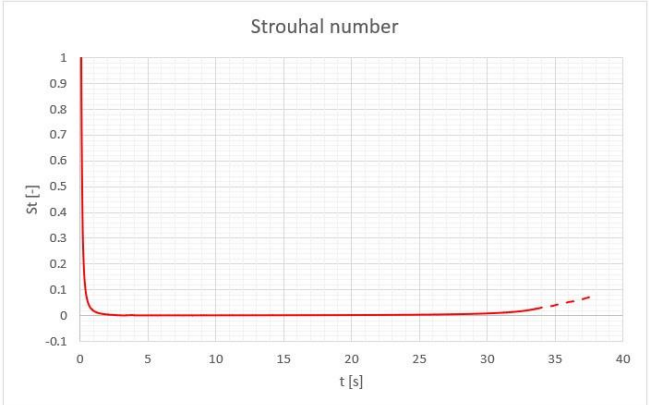

Fig. 9. Strouhal number as a function of time.

It is clear from the graph of Figure 9 that the Strouhal number condition is respected for most of the 38-seconds experiment (specifically, from t=0.5). At the beginning of the experiment the Strouhal number reaches very high values, since the flow rate is close to zero, whereas its rate of change is significant. At the end of the experiment, the Strouhal number is ill-defined since both the flow rate and the flow rate variation assume values close to zero.

Since the model used is 0-dimensional, it has not been possible to reproduce the varying geometry of the duct of the experimental setup. Instead, a circular duct with a constant diameter of 30 cm (equal to the impeller's diameter) has been represented. A free-flow experiment was performed, opening the gate-valves and letting the flow develop because of the water head difference of the two tanks, and putting the impeller in motion according to the drive train equation (3), with no motor torque and bearings frictional torque. Comparison of results for the tanks water levels are shown below.

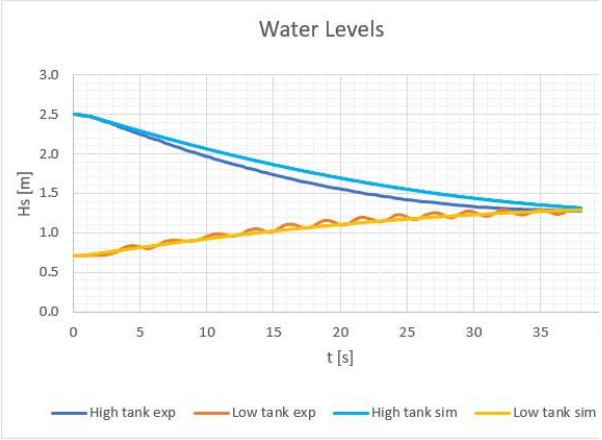

Fig. 10. Comparison of tanks water level as a function of time between experimental setup and model.

Since the experimental setup was not equipped to measure the flow rate, this has been calculated as the derivative of the water level of the high-water tank multiplied by its surface area. In addition, the speed of the pump was compared between model and experiments. The discrepancies in flow rate and shaft speed can be explained by the different geometry between the real setup and the modelled one. In fact, a larger average cross-sectional area of the duct is able to deliver a higher flow rate at the beginning of the experiment, therefore reducing the static head difference faster compared to the simulated case. This causes a quicker reduction of the flow rate. This higher flow rate also induces a faster rotation of the impeller.

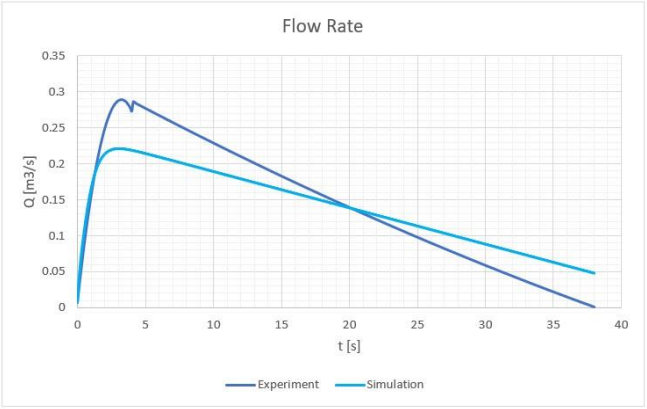

Fig. 11. Comparison of flow rate in function of time between experimental setup and model.

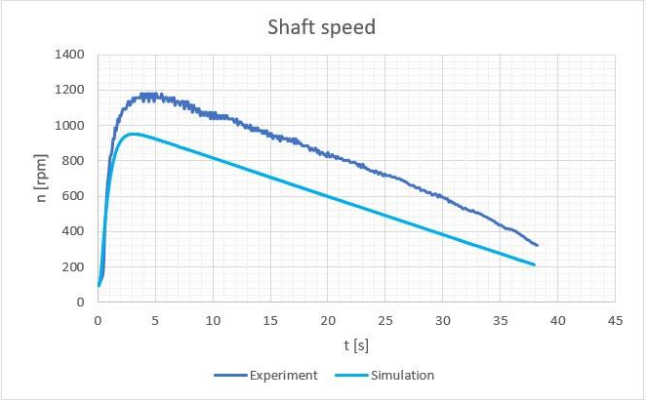

Fig. 12. Comparison of shaft speed in function of time between experimental setup and model.

In addition, the pressure head jump across the pump-turbine has been recorded and compared to the simulations.

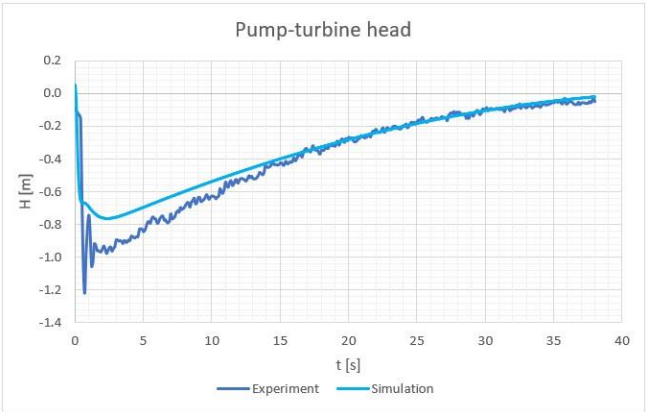

Fig. 13. Comparison of manometric head in function of time between experimental setup and model.

In order to check the behavior of the system, simulations have been run with a constant duct

diameter of 0.4 m. The results for flow rate and shaft speed are shown in the figures below.

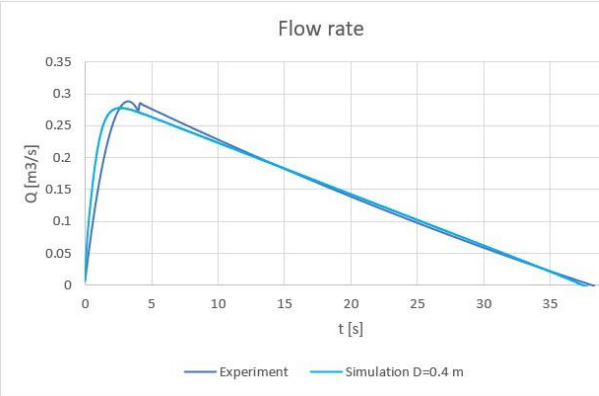

Fig. 14. Comparison of flow rate in function of time between experimental setup and model with increased diameter (0.4 m).

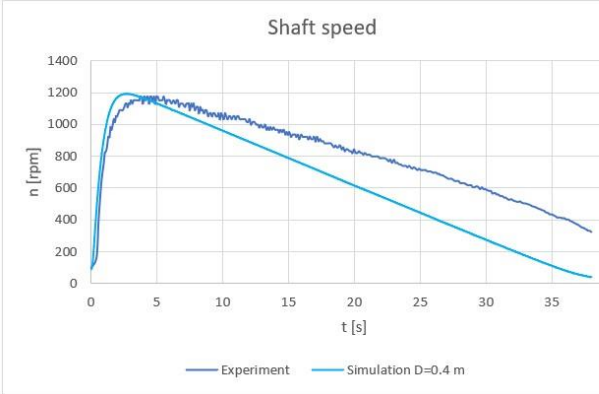

Fig. 15. Comparison of shaft speed in function of time between experimental setup and model with increased diameter (0.4 m).

This time the flow rate variation with time shows a better correspondence with the experimental results, suggesting that a duct with a diameter of 0.4 meters has a cross-sectional area (and therefore a pipe resistance) comparable to the average cross-sectional area of the experimental setup. The rpm graph shows a better correspondence as well, despite a faster decrease compared to the experimental results.

In conclusion, the results show some discrepancies between model and experimental setup. Although, these can be explained by the intrinsic approximations of the 0-D model and added mass moment estimation. A more accurate modelling of the test setup should be achieved in order to confirm these explanations.

IV. RESULTS

Simulations of the three starting procedures for the large-scale system have been performed. In Figure 16 the power trends during the start-up of the system are presented, with a static head difference of 1 meter. At t=0 the flow rate and shaft speed are assumed zero. Positive power represents consumption, whereas negative power represents generation. The shaft speed is also represented in Figure 17. The blue curve, representing the standard natural flow start-up of the system, starts generating power 11.5 seconds after the opening of the gate-valves, reaching nominal conditions in about 20 seconds. The red curve, representing the kickstart procedure without frequency controller, reaches generating conditions at 6.5 seconds, and steady-state generation at 15.5 seconds. It also shows a high peak in power demand at start-up, due to the system reaching the breakdown torque point. For pumps that are coupled to a motor without a frequency controller, this problem is usually solved with the use of a "soft starter", an electronic device that reduces the current surge at start-up. This in turn reduces the torque, which leads to a slower start. However, this approach has not been considered in this research. The green curve, corresponding to the kickstart procedure with frequency controller, reaches nominal power generation at 6 seconds.

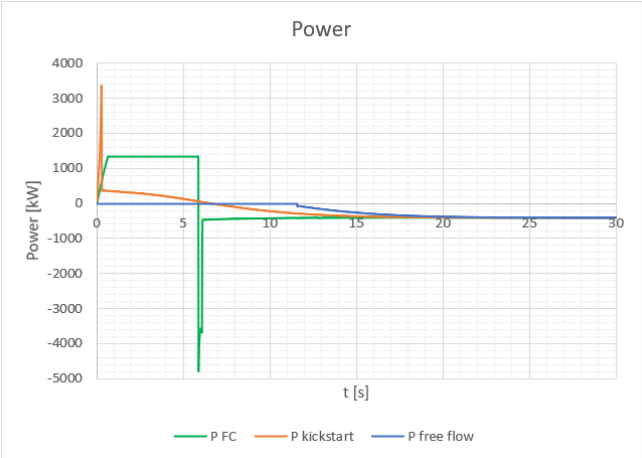

Fig. 16. Power consumed/generated with the three different starting procedures: kickstart with frequency controller (FC), normal kickstart and free flow. Static head difference of 1 meter.

The first increasing part of the green curve is the constant torque region, whereas the horizontal part is the constant power region. The observable large spike in power generation is

caused by the sudden reduction in current frequency. At that point the system rotates at around 24 rpm following the torque curve of Figure 6, so the electric machine is working as a motor. When generating conditions are reached by the flow, the frequency is reduced, so that the system starts working on the torque curve of Figure 5. After a few seconds, the system reaches its equilibrium point at about 400 kW.

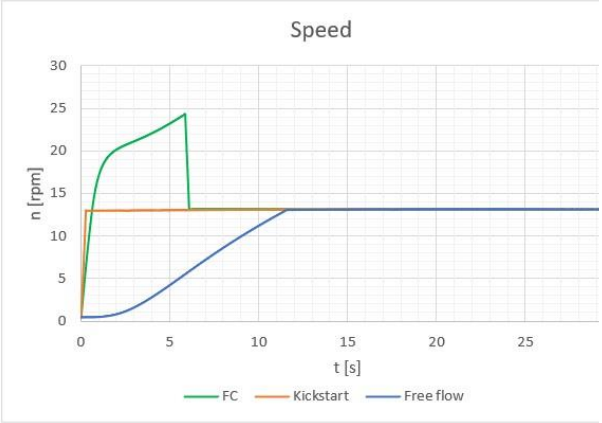

Fig. 17. Shaft speed in function of time for the three different starting procedures: kickstart with frequency controller (FC), normal kickstart and free flow.

The energy balance during the first 30 seconds of operation has also been tracked, to understand the amount of energy needed by the system during the kickstart procedures, and in how much time this energy would be recovered. This balance has been shown in Figure 18.

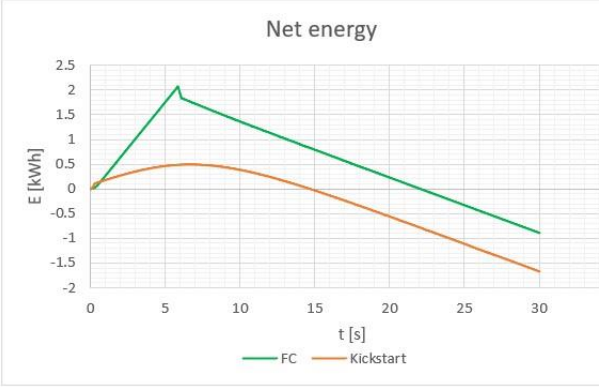

Fig. 18. Net energy balance for the two kickstart procedures: kickstart with frequency controller (FC) and fixed frequency kickstart.

The total energy needed by a single impeller/electric machine system is 0.5 kWh in case of fixed frequency kickstart and 2 kWh in case of kickstart with frequency controller. This energy is entirely recovered after 15 seconds and 22 seconds respectively.

V. Discussion of Results

From the results of section IV, it is clear that the only strategy able to reach nominal generating conditions in less than 10 seconds is the kickstart with frequency controller. The normal starting procedure, which relies only on the static head difference for the acceleration of the flow, which in turn puts the impeller into rotation, proved to be too slow given the set time constraint. In addition, the kickstart procedure at fixed frequency, despite having a fast acceleration in the first seconds, struggles to cross the synchronous speed of 13 rpm, since the mechanical torque in that speed range is small. This behaviour is shown by the red curve of Figure 17, where the shaft speed increases fast until it reaches values close to 13 rpm. In this sense, the advantage of the kickstart procedure with frequency controller lies in the fact that the system is able to accelerate up to a higher speed in a very short time, rapidly accelerating the flow and reaching nominal generating conditions.

A disadvantage of the kickstart procedures could be identified in the initial power demand of the system. In fact, if the grid experiences a demand increase and the power plant would have to be started to supply this power, the initial power consumption could cause an even greater grid imbalance. This problem could be solved by installing batteries that would store some of the energy generated during the turbine operation, to use it at the next start-up of the system. The size of these batteries can be estimated using the results shown in Figure 18.

VI. Conclusion

The study at hand has shown how a kickstart procedure with frequency controller is essential to comply with the timing restrictions of 10 seconds for nominal power generation. Especially for ultra-low head applications like in the case of the Brouwersdam, the flow development due to the water head difference alone turned out to be not sufficient to reach the prefixed goals.

As a recommendation for model accuracy improvements, it could be useful to adopt a 3-D modelling strategy, where the geometry of the experimental setup could be represented with higher accuracy. Moreover, for future research, it

could be also interesting to analyze how the system switches from a situation of steady-state pumping to the turbine operation, in particular how much time it would take for the system to slow down after the motor stops transmitting power to the shaft.

REFERENCES

[1] Z. Zhang, "Transient flows and computational method," in *Hydraulic transients and computations.* Springer, 2020

[2] M. Stewart, "Fluid flow and pressure drop," in *Surface production operations. Volume 3: facility piping and pipeline systems;* Elsevier, 2016

[3] D. J. Zigrang, N. D. Sylvester, "A review of explicit friction factor equations," *J. Energy Resour. Technol.*, vol. 107, issue 2, pp. 280–283, 1985.

[4] K. Sang-Hoon, "Alternating current motors: synchronous motor and induction motor," in *Electric motor control.* Elsevier, 2017

[5] A. Joshi et al., "Running torque of slow speed two-point and four-point contact bearings," *Lubricants*, 3, pp. 181–196, 2015.

[6] L. C. Burrill, W. Robson., "Virtual mass and moment of inertia of propellers," Marine and transport technology dept., TU Delft, 1962. [Online] Available: http://resolver.tudelft.nl/uuid:3a7ebb56-cb2f-4760-b5db-b29a2ef868d7

[7] D. M. MacPherson et al., "Estimation of entrained water added mass properties for vibration analysis," SNAME New England Section, 2005. [Online]. Available: https://www.hydrocompinc.com/wp-content/uploads/documents/MacPherson%202007%20EstimatioE%20of%20Entrained%20Water.pdf

[8] D. M. MacPherson et al., "Blade area ratio definition," HydroComp Inc., Report 135, 2007. [Online]. Available: https://www.hydrocompinc.com/wp-content/uploads/documents/HC135-BladeAreaRatio.pdf

[9] Holistic Numerical Methods, "Runge-Kutta 4th order methods for ordinary differential equations," 2010. [Online] Available: http://mathforcollege.com/nm/mws/gen/08ode/mws_gen_ode_txt_runge4th.pdf

[10] J. van Berkel et al., "Climate power plant for water safety and renewable energy", presented at the *13th EWTEC*, 2019

Appendix C – Solution of Non-linear Flow ODE

- $\frac{dQ}{dt} = \frac{gA}{L} H_s - \frac{f\frac{L}{D}+K_i+K_o}{2AL} Q^2$
- $\frac{dQ}{dt} + aQ^2 - b = 0$, Q(0)=0
- $\frac{dQ}{b-aQ^2} = dt$
- $\int \frac{dQ}{b-aQ^2} = \int dt$
- $\frac{1}{b}\int \frac{dQ}{1-\frac{aQ^2}{b}} = \int dt$, substitute $u = \frac{i*\sqrt{a}Q}{\sqrt{b}}$ with $du = \frac{i*\sqrt{a}}{\sqrt{b}} dQ$
- $-\frac{i}{\sqrt{a}\sqrt{b}}\int \frac{du}{u^2+1} = \int dt$
- $\int \frac{du}{u^2+1}$ is a known integral: $\int \frac{du}{u^2+1} = \arctan(u) + c_1$
- $-\frac{\mathrm{i}*\arctan(u)}{\sqrt{a}\sqrt{b}} + c_1 = t + c_2$, substitute again $u = \frac{i*\sqrt{a}Q}{\sqrt{b}}$
- $\frac{\operatorname{arctanh}\left(\frac{\sqrt{a}Q}{\sqrt{b}}\right)}{\sqrt{a}\sqrt{b}} = t + c$
- Solving for Q: $Q(t) = \frac{\sqrt{b}}{\sqrt{a}} * \tanh(\sqrt{ab} * t + \sqrt{ab} * c)$
- If Q(0)=0 then c=0
- $Q(t) = \frac{\sqrt{b}}{\sqrt{a}} * \tanh(\sqrt{ab} * t)$ and by definition $\tanh(x) = \frac{e^{2x}-1}{e^{2x}+1}$ so:
- $Q(t) = \frac{\sqrt{b}}{\sqrt{a}} * \frac{e^{2\sqrt{ab}*t}-1}{e^{2\sqrt{ab}*t}+1}$
- Calculating a and b for $Hs = 1\ m$, $A = 64\ m^2$, $L = 98\ m$, $f = 0.01575$, $D = 8\ m$, $K_i = 0.5$, $K_o = 1$:

  $a = 1.3496 * 10^{-4}\ m^{-3}$, $b = 6.407 \frac{m^3}{s^2}$
- $\frac{dQ}{dt} + 1.3496 * 10^{-4} * Q^2 - 6.407 = 0$, Q(0)=0
- $Q = 217.88 * \frac{e^{0.058811t}-1}{e^{0.058811t}+1}$

Appendix D – Matlab Functions

Scaling of experimental data

```
function [P, T, H] = characteristic(n,Q)
%% Characteristic Curves and H,P,T evaluation %%

%experimental data
n1=[649.400000000000,600.100000000000,550.400000000000,500.700000000000,451
,401.200000000000,351.300000000000,301.400000000000,251.600000000000,201.80
0000000000,151.900000000000,100,905.100000000000,850.300000000000,799.70000
0000000,750.300000000000,701.100000000000,651.800000000000,604.100000000000
,552.500000000000,502,452.400000000000,402.800000000000,352.700000000000,30
3.100000000000,253.200000000000,204.100000000000,100,925.600000000000,851.9
00000000000,801.800000000000,752.300000000000,702.500000000000,652.40000000
0000,602.800000000000,553,503.200000000000,403.900000000000,304.10000000000
0,204.200000000000,100,1128.30000000000,1102.30000000000,1051.60000000000,1
002.60000000000,952.200000000000,904,853.600000000000,803.700000000000,754.
200000000000,703.900000000000,655,604.300000000000,554.700000000000,505.100
000000000,455.400000000000,405.900000000000,306.400000000000,207.5000000000
00,100,500.400000000000,501.700000000000,498.800000000000,499.800000000000,
501.200000000000,500,498.900000000000,500.600000000000,500.900000000000,499
.500000000000,498.700000000000,499.400000000000,500.400000000000,499.800000
000000,499.500000000000,498.300000000000,500.100000000000,502.900000000000,
499.900000000000,500.100000000000,499.500000000000,499.300000000000,498.700
000000000,500.100000000000,499.900000000000,499.300000000000,504.2000000000
00,498.600000000000,501.700000000000,499.300000000000,498.800000000000,750,
750.200000000000,749.700000000000,749.300000000000,749.300000000000,749.600
000000000,749.600000000000,749.800000000000,749.300000000000,749.7000000000
00,749.500000000000,749.800000000000,750.600000000000,749.500000000000,749.
100000000000,749,749.200000000000,748.500000000000,749.100000000000,749.600
000000000];

Q1=1/3600*[562.800000000000,517.900000000000,481.800000000000,452.100000000
000,414,382.100000000000,348.300000000000,320.200000000000,291.100000000000
,260.200000000000,230.300000000000,201.100000000000,755.900000000000,712.50
0000000000,677.100000000000,644.200000000000,609.600000000000,575.600000000
000,545.300000000000,509,471.400000000000,441.900000000000,410.200000000000
,377.100000000000,350.900000000000,318.700000000000,293.100000000000,233.80
0000000000,782.400000000000,732.700000000000,693.600000000000,672.100000000
000,634.400000000000,602.200000000000,564.600000000000,533.700000000000,507
.400000000000,440.100000000000,380.200000000000,322.800000000000,263.600000
000000,966.400000000000,953.400000000000,906.800000000000,870,843.500000000
000,806.600000000000,775.200000000000,742.700000000000,705.800000000000,669
.200000000000,645.700000000000,609,582.300000000000,544.600000000000,520,48
8.400000000000,431.600000000000,372,326.600000000000,711.500000000000,661.2
00000000000,619.200000000000,571.100000000000,542.700000000000,524.30000000
0000,516.300000000000,488.900000000000,476.600000000000,457.400000000000,43
1.200000000000,423.800000000000,399.600000000000,386.200000000000,372.90000
0000000,345.300000000000,325,355.600000000000,349.400000000000,318.30000000
0000,310.700000000000,293,259,256,244.700000000000,220.500000000000,202.200
000000000,170.400000000000,156.100000000000,141.700000000000,80.80000000000
00,875.800000000000,830.500000000000,783.800000000000,737.100000000000,691.
800000000000,644.200000000000,606.300000000000,566.800000000000,544.9000000
00000,531.400000000000,526,502.100000000000,487.900000000000,480.6000000000
00,438.400000000000,395.300000000000,335.800000000000,256.100000000000,204.
500000000000,98.4000000000000];

H1=[-0.43739828, -0.464386369, -0.473150612, -0.463688227, -0.47342455, -
0.477662267, -0.480679041, -0.494087605, -0.480126042, -0.49043575, -
```

```
0.487040781, -0.493292402, -0.608724745, -0.650095743, -0.595632647, -
0.607911589, -0.63107558, -0.657223059, -0.634810022, -0.662018306, -
0.65899082, -0.658802169, -0.681525109, -0.660888651, -0.692982421, -
0.681292712, -0.696415241, -0.693847074, -0.908980237, -0.915169763, -
0.927645579, -0.945076731, -0.933380887, -0.959332408, -0.973450813, -
0.969034698, -0.956539806, -0.975831638, -0.9835162, -0.97705553, -
0.962567326, -1.363209448, -1.358725665, -1.347875318, -1.393397461, -
1.436204608, -1.351502992, -1.397695794, -1.391434402, -1.433335674, -
1.434634119, -1.447906661, -1.441516756, -1.440135345, -1.475972014, -
1.457586449, -1.451014328, -1.464223515, -1.474130846, -1.479734747, -
3.976678556, -3.158729358, -2.411836226, -1.766999521, -1.306562145, -
1.212004335, -1.052736703, -0.742744821, -0.713445494, -0.447515602, -
0.30604173, -0.193754354, 0.016856485, -0.000428775, 0.181755376,
0.338082854, 0.425805067, 0.273438283, 0.226338714, 0.432815242,
0.556850149, 0.558339958, 0.739536178, 0.807488904, 0.837183367,
0.923681572, 0.997343536, 1.073947178, 1.156599922, 1.262713586,
1.779044896, -4.438219882, -3.502850162, -2.680983545, -1.952138059, -
1.252512528, -0.702910256, -0.188386666, 0.227301359, 0.518312104,
0.588550642, 0.605661942, 0.834237612, 0.86814962, 1.137249235,
1.440713223, 1.745420682, 2.112250258, 2.429308015, 2.913908917,
4.518406997];

P1=1000*[-0.09,-0.197,-0.241,-0.246,-0.273,-0.274,-0.269,-0.258,-0.219,-
0.193,-0.153,-0.105,0.075,-0.143,-0.114,-0.213,-0.314,-0.409,-0.405,-
0.462,-0.47,-0.46,-0.465,-0.415,-0.401,-0.345,-0.301,-0.15,-0.47,-0.623,-
0.703,-0.763,-0.784,-0.835,-0.869,-0.847,-0.795,-0.731,-0.606,-0.438,-
0.205,-0.971,-0.975,-1.096,-1.289,-1.449,-1.327,-1.481,-1.495,-1.595,-
1.592,-1.573,-1.517,-1.432,-1.416,-1.297,-1.193,-0.974,-0.702,-0.325,-
4.165,-3.391,-2.493,-1.747,-1.22,-1.103,-0.925,-0.573,-0.531,-0.244,-
0.075,0.041,0.253,0.238,0.404,0.541,0.622,0.484,0.45,0.63,0.763,0.733,0.865
,0.944,0.937,0.995,1.086,1.129,1.218,1.273,1.644,-6.71,-5.167,-3.776,-
2.521,-1.312,-
0.375,0.43,1.058,1.45,1.584,1.574,1.88,1.947,2.302,2.654,2.979,3.336,3.755,
4.294,5.835];

T1=[-1.323431926,-3.134829907,-4.181287204,-4.69168556,-5.780394607,-
6.521703052,-7.312157078,-8.17424857,-8.311987092,-9.132875327,-
9.618448832,-10.02676141,0.791290735,-1.60596191,-1.361285245,-
2.710915864,-4.276820893,-5.992117679,-6.402028004,-7.985113163,-
8.940576484,-9.709718014,-11.02389005,-11.23605921,-12.63367843,-
13.01148231,-14.08299006,-14.32394488,-4.84892977,-6.983462581,-
8.372606011,-9.685116702,-10.65715092,-12.22204575,-13.76632172,-
14.62613781,-15.08682589,-17.2828319,-19.02950914,-20.4828203,-19.576058,-
8.217997859,-8.446488407,-9.952481036,-12.27712278,-14.53153828,-
14.01760682,-16.56807432,-17.76309369,-20.1950783,-21.59749988,-
22.93289088,-23.97200549,-24.65223132,-26.77054834,-27.19683283,-
28.06679189,-30.35579267,-32.30653592,-31.0352139,-79.48205491,-
64.54388025,-47.72733839,-33.37859371,-23.24449688,-21.06574827,-
17.70515001,-10.93037743,-10.12313134,-4.664721455,-
1.436128422,0.7839831,4.828081607,4.547284088,7.723555196,10.36758871,11.87
694956,9.19041469,8.596086144,12.02970776,14.5868134,14.01889525,16.5633478
,18.02546686,17.89896159,19.02974184,20.56829848,21.62285569,23.18326339,24
.34659434,31.47362387,-85.43437345,-65.77074841,-48.09676391,-32.12835539,-
16.72050863,-
4.777196131,5.477851563,13.47446757,18.47922067,20.17618486,20.05415987,23.
94328832,24.77015781,29.32952734,33.83237637,37.98044663,42.52062655,47.905
95682,54.73859236,74.33317179];


D1=0.3;     %experimental setup diameter [m]
D2=8;       %real diameter [m]
```

```
%variables initialization
Q2=zeros(1,length(n1));
H2=zeros(1,length(n1));
P2=zeros(1,length(n1));
T2=zeros(1,length(n1));
Q3=zeros(1,length(n1));
H3=zeros(1,length(n1));
P3=zeros(1,length(n1));
T3=zeros(1,length(n1));
C=zeros(length(n1),5);
D=zeros(length(n1),5);
E=zeros(length(n1),5);

%calculations
for i=1:length(n1)
    Q2(i)=Q1(i)*(n/n1(i));      %flow rate scaling (speed)      [m^3/s]
    H2(i)=H1(i)*(n/n1(i))^2;    %head scaling (speed)           [m]
    P2(i)=P1(i)*(n/n1(i))^3;    %power scaling (speed)          [W]
    T2(i)=T1(i)*(n/n1(i))^2;    %torque scaling (speed)         [Nm]
    Q3(i)=Q2(i)*(D2/D1)^3;      %flow rate scaling (diameter)   [m^3/s]
    H3(i)=H2(i)*(D2/D1)^2;      %head scaling (diameter)        [m]
    P3(i)=P2(i)*(D2/D1)^5;      %power scaling (diameter)       [W]
    T3(i)=T2(i)*(D2/D1)^5;      %torque scaling (diameter)      [Nm]

end

C=polyfit(Q3,H3,4);   %characteristic curves 4th rank
D=polyfit(Q3,P3,4);
E=polyfit(Q3,T3,4);

H=polyval(C,Q);       %evaluation of H(Q), P(Q), T(Q)
P=polyval(D,Q)/1000;
T=polyval(E,Q)/1000;

end
```

Mechanical Torque

```
function [T_el, T_mec, check] = Torque(n, Q, eta_mec, check)

T_rated=937.3285;                %[kNm]
P_const=T_rated*(13*pi/30);      %power in const. power region [kW]

%kickstart w/ FC
%if Q<80 && check==0;                  %pump operation (Q<80)
%    if n<=13                          %constant torque region
%        T_mec=T_rated;
%    else                              %constant power region
%        T_mec=P_const/(n*pi/30);
%    end
%else                %turbine operation (Q>80) OR kickstart w/o FC
%    check=1;        %switch pump/generation mode
%    if n<11.7
%        T_mec=T_rated*(0.01713*n^2-0.16185*n+2.33243);     %curve
fit from "torque curves.xlsx" [kNm]
    if n<13                       %no kick-start
```

```
        T_mec=0;
    elseif (n>=13) && (n<14.3)   %change interval (11.7->14.3 for
kickstart,13->14.3 for no kickstart)
        T_mec=T_rated*(0.89147*n^3-34.7674*n^2+448.36948*n-
1911.67617); %curve fit from "torque curves.xlsx" [kNm]
    else
        T_mec=T_rated*(-0.01713*n^2+0.72892*n-9.7044);      %curve
fit from "torque curves.xlsx" [kNm]
    end
%end
if T_mec>0
    T_el=T_mec/eta_mec; %efficiency effect
else
    T_el=T_mec*eta_mec; %efficiency effect
end
end
```

Acknowledgements

This report illustrates the work of my master's thesis, final project to complete the Master's Program of Sustainable Energy Technology at Eindhoven University of Technology. Firstly, I would like to thank my TU/e supervisor Prof. Bart van Esch and my external supervisor Prof. Jacob van Berkel. Thank you for giving me the opportunity to work on this subject, for your continued support and guidance, and for pushing me to do my best at every stage of the project. I would also like to thank the committee members for taking the time to review this thesis and be part of the defense committee. In addition, I would like to deeply thank the company Nijhuis Pompen BV and HZ University of Applied Sciences for the experimental data on which this project is based on. Moreover, I want to thank my family from the deepest of my heart for all the possibilities they have given to me during my life: their economic and moral support when I moved to the Netherlands are just the last chapter of a constant flow of love and care. A huge thank you to my girlfriend Elisa, for being such a lovely, caring, supportive and understanding partner during these challenging months. A socially-distanced hug to all my SET colleagues Arun, Giannis, Joost, Luis and Tito (thanks a lot for all the coding help!), and to all my friends around the world, especially Alessandro, Camilla, Flavio, Alessandro, Marco and Rute. Thank you everyone, from the bottom of my heart.